

Table 3.7 XPS data of the polymers resulting of the deposition at different conditions

<i>Peq</i>	<i>Atomic percentage</i>				<i>Ratio</i>	
	C1s	O1s	F1s	N1s	F/C	O/C
50W	38.73	34.31	0.15	0.29	0.004	0.88
25W	31.34	32.47	2.25	1.56	0.07	1.04
18W	40.34	26.63	5.53	7.83	0.04	0.66
10W	55.91	25.28	9.65	8.32	0.17	0.45
8.3W	57.31	24.58	11.62	6.35	0.20	0.43
5.5W	60.42	23.68	10.45	5.46	0.17	0.39
4.5W	62.28	16.50	17.87	3.36	0.29	0.27
0.2W	62.76	22.24	5.02	9.01	0.08	0.35
Theoretical values					0.5	0.2

3.4.2 INFLUENCE OF THE SAMPLE POSITION

Trying to get a better polymer structure on this reactor, a new parameter was introduced in the study. The geometry of this reactor is slightly different from *system 1*. The film structure was studied as a function of sample position keeping all other conditions constant. The changes in the location of the substrate relative to the plasma discharge zone have been shown to provide film chemistry variations.²² Following the best result of the previous study, the parameters will be fixed at 0.2 mbar monomer pressure, pulsed plasma at 50W and a duty cycle = 10/110, getting an equivalent power of 4.5W.

The samples were placed on a 55 cm glass holder. They were placed 10 cm from each other, placing position number 2 inside the coil, as it can be seen in Figure 3.11. The positions in the reactor were named arbitrarily from 1 to 5, starting at the right end and going against the monomer's flow direction.

Figure 3.11 shows also the XPS C1s peaks for the films achieved in these positions. It can be seen how the structure develops increasing the C-F group signal in front of other functionalities. In position 1 and 2, after and inside the coil, we can see how the structure is in concordance to the polymers gotten in the previous polymerizations. The structure is poorly achieved, having few C-F groups retained over the film. This is easy to be explained by the fact that the plasma is formed inside the coil. This is where it has its major power, and so where it achieves a wide degradation of the monomer. Also, the temperature is higher than in the rest of the reactor, and also a better degradation of the recent formed polymer occurs. Position 1 lays just after the coil, in the direction where the flow of monomer and excited species. The plasma here is still as strong as it is

inside the coil. Therefore the same kind of problem arises. Another important factor linked with these positions is the monomer residence time in the vessel. Being this time longer increases the opportunity for collision for every particle with an electron. That increases the degree of fragmentation of the monomer, being greatest adjacent to the vacuum outlet.²⁸

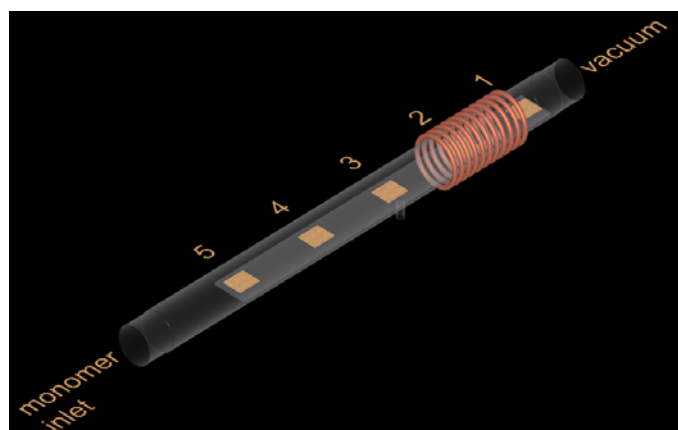
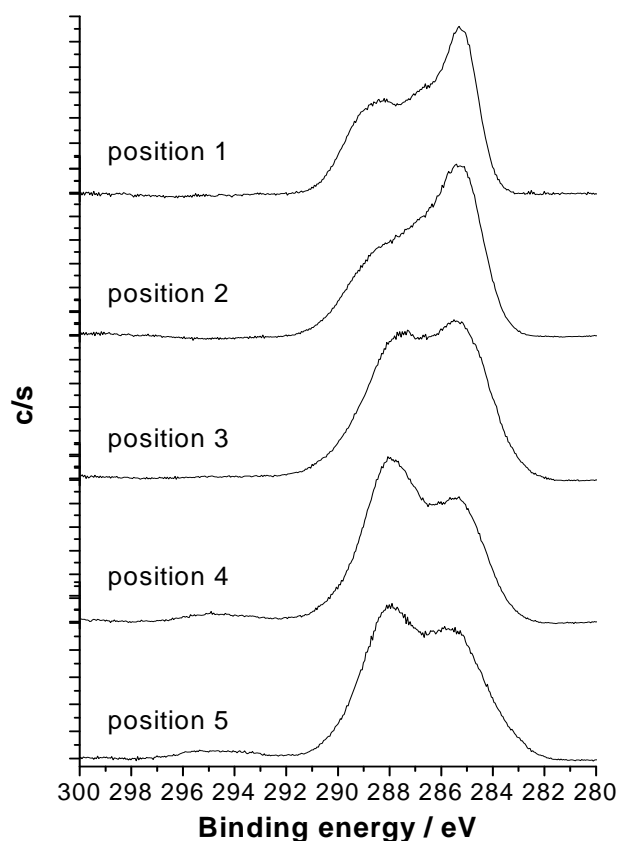


Figure 3.11 Drawing detail of the sample position in the reactor and its corresponding XPS C1s peak

Taking a look into Table 3.8 it can be seen how the fluorine content is very low, and still far from the ideal values. Instead of fluorine, there is a high value of oxygen and nitrogen for positions 1 and 2. This extended presence, particularly for nitrogen, and linked to the positional study, could indicate the presence of a small leak at this end of the reactor, leaving residual gas inside the chamber. The XPS can detect also silicon, which means that the polymerization wasn't successful in terms of deposition either.

As the sample was moved to positions 3 and 4, outside the coil in direction to the monomer inlet, against the flow, the C-F peak was seen to increase till it got predominant over the other functionalities. For the sample in position 4, a $\pi-\pi^*$ shake-up satellite signal can be observed for the first time, suggesting the presence of aromatic rings in the polymer. For this sample, the F/C and O/C are already near to the theoretical values (see Table 3.8), and the nitrogen presence decreases dramatically. No other species were present in the position.

Table 3.8 XPS data of the polymers resulting of the deposition at different positions

Position	Atomic percentage					Ratio	
	C1s	O1s	F1s	N1s	Si	F/C	O/C
1	51.32	26.87	4.58	11.20	5.94	0.09	0.52
2	61.97	23.24	5.56	7.98	0.80	0.09	0.37
3	61.42	16.35	18.82	3.31	-	0.31	0.27
4	58.55	13.27	27.44	0.66	-	0.47	0.23
5	59.00	12.16	27.81	0.70	0.32	0.47	0.21
Theoretical values						0.5	0.2

In these positions the plasma got weaker as the sample was nearer from the monomer inlet. There was still plasma present, but around the 4th position, already the light it generates wasn't extremely brightened anymore. The plasma was losing power, and new monomer got in contact to be excited at this position. Hence a better structure was achieved. There was less monomer degradation allowing low energy growth mechanisms, as polymerization over the allyl bonds retaining the phenyl functionalities intact. It has been reported in the literature that outside the glowing zone of the plasma, the recombination mechanisms usually result in the incorporation of molecular fragments with lower degrees of dissociation³¹, leading to better structure retention. Approaching position 5, though there was a good retention of the structure, a slightly loss of C-F groups could be observed. Here the plasma wasn't strong enough to get the best polymerization. The atomic composition was close to the theory, but again the presence of a small amount of silicon indicates an insufficient deposition rate. The film was too thin. At this position, the plasma generation core was too far and the power wasn't enough to polymerize the PFM properly.

The analysis of the samples showed, that by changing the sample position, it was possible to reach the desired structure in the polymer. From now on, position 4 was fixed for the all subsequent experiments, maintaining the other parameters fixed at 0.2 mbar monomer pressure, 50 W input power and pulsed plasma with a duty cycle 10/110.

ToF-SIMS analysis was used to get a complementary data to the XPS. Positive and negative spectra of the obtained polymers were studied to determine the structure of the films.

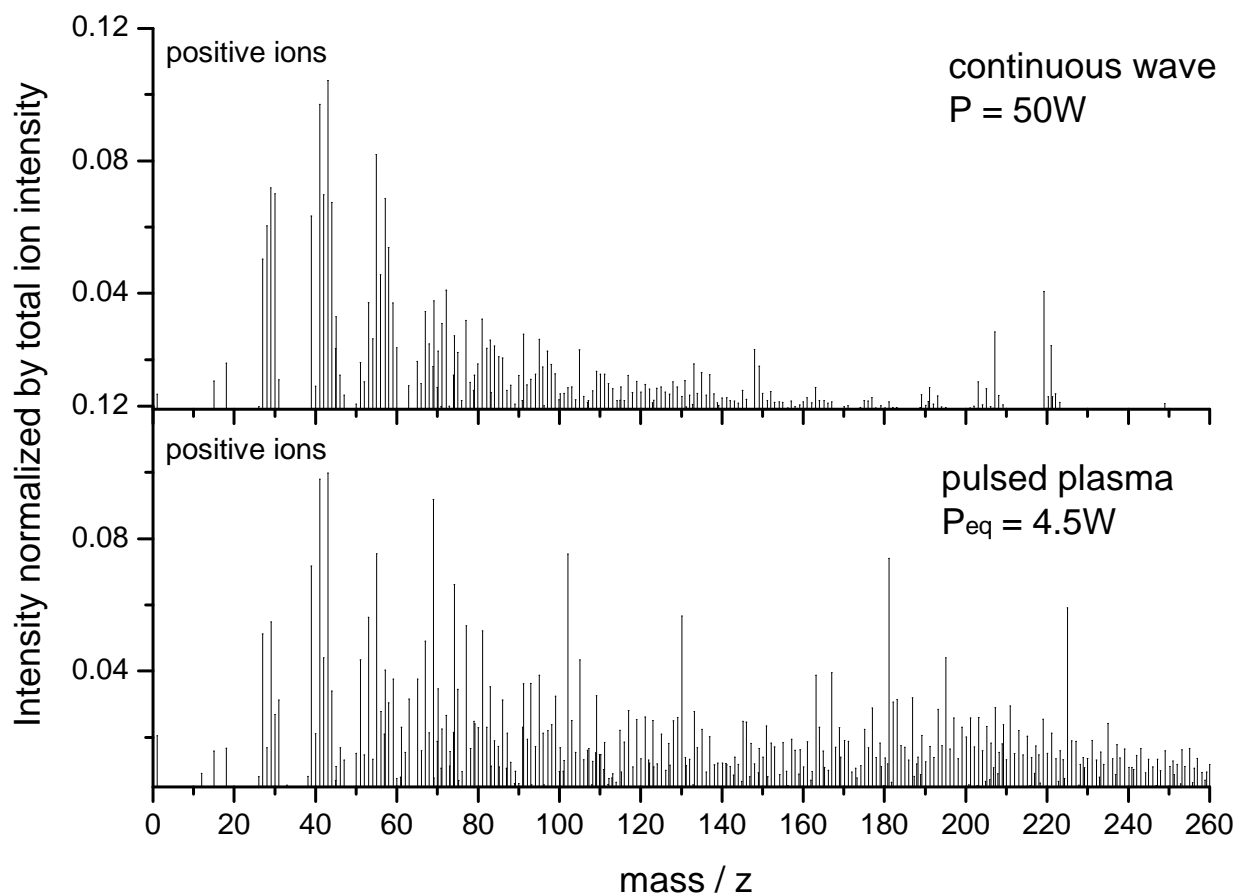


Figure 3.12 Averaged and normalized positive ToF-SIMS spectra of PFM polymerized under different conditions: ppPFM under 50W continuous wave in position 1 in the reactor, and pp-PFM under 4.5W equivalent power DC=10/110, in position 4.

Figure 3.12 presents a comparison between the positive spectra of the sample polymerized under continuous wave with a power input of 50 W and a second sample polymerized under pulsed plasma with a duty cycle of 10/110 with an equivalent power of 4.5W and the sample positioned in position 4. Under ToF-SIMS analysis conditions, the two samples present different behavior. The first sample presents a higher concentration of low masses, while the second sample presents a higher concentration of high masses. This presence of high masses indicates a better retention of the monomer's structure, in front of the sample polymerized under continuous wave conditions, supporting the previous gotten results. The better structure retention at lower plasma powers determined by ToF-SIMS analysis has already been reported for other monomers.³²

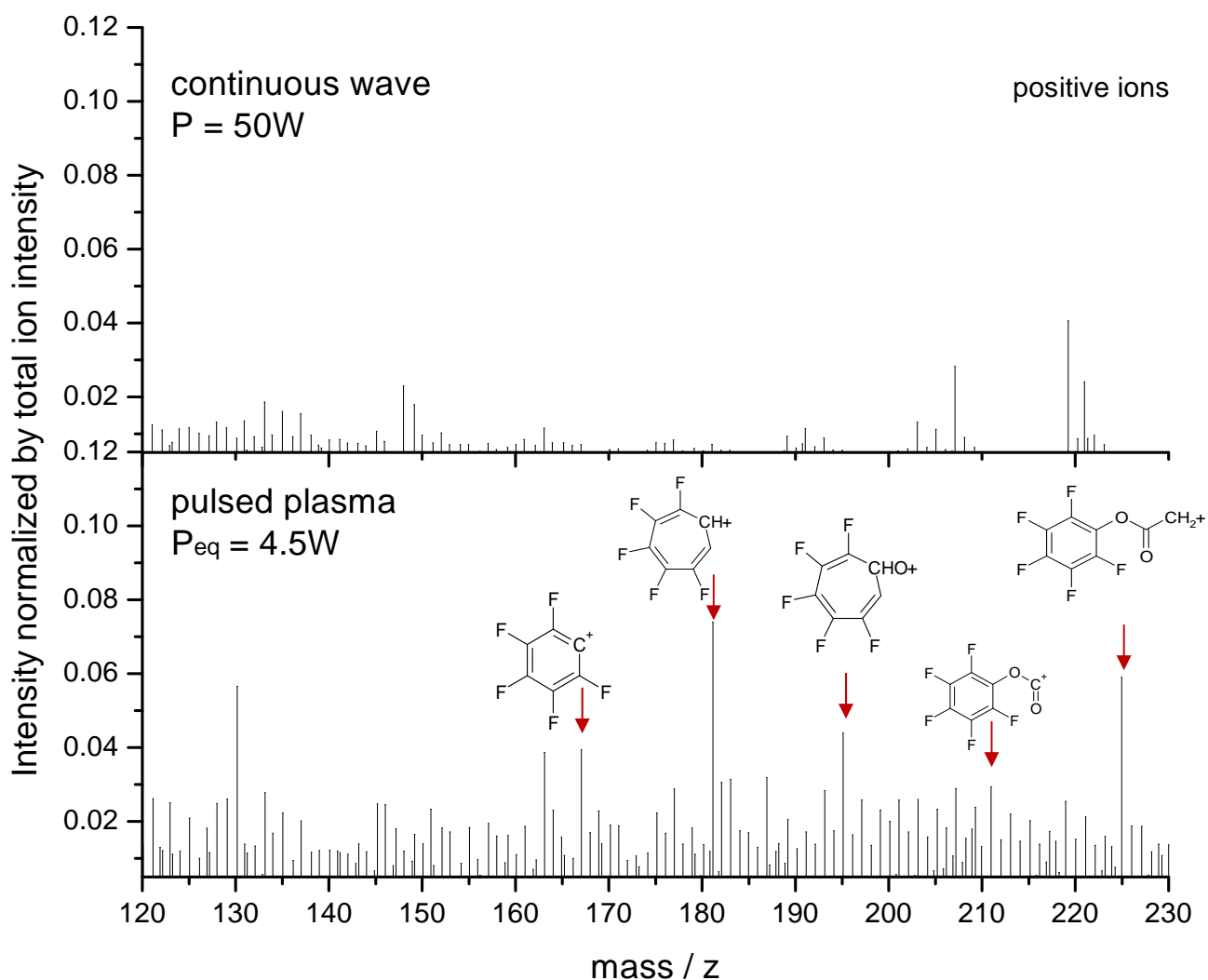
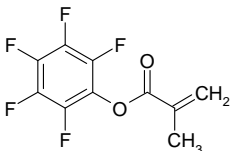
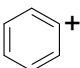
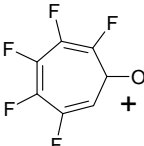
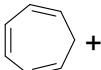
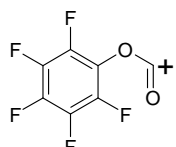
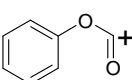
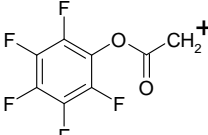
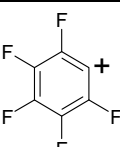
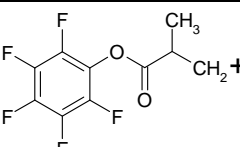
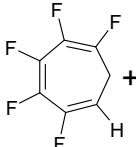
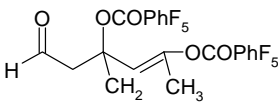


Figure 3.13 Zoom over the 120-230 mass area in ToF-SIMS spectra in Figure 2.14

Figure 3.13 presents a zoom over the m/z 120-230 area, showing the most significant differences between the two samples. This area was chosen due to the presence of some interesting masses for the characterization of the polymer (see next page in Table 3.9). The sample polymerized under pulsed plasma conditions shows the presence of some indicative peaks for the monomer, showing the retention of the monomeric structure. In the same range, the sample polymerized under continuous wave conditions shows only small peaks, indicating small structure retention.

Table 3.9 presents the possible ion structures for the found indicative peaks of the pp-PFM at high masses.

Table 3.9 Possible structure of the secondary ions for the found characteristic peaks of the pp-PFM under pulsed plasma conditions

Monomer Structure		m/z	
		252.14	
Possible Ion Structure	m/z	Possible Ion Structure	m/z
	77		195.2
	91		210.96
	121		224.94
	167.06		253.11
	181.12		333.26

In comparison to the monomer structure, also drawn in Table 3.9, at high masses it is possible to find structures that resemble the original monomer structure. The presence of benzene ($C_6H_6^+$, $m/z=77$) and cyclic tropylium ion ($C_7H_7^+$, $m/z=91$) can be found easily in the data. These peaks have already been reported for plasma polymers with aromatic rings in their side chains (e.g. polystyrene)^{6,33}. The analogues of these structures can be observed also substituted by fluorine atoms ($C_6F_5^+$, $m/z=167.06$ and $C_6F_5H^+$, $m/z=181.12$), showing the retention of the fluorinated rings in the polymeric structure. Indicative ions revealing the monomer structure have also been detected, showing the retention of the ester group at higher masses, like $m/z=210.96$ and $m/z=224.94$. The presence of the molecular ion can be detected at $M+1$, $m/z=253.11$, although it is only in a small amount. At higher masses some oligomeric structures can be found, like the one

detected at $m/z=333.26$ that are not shown in the presented spectra. These structures are present in small amounts.

In the case of the negative spectrum, the presence of fluorine (F^- , $m/z=19$) is dominating the rest of the spectrum, showing the highest intensity. The rest of the spectrum doesn't add any information to the already presented information from the positive data, and therefore, it won't be presented in further detail. The only remarkable fact is that also this spectrum corroborates the presence of high mass peaks revealing the presence of oligomeric particles with a high retention of the monomeric structure (e.g. $m/z=308.73$ and $m/z=327.9$).

3.4.3 SUMMARY FOR WORK IN SYSTEM 2

After adjusting the working parameters, it was possible to polymerize PFM in a new built system. Not only the input power and the duty cycle needed to be adjusted, but it was also demonstrated that the sample position plays a key role in determining the subsequent structure. It has been possible to repeat the previously achieved structure by working under very specific conditions. As in the preceding system, there is a small range of parameters that allows reaching a polymer with high retention of the reactive groups. These results show a repeatability success in the new built system.

3.5 FILM STABILITY AND REACTIVITY

In the preceding sections, a PFM polymer film with high retention structure was developed. This polymer offers a highly reactive ester group that can potentially be used to react with the amino groups on proteins, e.g. integrins and other biological ligands.¹ The interaction of biological molecules with reactive surfaces always occurs in an aqueous environment and often in the presence of other, possibly competing fluid components. In order to achieve a fundamental understanding of the chemical reactivity of the pp-PFM surface towards proteins, we investigated the basic reaction of the perfluoroester group with a simple amine using FTIR, XPS and Surface Plasmon Resonance Spectroscopy.

Knowing that the solvent plays an active part in any subsequent chemical reactions, there is an interest to investigate how this affects the reactivity of the active ester towards a simple diamine and a protein in PBS solution. This was done by reacting the surface with amine in aqueous buffer solution (PBS) after different immersion times in pure buffer.

3.5.1 EFFECT OF THE SOLVENT ON PP-PFM: THICKNESS AND COMPOSITION

Before the reactivity of the plasma polymerized PFM film towards amines or proteins could be tested, it was necessary to understand the reactivity towards the solvent (PBS). In a series of experiments, the effect on the polymer of an immersion in PBS solution was studied. The samples were placed in contact with the solution right after deposition in the plasma chamber. For the FTIR analysis, it was only possible to follow the reaction off-line, always working on the same sample. For the SPR a reaction on-line could be observed.

The FTIR spectra in Figure 3.14 show that the plasma polymerized PFM undergoes some change in chemical structure upon immersion. The reaction of the ester group with the water is observed as a decrease of the band at 1730 cm^{-1} accompanied by the appearance of a band at 1650 cm^{-1} . At the same time, a decrease in the intensity of the band at $1000\text{-}1400\text{ cm}^{-1}$ indicates a loss of the fluorinated group. After approximately 100 minutes the films appeared to be sufficiently stable. From the changes in the FTIR spectra, it is seen that with extended immersion time in PBS the active ester group dissociates to give the free acid and the pentafluorophenyl group (PFP). Since, however, there is still significant relative intensity at wavenumbers of 1730 and 1525 cm^{-1} , it can be assumed that only the perfluorinated ester within the uppermost layers are reacting and that functional groups deeper within the film remain intact over the time period studied here.

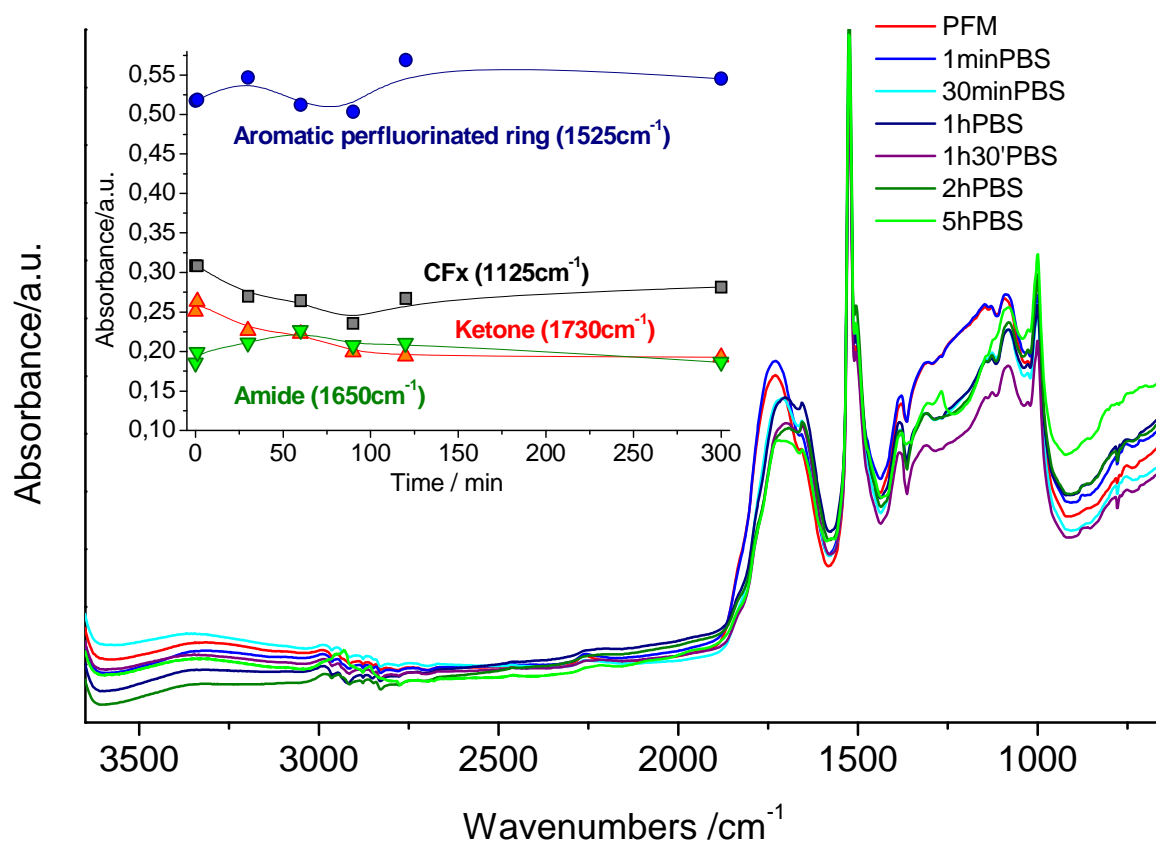


Figure 3.14 FTIR spectra showing the change in the surface chemistry after several hours immersion in PBS

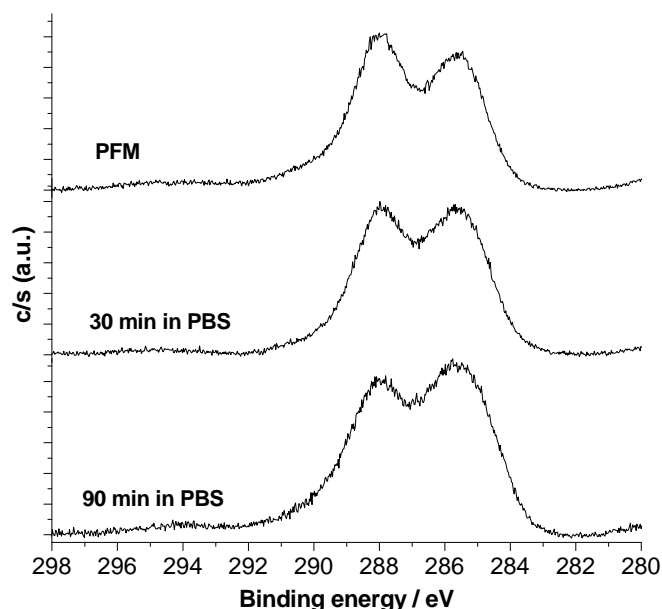


Table 3.10 XPS data of the polymer after immersion in PBS

Sample	Ratio	
	F/C	O/C
PFM	0.48	0.19
+ 30 min in PBS	0.43	0.19
+ 90 min in PBS	0.39	0.21
Theoretical values	0.5	0.2

Figure 3.15 XPS spectra showing the change in the surface chemistry after immersion in PBS

Figure 3.15 presents a comparison between the XPS C1s peaks before and after exposure to a PBS solution. There is an evident change on the curves' profiles, showing a decrease on the C-F groups. The changes in the C-O groups are difficult to identify, due to the overlapped position of the peaks. The C-O peak is positioned in

the middle of the curve (see Figure 3.8 and related Table 3.5), making any alteration in the peak area impossible to identify. The data presented in Table 3.10 shows how the F/C ratio decreases, supporting the profiles, while the O/C ratio shows a small increase. The immersion in PBS solution leads to a loss in fluorine, yet only a comparatively small change in oxygen, which may suggest the loss of the fluorinated, aromatic ring to give free carboxylic acid groups. The longer the immersion time in PBS, the more fluorine was seen to be lost.

Complementary experiments were done using SPR, to follow the change within the polymer upon the immersion in PBS for 14 hours.

Figure 3.16 shows the SPR kinetic curve of the polymer's exposure to PBS. The curve of the polymer was compared to gold reference under the same conditions. A small slope on gold curve can be observed. This is believed to be due to the increase of the temperature of the circulating solution by exposure to the laser beam, as work is done usually with small volumes.

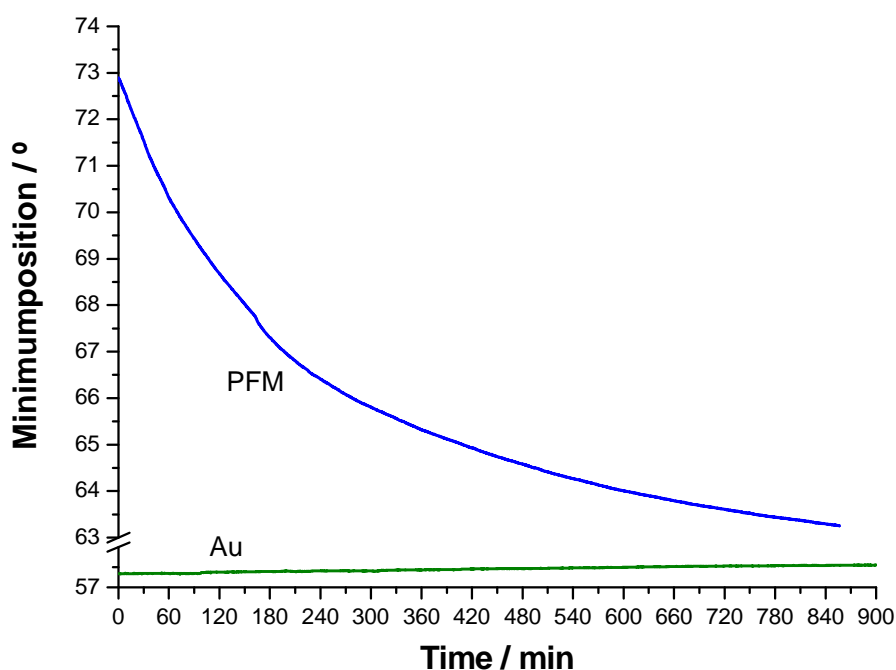


Figure 3.16 SPR kinetic study of the relation film thickness – refractive index during 14 hours of immersion in PBS

The PFM curve shows a decrease in the resonance angle ($\Delta=9^\circ$). This decrease in the resonance angle is due to a number of effects taking place simultaneously and which cannot be distinguished in the SPR data. Firstly, the active ester group is expected to hydrolyse in water, the PFP-group is lost and may or may not be able to desorb from the surface. Secondly, at low duty cycle plasma deposition conditions unreacted monomer or dimer may become trapped within the structure and may be slowly released from the film when this is immersed in solution. Thirdly, all polymers swell in aqueous solution. This results in an increase in film

thickness, such that the overall effect observed in the SPR experiment is merely the sum of these three basic phenomena. Care has been taken to include this in the experimental procedure and the interpretation.

The presented data clarifies that there exists a reaction of the active ester group versus the 0.01 M PBS solution, i.e. water. Even though the reaction isn't as fast as that expected from the theoretical point of view.

3.5.2 SURFACE REACTIVITY VERSUS AMINE

Knowing that the solvent plays a small but measurable part in any subsequent chemical reaction, it was interesting to investigate the reactivity of the active ester towards a simple diamine, 1,6-diaminohexane.

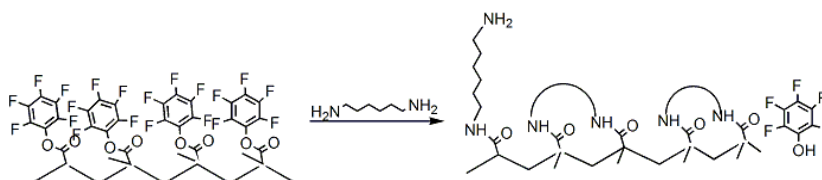


Figure 3.17 Possible reaction of the pp-PFM with the 1,6-diaminohexane used for the experiments

In order to investigate the rate at which reactivity of the active ester group was lost, a set of experiments was performed after different immersion times in PBS.

Experiments at time 0

The polymer was allowed to react with an amine without prior immersion/stabilization in PBS in order to test the reactivity of the fresh deposited polymer.

The relative change in chemical structure of the polymer film subjected to 10 mM diamino-hexane in PBS, could be seen in the FTIR spectra in Figure 3.18. It showed the change in relative FTIR peak intensities for the bands at 1655 cm^{-1} (amide formation, $\text{O}=\text{C}-\text{NH}-$), 1525 cm^{-1} (the PFP group) and 1125 cm^{-1} (C-F) with immersion time. Similar data analysis was not performed for the ester group (1730 cm^{-1}) since this was not a clearly defined band in all the spectra. The contribution due to the aromatic ring (at 1525 cm^{-1}) was seen not to change significantly over the time studied. However, the $\text{C}-\text{F}_x$ bands decreased in intensity, while the amide band (1655 cm^{-1}) increased within about 10 minutes, after which time it remained relatively stable. It was thus assumed that the reaction between the ester groups in the film (of $d = 60\text{ nm}$) and the diamine was complete after 10 minutes, suggesting that the rate of reaction of the diamine is a factor 10 faster than that of the

solvent (PBS). With increasing immersion time in diamine/PBS, the FTIR spectrum also shows an increase in the intensity of the hydrocarbon component (around 3000 cm^{-1}) and a decrease in the band at 2250 cm^{-1} . The latter could suggest that there was some dissolution of unbonded dissociation products containing $\text{C}\equiv\text{C}$. The intensity increase of the hydrocarbon component probably originated from the surface attached amines.

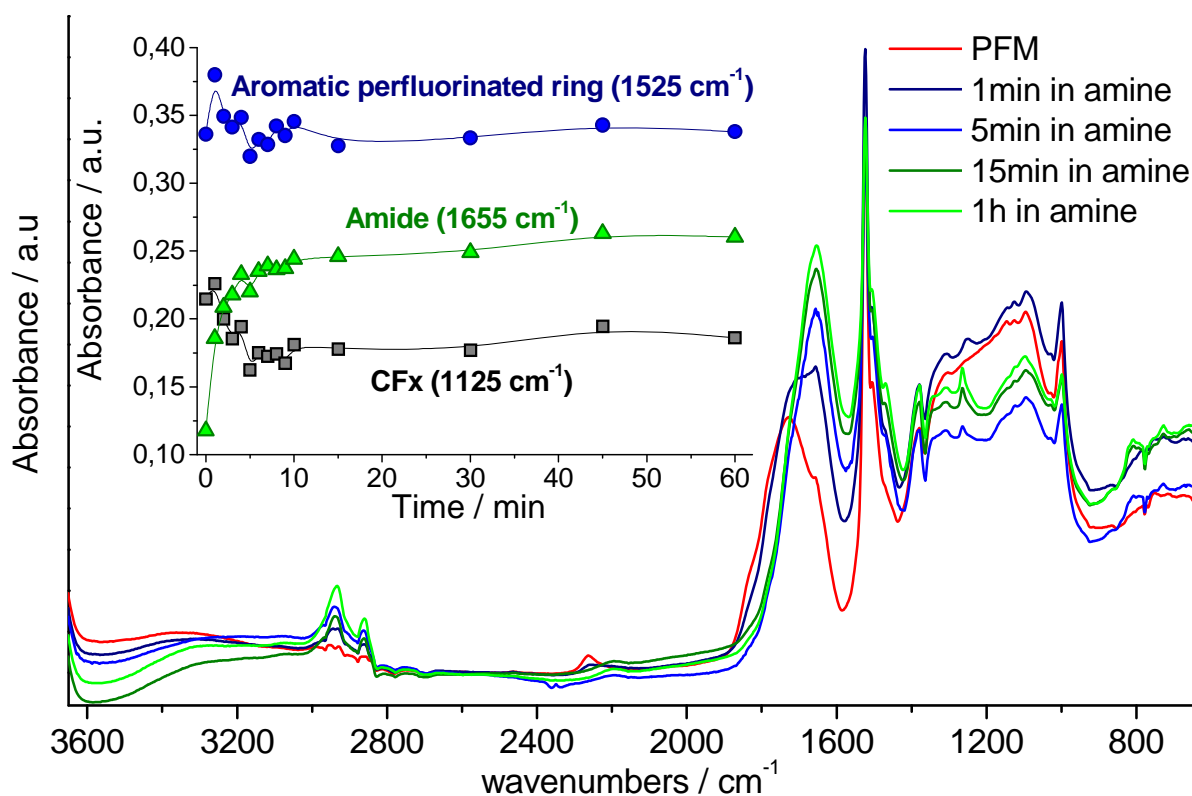


Figure 3.18 FTIR analysis of pp-PFM reacted with amine immediately after deposition

Table 3.11 Static contact angle values after polymer treatment

Sample	Contact angle
PFM	98.6 ± 1.5
after 1h min in PBS	92.5 ± 1.2
after 1h in amine	79.4 ± 1.3

The contact angle values presented in Table 3.11 show how the surface characteristics change as it reacts with the different species. Accordingly to the previous presented data, the PBS treatment showed a small decrease of the on the contact angle, while the reaction with the amine showed a more extended action, as it decreased the angle in around 19° from the original polymer. That indicated that the amine reacted over a higher amount of PFP groups that leave the surface now exhibiting a hydrocarbonated chain or amine.

Experiments at time 30 min

The reaction of the pp-PFM films with the diamine in PBS after immersion in PBS for 30 minutes is shown in Figure 3.19. The solvent has had time to interact with the active ester during the 30 minutes in PBS, like the decrease of ester band at 1730 cm^{-1} shows. But when coming on contact with the amine, the FTIR data suggests a conversion of ester groups to the amide for the duration of the experiment. This is seen as a decrease in the ester band at 1730 cm^{-1} accompanied by an increase in the intensity of the amide band at 1655 cm^{-1} . At the same time, the intensity of the bands associated with the aromatic ring and the C-F bonds also decreased. In comparison to the reaction without prior immersion in PBS (see Figure 3.18) the reaction seems to go slower and there is less formation of amide after the exposure to the amine.

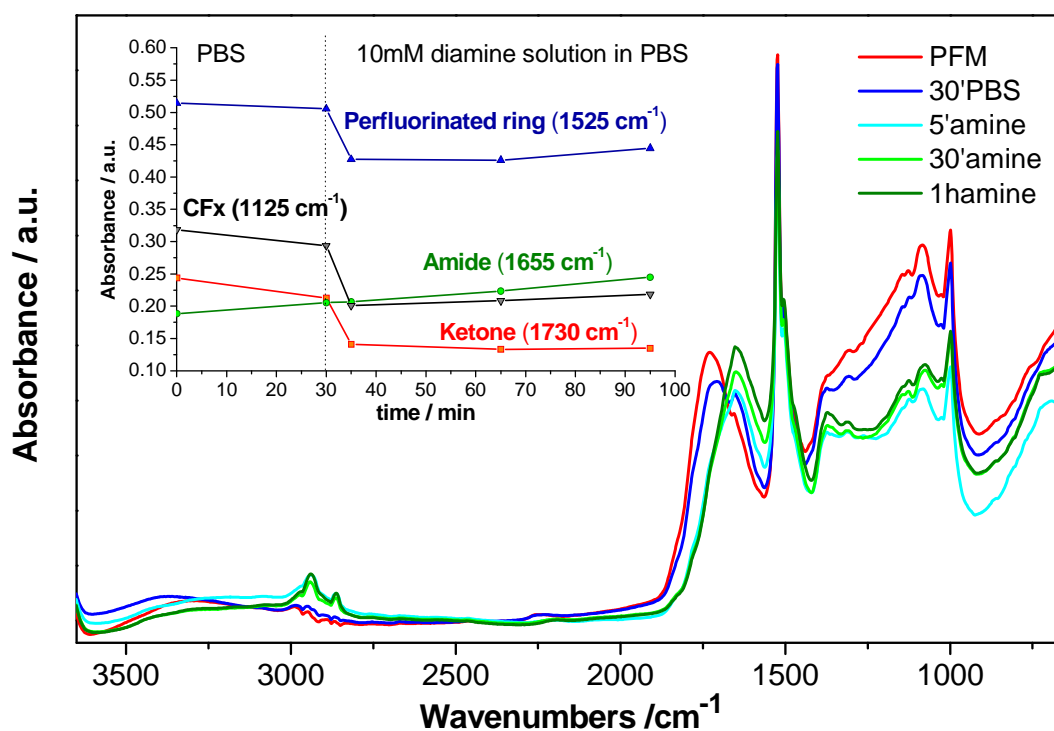


Figure 3.19 FTIR analysis of pp-PFM reacted with amine 30min immersed in PBS

Experiments at time 90 min

The reaction of the pp-PFM films with the diamine in PBS after immersion in PBS for 90 minutes is shown in Figure 3.20. Like in the prior experiment, after exposure to the solvent, the FTIR data suggests a conversion of ester groups to the amide for the duration of the experiment, by the shift of the ester band to the amine zone and the decrease of the C-F bonds. In comparison to the other experiments, the rate of reaction seems to be much slower and the density of amides within the film after 1 hour of reaction was considerably less.

A semi-quantitative consideration of the relative intensities observed for the amide band at 1655 cm^{-1} would suggest the density of amide groups forming is least after 90 minutes of pre-treatment in PBS and highest without any preconditioning in PBS.

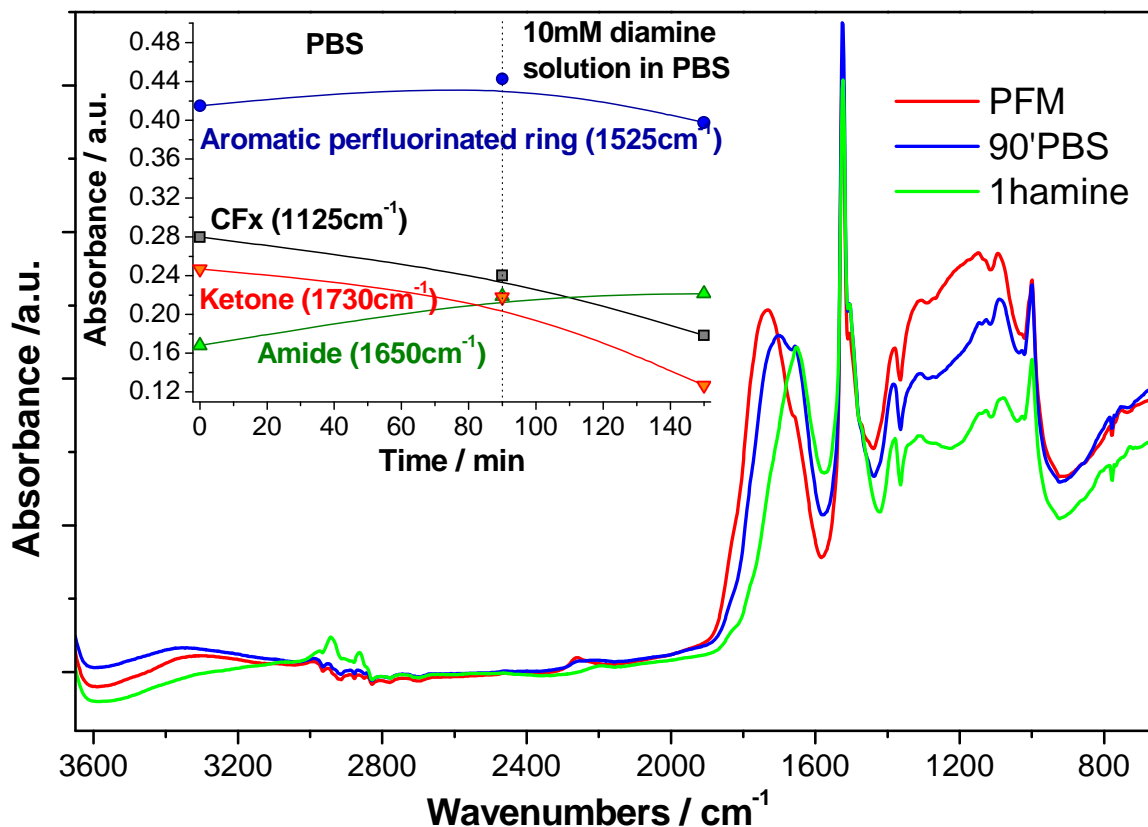


Figure 3.20 FTIR analysis of pp-PFM reacted with amine 90min immersed in PBS

Complementary experiments were done using SPR to follow the reaction of the pp-PFM with the diamine after a short immersion time in PBS. This was done by first exposing the pp-PFM films to PBS for a few minutes to obtain a baseline. The solution in the SPR reaction cell was then exchanged for 10 mM diamino-hexane in PBS, while a kinetic SPR scan was recorded. The initial immersion of the pp-PFM film in PBS solution led to a slow decrease in the resonance, which is due to a number of effects taking place simultaneously that cannot be distinguished in the SPR data. First, as demonstrated in section 3.6.1, the active ester group slowly hydrolyzes in water, leading to some loss of the PFP group, which may or may not be able to desorb from the surface. Second, at low duty cycle plasma deposition conditions, unreacted monomers or dimers may become trapped within the structure and may be slowly released from the film when it is immersed in solution. Third, all polymers swell in aqueous solution, which should result in an increase in film thickness. The overall effect observed in the SPR experiment was merely the sum of these three basic phenomena. Care was taken to include this in the experimental procedure and in the interpretation. A more quantitative evaluation of the data was therefore difficult. The addition of a solution of the amine in PBS led to an increase in the surface

plasmon resonance angle, which could be directly related to the reaction of the amine to the pp-PFM surface (Figure 3.21). After immersion for 10 min, no further significant change was observed in the resonance angle, suggesting that the reaction was complete. This is in agreement with the data observed by FTIR. Rinsing the surface with PBS led to a small decrease in the resonance angle, which may be associated with the loss of physisorbed material from the surface.

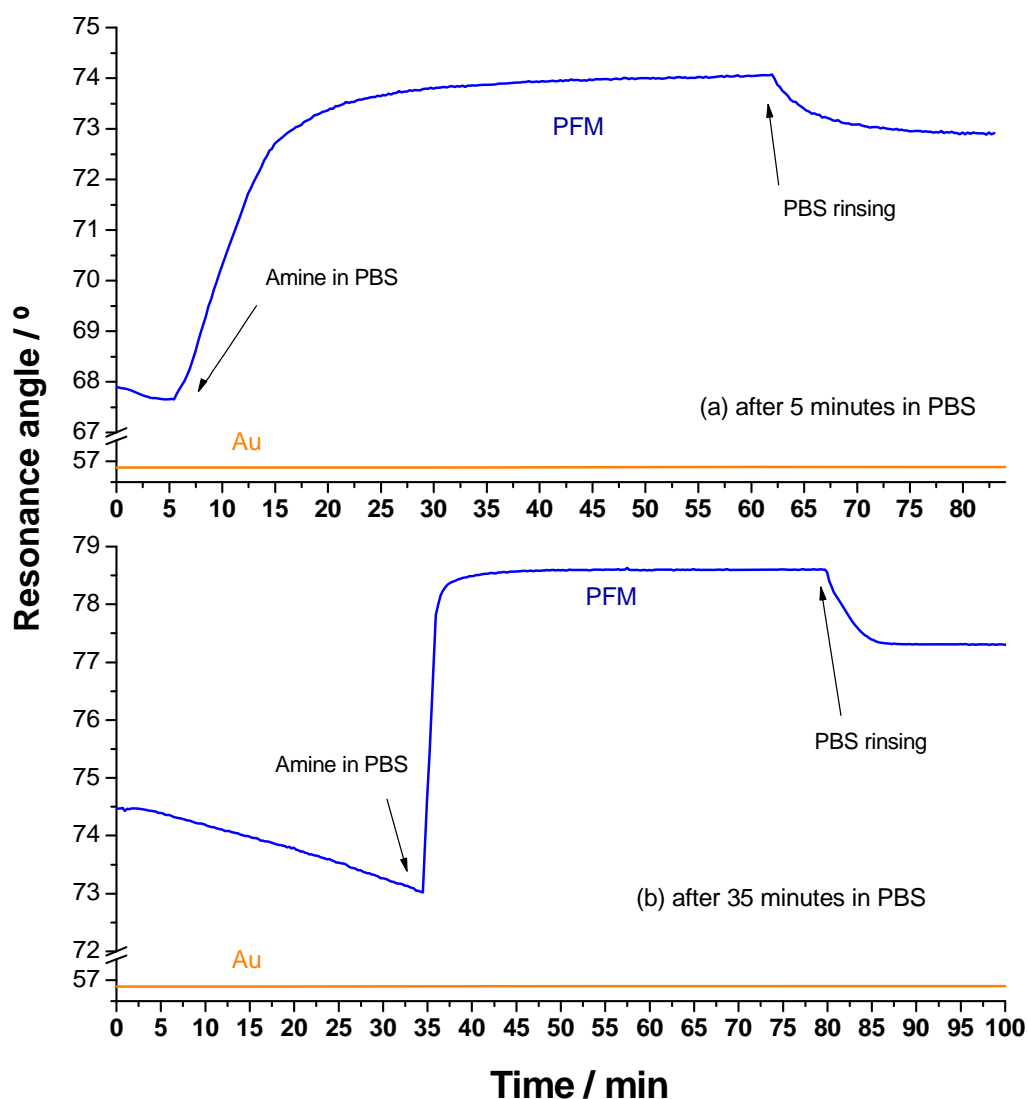


Figure 3.21 Kinetics of the reaction of diaminoethane with pp-PFM (a) right after deposition, (b) after 35min immersion in PBS

After 35 min in PBS, the reaction seems faster than the one done after 5min. This may be due to the loss of material and consequent reaction of PFP groups in inner layers.

The XPS C1s spectra, in Figure 3.22, show the PFM coatings before and after reaction with the diamine. The first one is the PFM polymer after deposition, while (b) and (c) show reacted films. The second curve presents

the film reacted right after deposition with the 10mM diamine solution. The last peak shows the film reacted with the amine solution after prior immersion in PBS during 30 min.

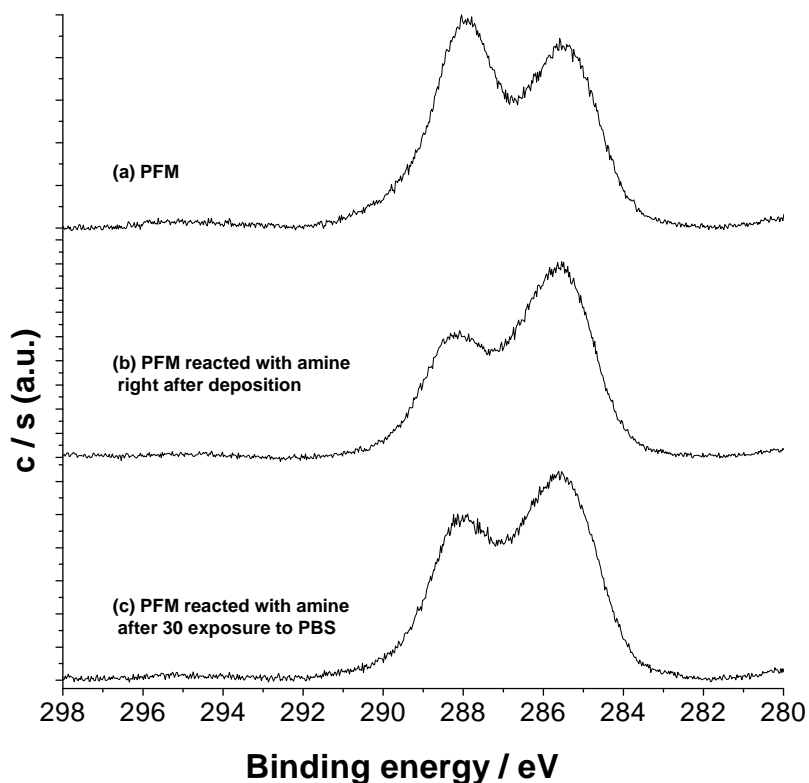


Figure 3.22 XPS spectra showing the chemical structure of reacted PFM

The reacted polymer curves show how the intensity of the high energy peak decreases significantly, indicating a loss of C-F bonds, as the surface comes into contact with the amine. Any changes due to the reaction of the ester to the amide are unfortunately hidden under the tail of the high energy peak at 288.2 eV. Comparing these two peaks it is clear that the reaction goes further in the case of the sample without immersion in PBS. The profile of the curve shows a higher decrease in the C-F bonds. These results support the FTIR observations.

Table 3.12 XPS data of the polymer after reaction with amine

Sample	Atomic percentage				Ratio		
	C1s	O1s	F1s	N1s	F/C	O/C	N/C
PFM	58.97	11.30	27.80	1.94	0.47	0.19	0.03
reacted vs. amine	66.12	10.38	19.20	4.29	0.29	0.16	0.07
reacted after 30 min in PBS	62.50	11.13	22.18	4.19	0.35	0.18	0.07

From the changes in the XPS elemental composition, in Table 3.12, it can be concluded that there is a loss of the fluorinated aromatic ring upon reaction of the pp-PFM with either of the reaction, though the F/C ratio decreases further in the case of the surface non-exposed to PBS. The reaction of the amine led to a loss of oxygen as well as fluorine, accompanied by a gain in nitrogen, which is in agreement with the formation of amide groups. At this point, there was no a clear difference between the N/C ratios of both samples, even if the ratio of the other element showed an obvious variation.

An additional study was done by taking a better look into the XPS data of the experiment of the reaction with amine right after deposition. Further experiments showed a higher degree of reaction for the F/C and N/C ratios, arriving at values of N/C= 0.11.

The results presented in this section make clear that the kinetic of reaction between the active ester group and the amine is much faster than the kinetic of reaction solvent. This is a great advantage to let amino-terminated molecules react in the presence of water, without having to take into account a possible competition between the two species.

A partial deactivation of the surface is to be seen when doing a prior immersion of the film in solvent. Even so, the time to deactivate the surface are so high, that any performance times to get the amine in contact to the surface are much faster, avoiding so any extended deactivation of the reactive sites.

Further studies of the reaction with amines, to try to understand completely how the polymer is responding, were performed with the help of the microcantilever sensors technology. The results obtained will be presented in Chapter 4.

3.5.3 SURFACE REACTIVITY WITH THE PEPTIDE (CYS0) - LAMININ A (2091-2108)

After seeing that a reaction of amines on the surface is possible and measurable, the binding of a peptide to the film was investigated.

The peptide used in this work was (Cys0) - Laminin A (2091-2108). This peptide is a synthetic short peptide chain based on laminin. Laminin is a multiadherent protein present in the extracellular matrix (see Figure 3.23). It has binding sites with a high affinity for cellular adhesion molecules present on the surface of many cells.³⁴

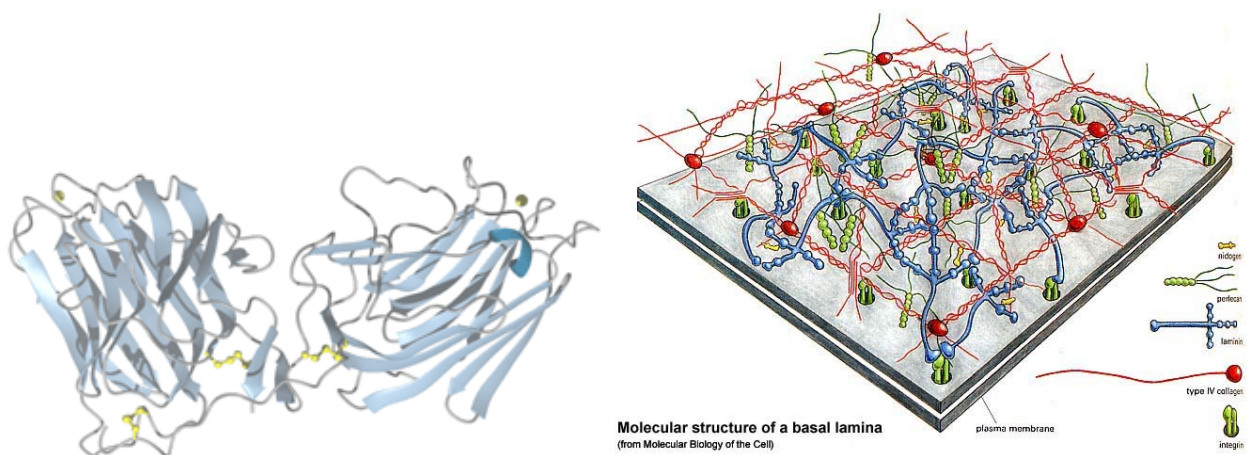


Figure 3.23 Structure of laminin and its distribution in the ECM within the basal lamina (laminin represented in blue)^{35,36}

(Cys0) - Laminin A (2091-2108) is a chain synthetic peptide from the long arm of the laminin A chain is capable of stimulating neuronal-like process formation to almost the same extent as laminin and competes with laminin for stimulation of neurite outgrowth.^{37,38}

This peptide is composed by the subsequent chain of 19 aminoacids (CSRARKQAASIKVAVSADR):

Cysteine – Serine – Arginine – Alanine – Arginine – Lysine – Glutamine – Alanine - Alanine – Serine –
Isoleucine – Lysine – Valine – Alanine – Valine – Serine – Alanine -Aspartic acid – Arginine

Its primary structure is displayed in Figure 3.24 (see next page). Just looking at the primary structure, eight primary amines can be seen; therefore eight potential binding sites to the PFP active sites on the surface are present in this molecule. Many of these sites are possible hidden in the tertiary structure of the peptide, but others may be exposed to the surface and react with the active groups, binding covalently to the surface.

Another interesting character of this peptide is the content of a sulfur atom, which will be easily recognized by the XPS analysis.

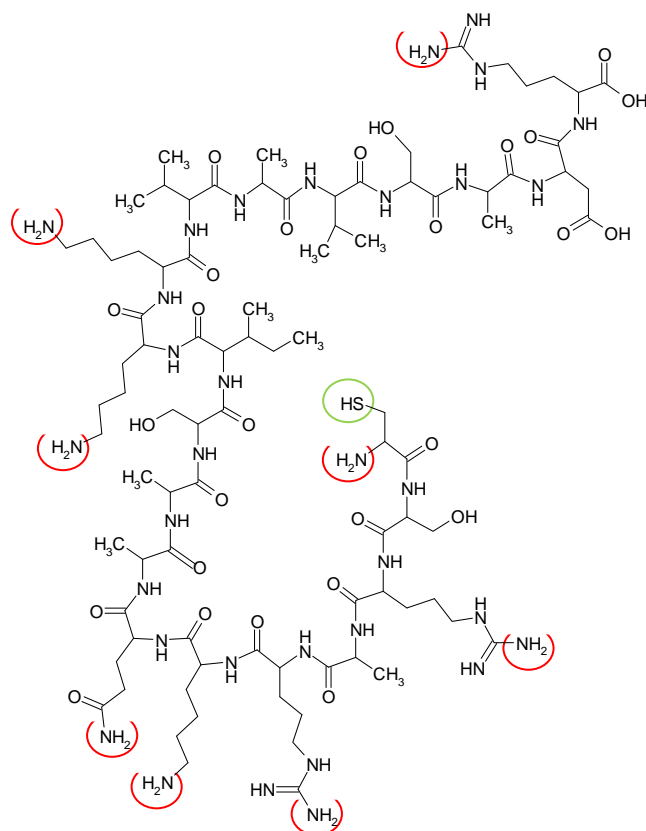


Figure 3.24 Chemical structure of (Cys0) - Laminin A (2091-2108)

Figure 3.25 presents the FTIR and XPS spectra of the surfaces before and after reaction. The FTIR data did not show a clear binding of the peptide to the polymer, even though a slight change in the ketone peak moving to lower wavenumbers was observed.

The XPS data shows the binding of the peptide through the C-F peak of the reacted surface. This peak decreases in comparison to the pp-PFM, as the π - π^* *shake-up* satellite peak corresponding to the ring disappears, showing a loss of the perfluorinated phenyl ring.

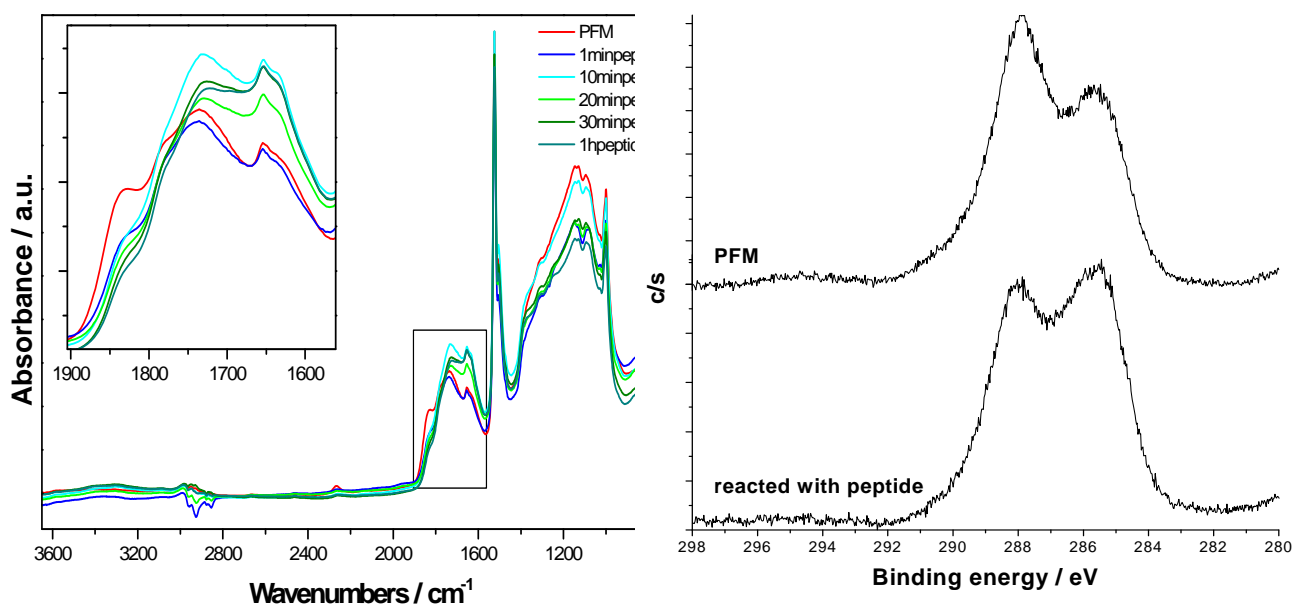


Figure 3.25 FTIR and XPS analysis of pp-PFM reacted with peptide immediately after deposition

The XPS data of the atomic percentage corresponding to the polymer and the polymer reacted with peptide presented in Table 3.13 show an evident difference between the two samples. The F/C ratio decreases dramatically as the N/C increases when reacting the peptide to the PFM surface. There is a rising in the O/C also, easy to explain by the big amount of oxygen contained in the peptide's structure. Also a small presence of sulfur can be seen on the reacted surface, which indicates without a doubt the presence of the peptide.

Table 3.13 XPS data of the polymer after reaction with peptide

Sample	Atomic percentage					Ratio		
	C1s	O1s	F1s	N1s	S2p	F/C	O/C	N/C
PFM	59.18	10.09	28.96	1.77	-	0.49	0.17	0.03
reacted vs. peptide	62.12	14.90	14.24	8.56	0.18	0.23	0.24	0.14

The XPS spectra prove the reaction of the peptide with the polymer. The presence of Tween 20 in the solution discards possible undesired adhesion of the molecule to the surface, elucidating the covalent binding of the peptide to the polymer.

3.5.4 REPRODUCIBILITY FOR POLYMER IN SYSTEM 2

In the previous sections it was determined that the plasma polymerized film of PFM in the first system was able to react with amines and peptides. The desired structure of the polymer was also achieved in a second system. In this section, the reactivity of this film will be checked, in order to determine if the reaction with the desired substances is the same as in polymer of the first system.

Effect of the solvent

Once more, the reactivity of the polymer synthesized in *system 2* was tested in the solvent (PBS) before going to the reactivity of amines or peptides. In a series of experiments, the effect on the polymer after immersion in PBS solution was studied. The samples were placed in contact with the solution immediately after deposition in the plasma chamber. It was only possible to follow the reactions off-line, with XPS and ToF-SIMS analyses.

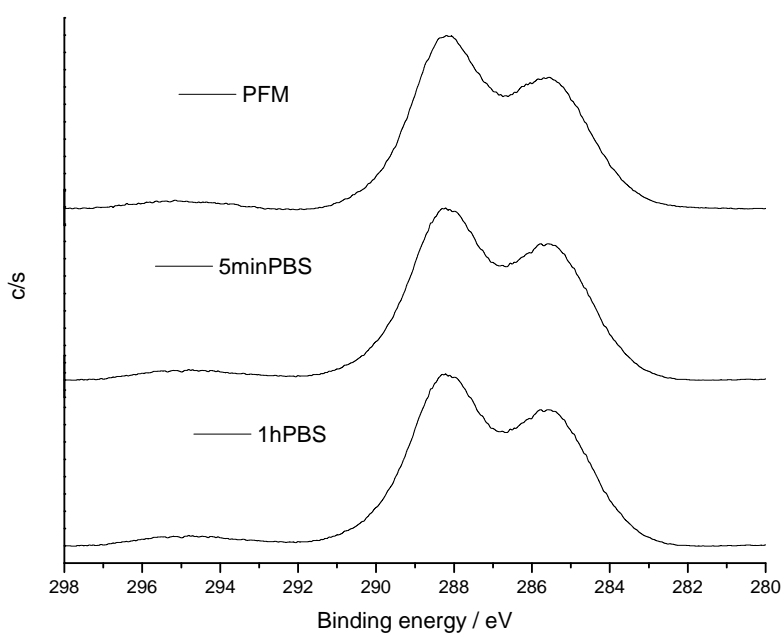


Table 3.14 XPS data of the polymer of *system 2* after immersion in PBS

Sample	Ratio	
	F/C	O/C
PFM	0.52	0.18
+ 5 min in PBS	0.49	0.19
+ 60 min in PBS	0.37	0.21
Theoretical values	0.5	0.2

Figure 3.26 XPS Kinetic study of the different elemental ratios for pp-PFM reacted with diamine right after deposition

Figure 3.26 and Table 3.14 present a comparison between the XPS data before and after exposure to a PBS solution. Any changes in C-O group are very hard to identify, due to the position of the peaks. This is positioned at 286.2 eV (see Figure 3.8 and related table 3.5), making any alteration in the peak area impossible to identify. The data presented in table 3.14 shows how the F/C ratio decreases, while the O/C ratio shows a small increase. These results are comparable with the ones obtained with the polymer from

system 1, even though the films obtained in *system 2* seem to present higher stability against the solvent than the ones from *system 1*.

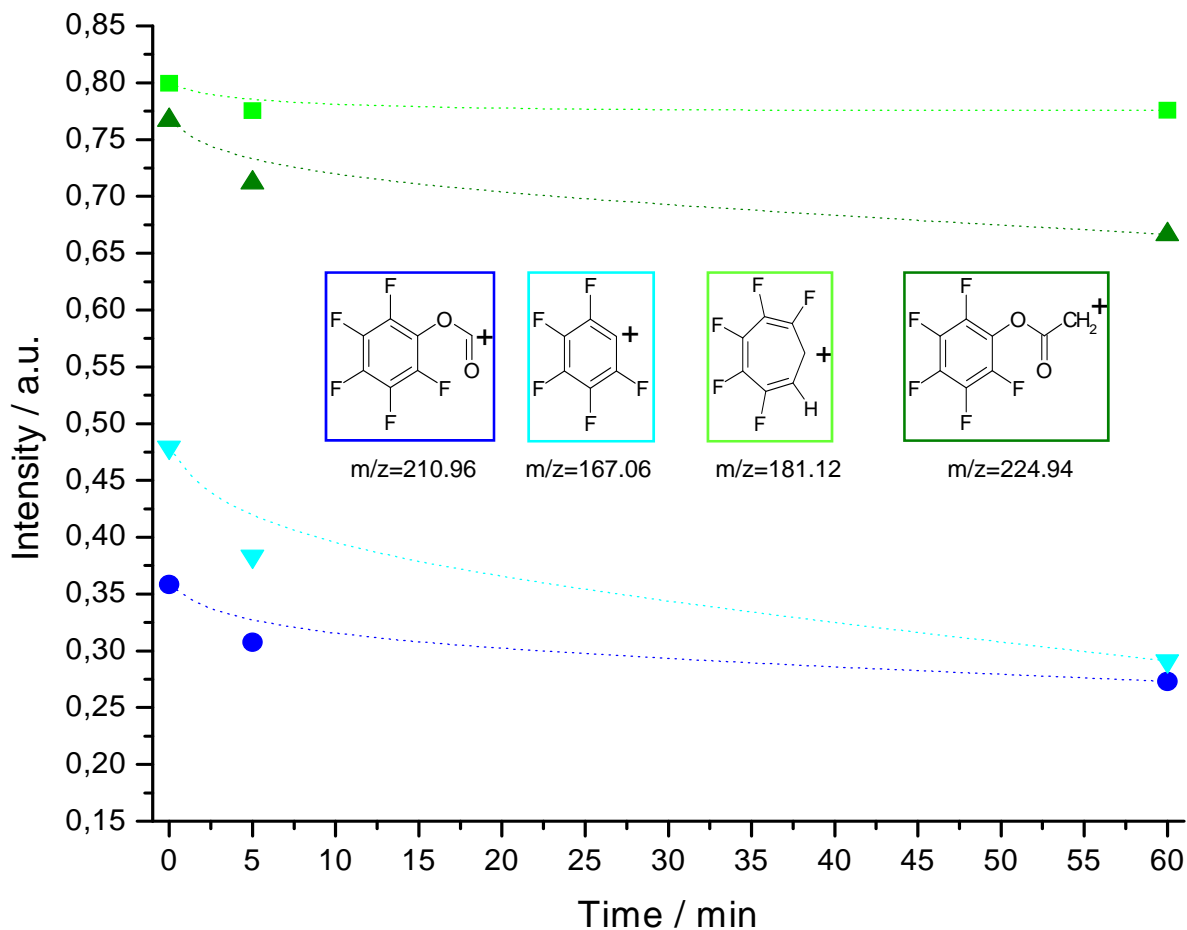


Figure 3.27 ToF-SIMS Kinetic of immersion in PBS

Figure 3.27 presents the kinetic profile of the ToF-SIMS analyses of the immersion of the pp-PFM in PBS, concentrating only in the previous presented groups of interest (see section 3.4.2). The masses of interest are the ones that were lost after reaction through the ester bond.

The kinetic profile shows that there is a small loss of the characteristic groups showing the pentafluorophenyl structure on the surface. After the exposure of the samples during one hour to the solvent, the groups are still to be seen in a similar amount than before the exposure. The ToF-SIMS results support the previous presented XPS analyses.

Experiments with 1,6-diaminohexane

Once the stability was verified, the reactivity of the active ester towards a simple diamine, 1,6-diaminohexane, was studied.

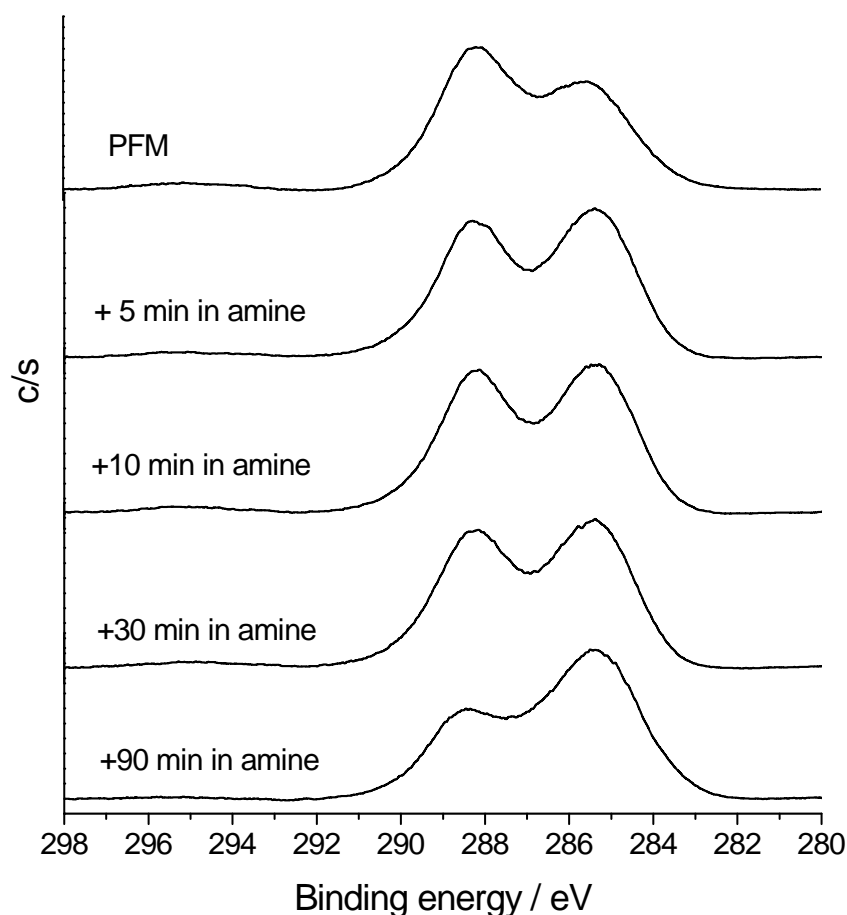


Table 3.15 XPS data of the polymer of system 2 after reaction with amine

Sample	Ratio		
	F/C	O/C	N/C
PFM	0.52	0.18	-
+ 5 min in amine	0.38	0.21	0.02
+ 10 min in amine	0.39	0.20	0.03
+ 30 min in amine	0.39	0.20	0.03
+ 90 min in amine	0.25	0.26	0.05

Figure 3.28 XPS spectra showing the chemical structure of (a) pp-PFM, reacted with 10 mM diamino-hexane (b) for 20 min and (c) 90 min

The XPS C1s spectra, in Figure 3.28, show the PFM coatings before and after reaction with the diamine. The first peak represents the C1s narrow scan of the PFM polymer after deposition, while the other curves present the reacted films after different times of exposure to a 10 mM diamine solution in PBS.

As the reactivity showed for polymer developed in *system 1*, the pp-PFM coming from the *system 2* presents a decrease of the high energy component, indicating the loss of C-F bonds, as the samples are exposed to the amine solution. The results of the XPS elemental ratios, in Table 3.15, indicate a loss of fluorine, higher than in the case of immersion in PBS. The nitrogen content increases at the same time.

Figure 3.29 presents a ToF-SIMS kinetic study of the same reaction. The monitoring of the representative peaks for the pentafluorophenyl functionality show an obvious decrease with time of exposure to the amine

solution. In comparison to the PBS kinetic, the change in the surface structures is much more evident as a rapid loss of the characteristic groups was observed, showing a faster kinetic.

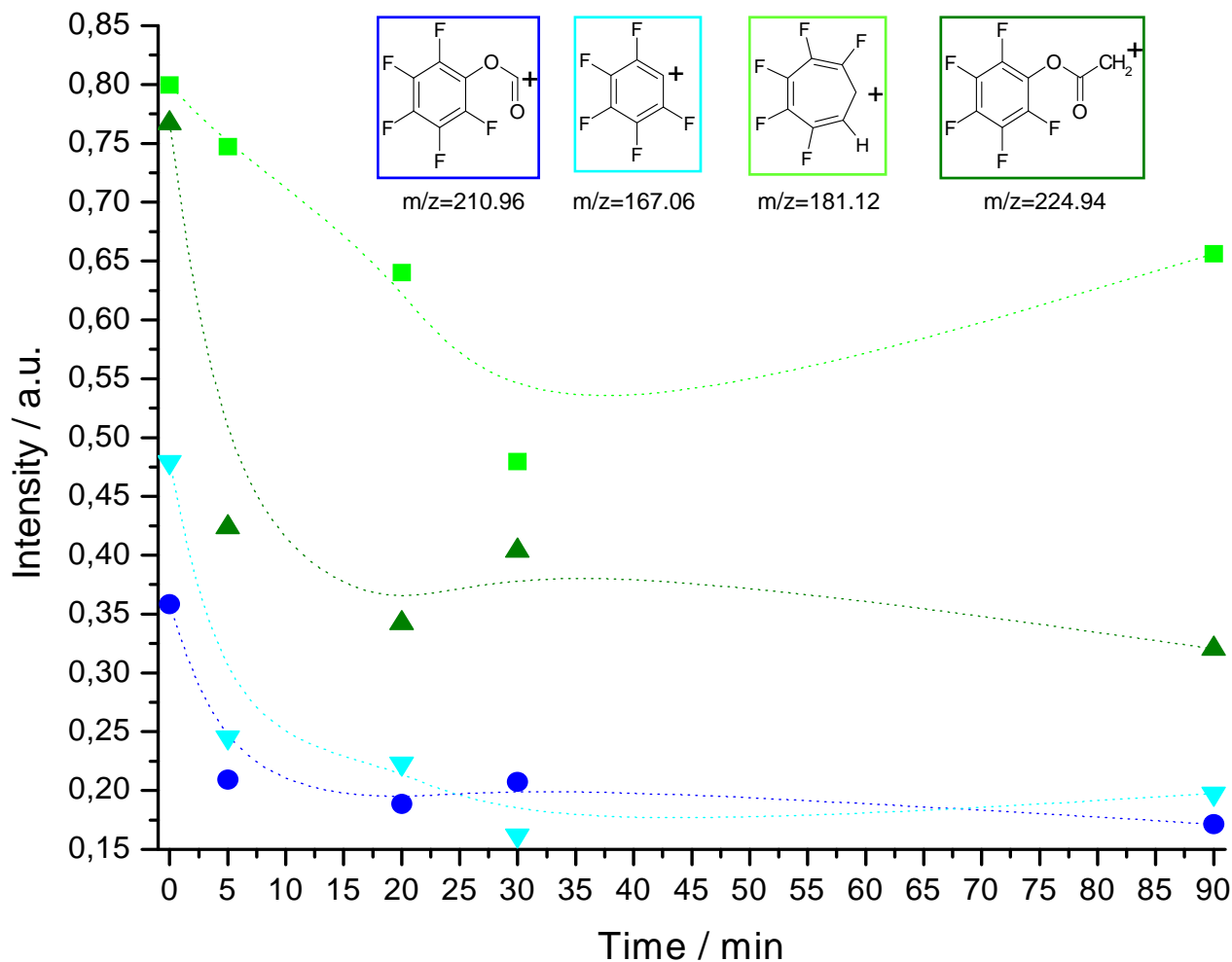


Figure 3.29 ToF-SIMS Kinetic of reaction with amine

The peak at $m/z=181.12$ presents a different profile than the other one, showing an increase of this group after 90 min in solution. The other groups show a kinetic profile similar to the ones presented in Figure 3.18. The time scale in both cases show a fast reaction for the initial minutes, while the reaction slows down until stability after 20 min exposure.

This study reflects that the reproducibility of the polymer was achieved on the polymer's chemical structure, and also in its reactivity, as expected. The kinetic of reaction of the amino terminated molecules is much faster than the kinetic if reaction of the solvent. This is a great advantage for the functionalization of the surface with amino-terminated molecules in water, without any remarkable competition between the molecule of interest and the solvent.

Experiments with peptide

The binding of a peptide to the surface was tested. The peptide used is (Cys0) – Laminin A (2091-2108), described in section 3.5.3.

Figure 3.30 presents the C1s narrow scans of pp-PFM films before and after reaction with the peptide solution at different times.

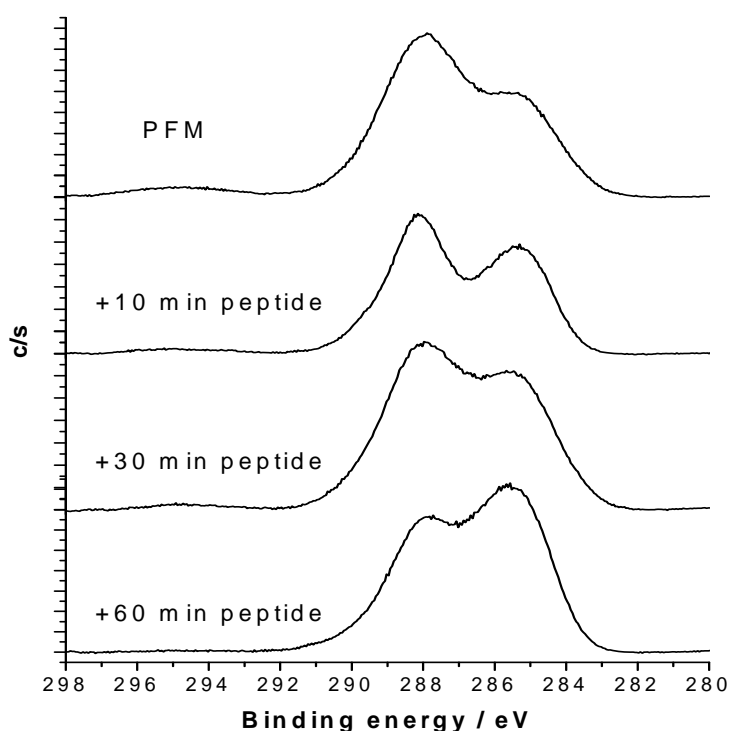


Table 3.16 XPS data of the polymer of system 2 after reaction with peptide

Sample	Ratio			
	F/C	O/C	N/C	S2p
PFM	0.56	0.19	0.02	-
+ 10 min in peptide	0.39	0.29	0.09	0.24
+ 30 min in peptide	0.37	0.27	0.10	0.23
+ 60 min in peptide	0.18	0.30	0.17	0.22

Figure 3.30 XPS spectra showing the chemical structure of C1s scans of PFM and PFM reacted with peptide at different times

The XPS profiles show a loss of the C-F groups with time. On the other hand, by taking a look into the atomic ratios, it can be observed how the nitrogen content rises as the sample reacts with the peptide. A presence of sulfur can be tracked, indicating the presence of the peptide on the surface. The combination of nitrogen and sulfur prove the presence of the peptide on the surface.

The ToF-SIMS kinetic profile presented in Figure 3.31 shows a kinetic of reaction with a fast change in the first minutes. Similar results are achieved when working with the amine, as presented above, although in the case of working with the peptide, the curves show a less stable profile, but with the same results. In comparison to the samples from system 1, where the kinetic profile of reaction between the peptide and the polymer was

impossible to be tracked by FTIR analyses, in this case, the ToF-SIMS analyses show a better sensibility to the reaction, even when this happens just on the outermost layer of the film.

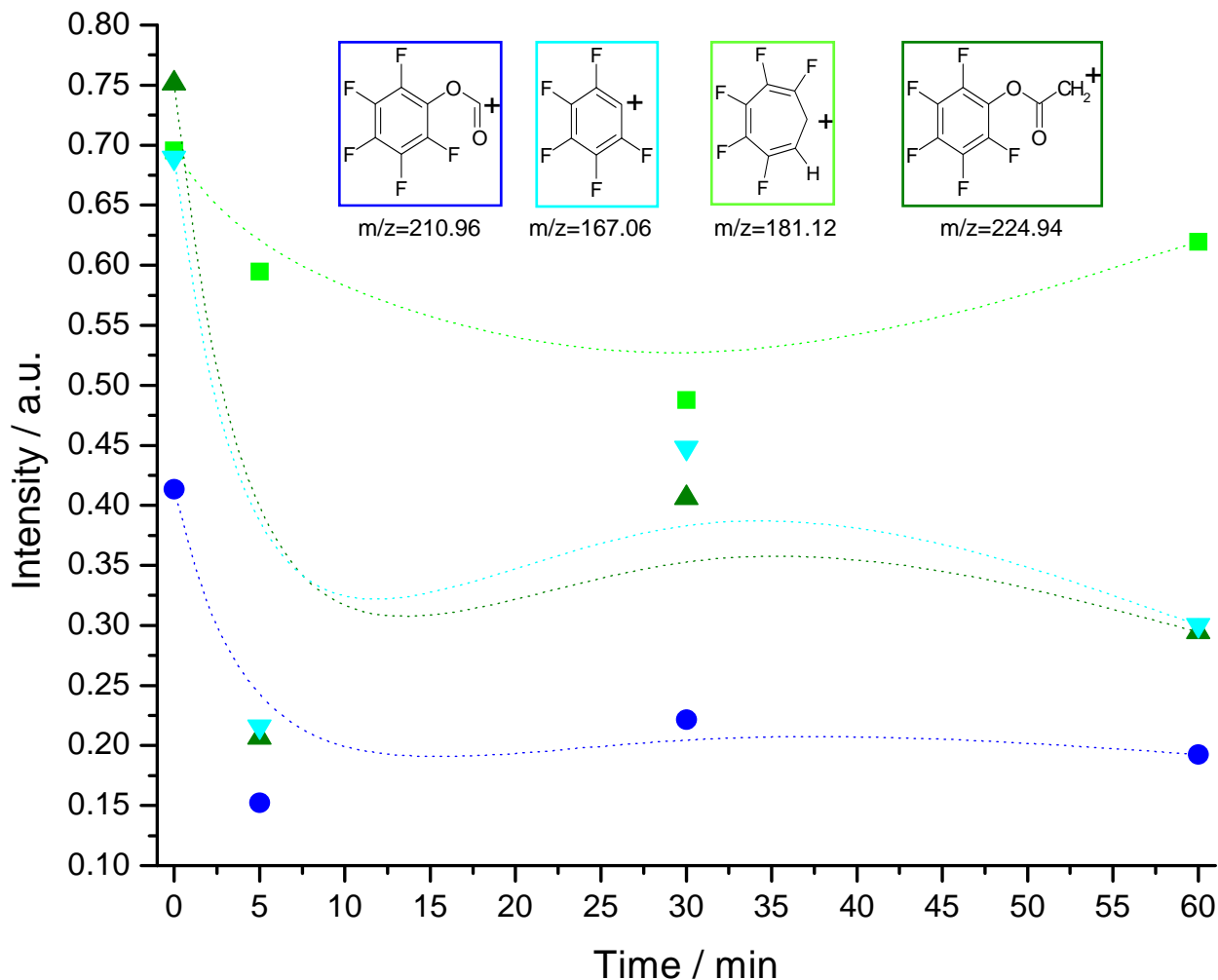


Figure 3.31 ToF-SIMS Kinetic of reaction with peptide

These experiments have shown that the binding reaction with peptide was also equally successful with the polymer obtained in *system 2*.

In this section, the reproducibility of the reaction on this second polymer has been achieved, showing the independency of the reactor, when studying the deposition's parameters.

3.5.5 SUMMARY

The work presented in this section centers over the reactivity of the pp-PFM against different species.

The first big question answered was the fact of the reactivity of the ester group against the solvent, the 0.01 M PBS solution, i.e. water. It has been shown that the reaction was not as fast as that expected from the theoretical point of view, possibly leaving an amount of reactive groups on the surface to be able to link other molecules.

When making the solvent compete with a simple amine, the kinetic of reaction between the active ester group and the amine was much faster than the kinetic of reaction in front of the solvent. This was a great advantage to let amino-terminated molecules to react in the presence of water, without having to take into account a possible competition between the two species.

A partial deactivation of the surface was to be seen when doing a prior immersion of the film in the solvent. Even so, the times for a deactivation are high enough, that the times required for the amine to react with the surface are much faster. Binding of a peptide to the surface was achieved.

The reactivity profile of the pp-PFM polymer was independent of the system where the polymer was deposited. As long as the chemical structure of the polymers obtained in both systems resemble, the reactivity shown is the same, even matching in the time scale. This is an important point, as it contributes to a certain independency to the reactor for depositing the pp-PFM polymer, always achieving the same kind of covalent binding with the molecules of interest.

3.6 CELL CULTURE

The differentiation and morphogenesis of neural tissues is highly affected by the diverse interaction between neural cells and the surrounding ECM.³⁹ The adhesion of neural cells to ECM molecules is mediated by the interaction between cell binding domains in ECM and cell surface receptors. This can control neural cell morphogenesis. An active promoter of neural cell attachment and differentiation is laminin⁴⁰, especially the IKVAV domain present in the alpha chain.³⁸

In this section, an approach to cell culture was developed for the pp-PFM polymer reacted with the (Cys0) - Laminin A (2091-2108).

3.6.1 STABILITY OF THE FILM AGAINST DIFFERENT STERILIZATION TECHNIQUES

The polymer that was developed in the previous section should serve as a platform for cell binding and proliferation. Therefore, it was important to test the stability of the polymer in front of different sterilization techniques, as it was needed a sterile polymer to be used for cell culture. This section concentrates in this issue.

Taking a look at the structure of the polymer and its labile group, the most conventional sterilization methods turn out to be a problem. The work with an autoclave, under conditions of moist heat, would deactivate all the linking sites. For that reason this technique was rejected.

70% Ethanol is one of the most common ways to sterilize substrates before working with them. Exposing the polymer to ethanol was impossible, by the fact that it dissolved the plasma polymer.

Another common process is exposure of the substrates to UV light. This method was investigated by FTIR analysis to see if the structure of the polymer is able to resist the treatment.

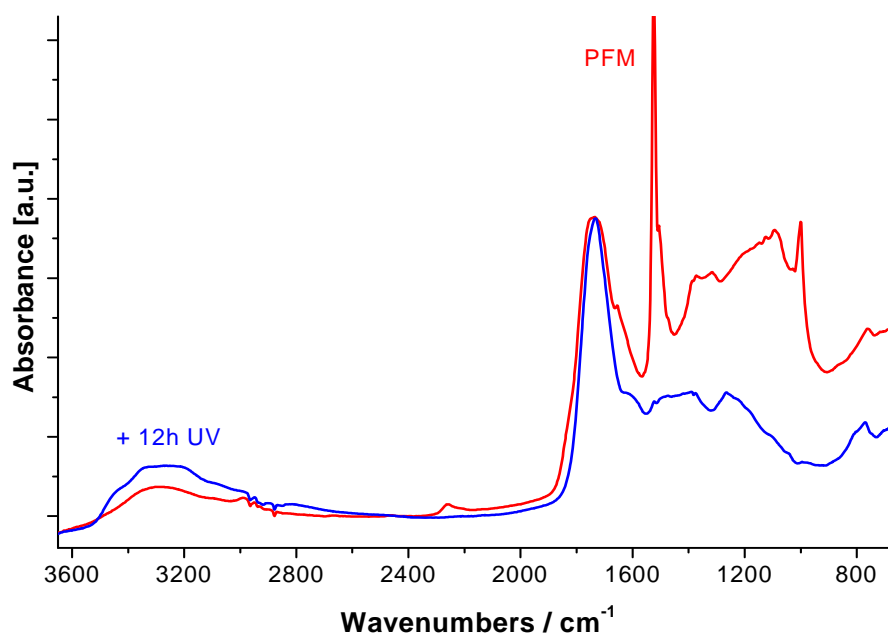


Figure 3.32 FTIR analysis of pp-PFM exposed during 12 h to UV radiation

Figure 3.32 presents the FTIR spectra of the pp-PFM prior and after exposure to 12 h of UV-light. By comparing the two spectra, it is obvious that the exposed polymer lost the labile group containing the C-F_x and the ring bands under 1600 cm⁻¹. As the other techniques, the UV-light exposure of the polymer destroys its reactivity. Therefore it is not possible to use this sterilization method either.

As an alternative, plasma exposure is proposed as sterilization technique. The samples can be sterilized prior to polymerization, and then be isolated in an argon atmosphere. Further treatments can be done in a laminar flow fume hood, avoiding contamination.

Plasma sterilization mechanisms are based on synergistic effect of etching by direct plasma exposure and UV radiation, depending on the plasma parameters, having been proved to be microbiologically safe, not only killing virus and bacteria, but also removing them from the system, as it works in a similar way than plasma etching.⁴¹ These have to be chosen in a compromise between plasma efficiency for sterilization and damage of the samples.⁴²⁻⁴⁴

Based on the group's experience, samples were exposed to an Ar/O₂ plasma (90/10) for 10 min. In this case the substrates were polystyrene dishes. The power was fixed at 50W in continuous wave.

After sterilization, polymerization was performed directly on the samples, without removing them from the reactor chamber or breaking the vacuum. Once the polymer was formed, the samples were stored under Argon atmosphere as explained above. Experience showed that they were maintained sterile up to four weeks.

3.6.2 QUALITATIVE ANALYSIS OF CELL CULTURE STUDY ON PLASMA POLYMERIZED SURFACE

The behavior of the P19 embryonic carcinoma derived neurons was analyzed in this section. The morphology of these kinds of cells, before differentiation is presented in Figure 3.33, from the ATCC Cell Biology Collection, which is the most comprehensive and diverse of its kind in the world, consisting of over 3,600 cell lines from over 80 different species.⁴⁵

Figure 3.33 will help us as reference to understand if our samples are developing correctly, in the first days. It shows attached P19 cells, although it must be remarked that they are not derived neurons.

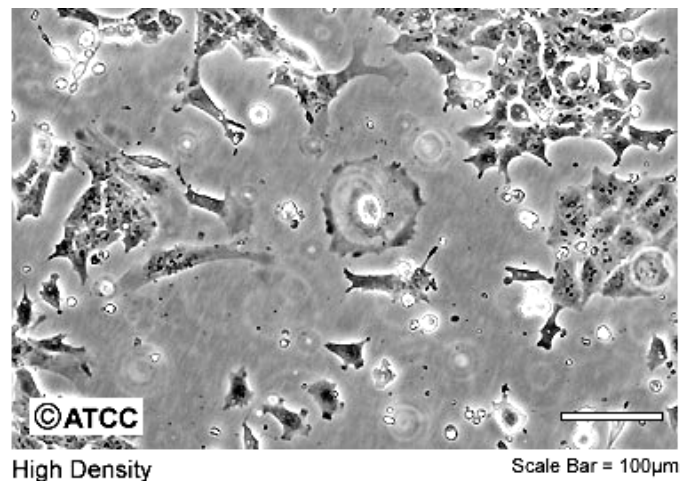


Figure 3.33 P19 non differentiated cells from the ATCC collection

For these experiments, the Petri dishes were prepared as described before in section 3.2, to do the cells seeding. The following pictures in Figures 3.34 – 3.37 show the cell behavior on the different surfaces. Pictures were taking at different days, to see how the cells were developing in time over the different stages.

Cell attachment (Day 1)

As Figure 3.34 P19 neurons (P19N) were attached to all the surfaces. They formed larger cell colonies on the P/LC surface, i.e. dish with PFM polymer reacted with the (Cys0) - Laminin A solution. The colonies had on average more than 30 cells each and some of them consist of more than 1 cell layer. Dishes with the PFM polymer but without being reacted with the laminin, P/NLC surface, has small colonies consisting of multi cell layers attached. The reference samples without polymer and with or without laminin have small colonies attached. Short neurite extensions were observed on all surfaces.

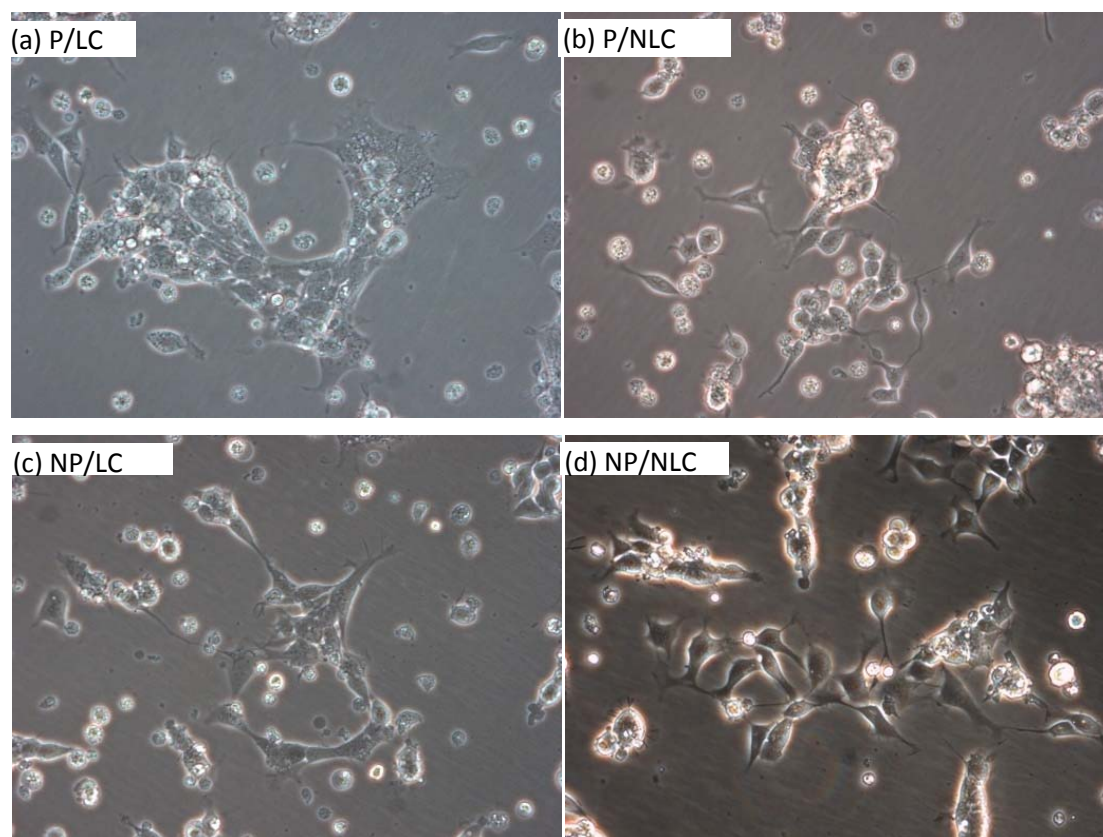


Figure 3.34 Cells after 1 day culture (20x). Attachment phase. (a) with PFM polymer and reacted with laminin (P/LC), (b) with PFM polymer without laminin coating (P/NLC), and reference samples (c) without PFM polymer and with laminin coating (NP/LC) and (d) without PFM polymer or laminin coating (NP/NLC)

P19N proliferation and neurite formation

Figure 3.35 presents the growing of the cells in all samples after three days in culture. Large necrotic cell aggregates were observed on the P/NLC (see Figure 3.35b). The polymerized surface alone was unable to support P19N proliferation and neurite formation. All other three surfaces, including the reference surfaces and the polymerized laminin coated sample, were able to support the growth of neuronal progenitors, an increased in neurite formation was observed for all three samples by the third day. Samples seem close to each other.

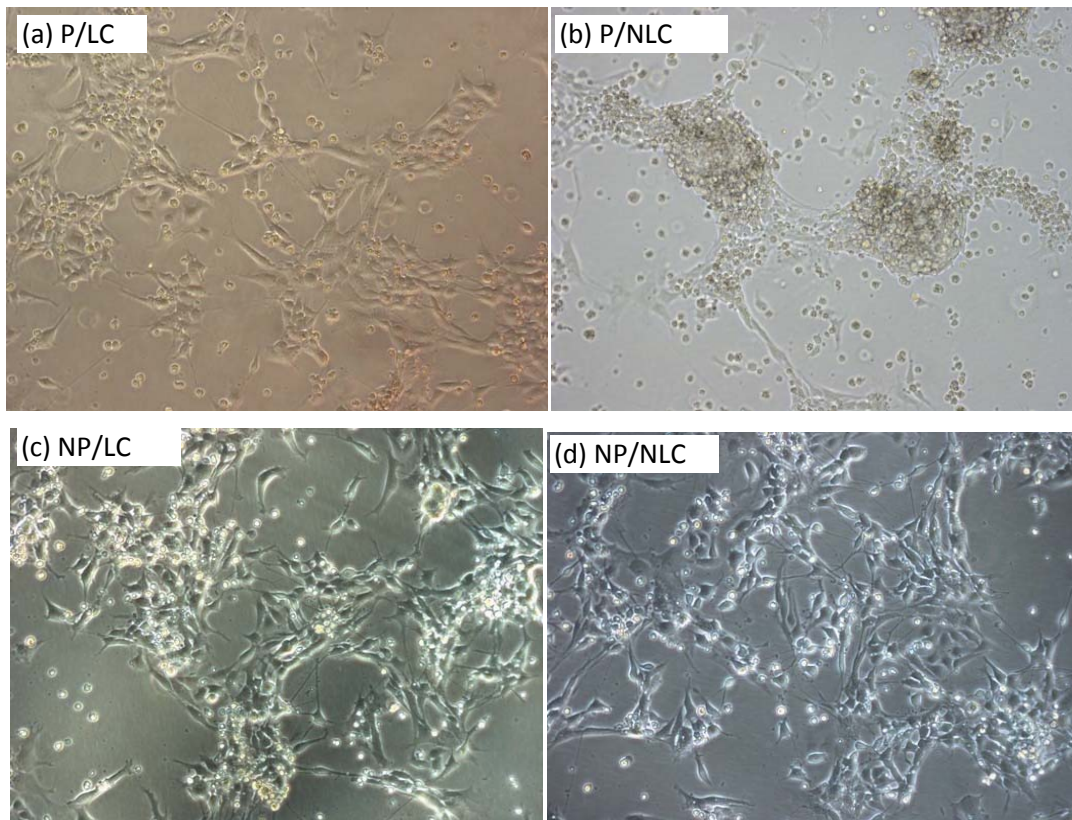


Figure 3.35 Cells after 3 days culture (10x). Proliferation phase

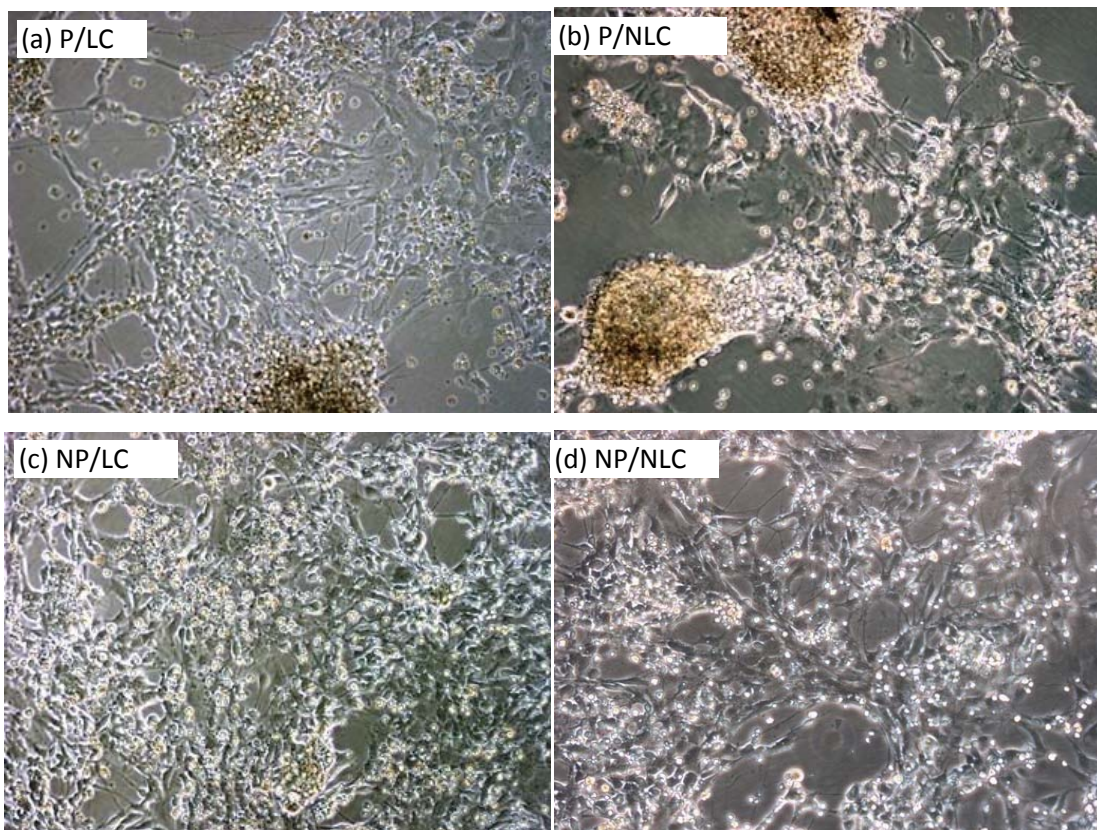


Figure 3.36 Cells after 6 days culture (10x). Proliferation phase

Figure 3.36 shows the cell cultures after six days. In the reference sample NP/LC, by the sixth day, there is a monolayer of P19N growing on a homogenous underlying layer of non-neuronal cells which increased in density until the end of the study (13 days, see Figure 3.37) on the substrates. P19N were able to form close connecting neurites with one another, which is an indication of synaptogenesis, on these substrates, NP/LC dishes.

Less extensive neurites were formed by the end of the 6th day on both P/LC and NP/NLC surfaces. Even so, the cells are still forming neurites.

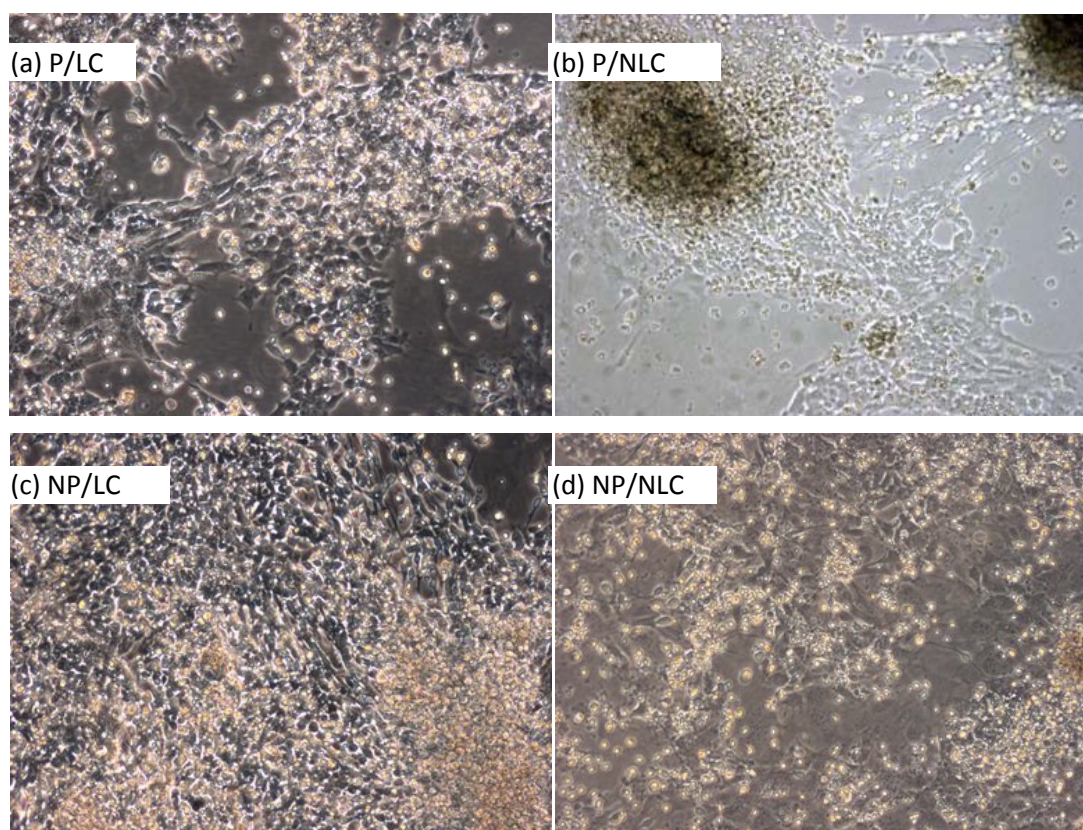


Figure 3.37 Cells after 13 days culture (10x). Proliferation phase. Proliferation phase. (a) P/LC, (b) P/NLC, and reference samples (c) NP/LC and (d) NP/NLC

Taking a look at the pictures presented in Figure 3.37, For P/NLC there was widespread proliferation of flat non-neuronal cells by day 13 in vitro.

NP/NLC (in fig 3.37 d) surfaces were not able to support further neurite formation by the 13th day, with a sparse population of P19N growing on a monolayer of flattened non-neuronal cells. After 13th days of culture, the developing of the neurons on the P/LC samples seemed to be reactivated and scattered pockets of P19N were found growing on an underlying layer of non-neuronal cells on the P/LC surface even on the 13th day of culture.

The reference (non polymerized laminin coated sample, fig 3.37 c) showed the best results on neuron growth and formation of close neurite, as expected. The other reference sample, non polymerized and non laminin coated showed the expected results as well, as the neurite formation is impossible. Comparing these reference samples to the ones with polymer, the evidence of cells dying on the non laminin coated dish, made clear that the direct exposure of the cells to the polymer killed them, showing the poisoning effect of the chemistry on the surface, probably due to the presence of the fluorine containing groups in the polymer. On the other side, the polymerized and laminin coated surface showed to be a viable surface for cell culture, even if the growth was slower as in the reference samples.

For additional information about the cells growth and behavior on the surfaces, further tests should be done. In future works, it could be tested if the cell retain the own characteristics, by checking if they still express their characteristic proteins. Another interesting study would be their growing curve. Some other tests could be done, always trying to determine if the cells still feel comfortable on the treated surface for further applications.

3.6.3 SUMMARY

Using the results of the reactivity study in the previous section, a new protocol for sample preparation has been developed in this part of the work, to be completed with cells seeding and culture on modified substrates.

Common techniques to sterilize the substrates have demonstrated the deactivation of the reactive sites or total destruction of the PFM polymer. Therefore, a sterilization method based on plasma techniques has been exposed as a promising way to sterilize the substrates and deposit the polymer directly on them, without exposure to the air.

After the treatment of the modified surfaces with the peptide, (Cys0) – Laminin A, they were used for cell seeding. The sample of interest shows its viability for the growing of neurons that lived upon to 13 days on the surface. At this point, the test was stopped.

Cells exposed to the polymer directly, without the laminin coating, died after several days.

The order of good neuron propagation was the following:

$$P/NLC < NP/NLC < P/LC < NP/LC$$

The fact that cells, in this case neurons, are able to grow on top of the polymerized surface after covalent peptide attaching shows a promising platform for cell-substrate interaction.

3.7 CONCLUDING REMARKS

This chapter presents the development of the pentafluorophenyl methacrylate films by polymerization techniques.

It has been shown that even monomers containing reactive groups, such as pentafluorophenyl methacrylate, can be polymerized with high functional group retention using pulsed plasma deposition conditions. Depending on the system used polymerization parameters have been fixed, obtaining good group retention. In the case of *system 1*, a maximum retention of the desired structure has been achieved by working at 50W with a duty cycle fixed at 2/52. The electrode's distance was fixed at 13 cm. In *system 2*, the parameters have been fixed at 50W with a duty cycle at 10/100, and the sample position has been revealed as a key factor to get a good structural retention.

The surfaces of the deposits are highly reactive and react readily in aqueous solution and with primary amines. It has been shown, that the reaction with aqueous buffer is much slower than that with primary amines. Thus, the reaction between an amine terminated reagent and the ester groups will always dominate reaction pathways in a solvent environment. It has been further shown, that the reactivity of the plasma deposits is reduced considerably if the surfaces are immersed in aqueous solution prior to reaction with the amine. These insights are of particular importance when applying these surfaces as supports for the covalent attachment of peptides and other biomolecules containing amines or alcohols. Binding of a peptide to the surface has been achieved, accomplishing one of the main goals of this work.

Further on, a new protocol for sample preparation has been developed to be completed with cells seeding and culture on modified substrates. Cells seeding has been accomplished, after binding of a peptide to the surface, by a successful growing of neurons living up to 13 days on the platform.

The fact that cells are able to grow on top of the polymerized surface after covalent peptide attaching shows a promising platform for cell-substrate interaction.

After this platform has been achieved, and its reactivity proved, the next chapter concentrates in two possible applications for the pp-PFM related to all that has been studied till the moment.

3.8 REFERENCES

1. Francesch, L.; Garreta, E.; Balcells, M.; Edelman, E. R.; Borros, S. Fabrication of bioactive surfaces by plasma polymerization techniques using a novel acrylate-derived monomer. *Plasma Processes and Polymers* **2005**, *2* (8), 605-611.
2. Papra, A.; Gadegaard, N.; Larsen, N. B. Characterization of ultrathin poly(ethylene glycol) monolayers on silicon substrates. *Langmuir* **2001**, *17* (5), 1457-1460.
3. Backmann, N.; Zahnd, C.; Huber, F.; Bietsch, A.; Pluckthun, A.; Lang, H. P.; Guntherodt, H. J.; Hegner, M.; Gerber, C. A label-free immunosensor array using single-chain antibody fragments. *Proceedings of the National Academy of Sciences of the United States of America* **2005**, *102* (41), 14587-14592.
4. Padeste, C.; Sorribas, H.; Tlefemauer, L. Photolithographic Generation of Protein Micropatterns. *PSI Anual Scientific Report* **2000**.
5. Coulson, S. R.; Woodward, I. S.; Badyal, J. P. S.; Brewer, S. A.; Willis, C. Ultralow Surface Energy Plasma Polymer Films. *Chem. Mater.* **2000**, *12* (7), 2031-2038.
6. Mackie, N. M.; Castner, D. G.; Fisher, E. R. Characterization of pulsed-plasma-polymerized aromatic films. *Langmuir* **1998**, *14* (5), 1227-1235.
7. Wei, T. C.; Liu, C. H. Evaluation of plasma deposited fluorocarbon films using experimental design methodology. *Surface and Coatings Technology* **2005**, *200* (7), 2214-2222.
8. Hynes, A.; Badyal, J. P. S. Selective Incorporation of Perfluorinated Phenyl Rings during Pulsed Plasma Polymerization of Perfluoroallylbenzene. *Chem. Mater.* **1998**, *10* (8), 2177-2182.
9. Zhang, J.; van Ooij, W.; France, P.; Datta, S.; Radomyselskiy, A.; Xie, H. Investigation of deposition rate and structure of pulse DC plasma polymers. *Thin Solid Films* **2001**, *390* (1,2), 123-129.
10. Mackie, N. M.; Dalleska, N. F.; Castner, D. G.; Fisher, E. R. Comparison of Pulsed and Continuous-Wave Deposition of Thin Films from Saturated Fluorocarbon/H₂ Inductively Coupled rf Plasmas. *Chem. Mater.* **1997**, *9* (1), 349-362.
11. Pretsch, E.; Bühlmann, P.; Affolter, C.; Herrera, A.; Martinez, R. *Determinacion estructural de compuestos organicos*; Springer-Verlag Iberica: Barcelona, **2001**.
12. d'Agostino, R. *Plasma Deposition, Treatment and Etching of Polymer Films*; Academic Press: Boston, MA, **1990**.
13. Panchalingam, V.; Chen, X.; Savage, C. R.; Timmons, R. B.; Eberhart, R. C. Molecular tailoring of surfaces via pulsed RF plasma depositions. *Journal of Applied Polymer Science: Applied Polymer Symposium* **1994**, *54* (Plasma Deposition of Polymeric Thin Films), 123-141.
14. Yasuda, H. *Luminous Chemical Vapor Deposition and Interface Engineering*; Marcel Dekker: New York, **2004**.
15. Bai, Y. L.; Koh, C. G.; Boreman, M.; Juang, Y. J.; Tang, I. C.; Lee, L. J.; Yang, S. T. Surface modification for enhancing antibody binding on polymer-based microfluidic device for enzyme-linked immunosorbent assay. *Langmuir* **2006**, *22* (22), 9458-9467.
16. Calderon, J. G.; Timmons, R. B. Surface molecular tailoring via pulsed plasma-generated acryloyl chloride polymers: synthesis and reactivity. *Macromolecules* **1998**, *31* (10), 3216-3224.
17. Panchalingam, V.; Poon, B.; Huo, H.-H.; Savage, C. R.; Timmons, R. B.; Eberhart, R. C. *Journal of Biomaterials Science, Polymer Edition* **1993**, *5*, 131.
18. McCurdy, P. R.; Truitt, J. M.; Fisher, E. R. Comparison of oxidation rates for a-Si_{1-x}C_x:H films deposited from pulsed and continuous wave RF plasmas. 145 ed.; **1998**; pp 3271-3277.
19. Sciaratta, V.; Vohrer, U.; Hegemann, D.; Muller, M.; Oehr, C. Plasma functionalization of polypropylene with acrylic acid. *Surface and Coatings Technology* **2003**, *174-175*, 805-810.
20. Watkins, L.; Bismarck, A.; Brain, A.; Lee, A. F.; Maughan, J.; Wilson, D.; Wilson, K. An XPS study of pulsed plasma poly-allyl-alcohol film growth on polyurethane. *Abstracts of Papers, 230th ACS National Meeting, Washington, DC, United States, Aug. 28-Sept. 1, 2005* **2005**, OLY-605.
21. Fraser, S.; Short, R. D.; Barton, D.; Bradley, J. W. A Multi-Technique Investigation of the Pulsed Plasma and Plasma Polymers of Acrylic Acid: Millisecond Pulse Regime. *Journal of Physical Chemistry B* **2002**, *106* (22), 5596-5603.

22. Rinsch, C. L.; Chen, X.; Panchalingam, V.; Eberhart, R. C.; Wang, J. H.; Timmons, R. B. Pulsed Radio Frequency Plasma Polymerization of Allyl Alcohol: Controlled Deposition of Surface Hydroxyl Groups. *Langmuir* **1996**, *12* (12), 2995-3002.
23. Forch, R.; Zhang, Z. H.; Knoll, W. Soft plasma treated surfaces: Tailoring of structure and properties for biomaterial applications. *Plasma Processes and Polymers* **2005**, *2* (5), 351-372.
24. Swaraj, S.; Oran, U.; Lippitz, A.; Friedrich, J. F.; Unger, W. E. S. Study of influence of external plasma parameters on plasma polymerised films prepared from organic molecules (acrylic acid, allyl alcohol, allyl amine) using XPS and NEXAFS. *Surface and Coatings Technology* **2005**, *200* (1-4), 494-497.
25. Bodas, D. S.; Mandale, A. B.; Gangal, S. A. Deposition of PTFE thin films by RF plasma sputtering on {1 0 0} silicon substrates. *Applied Surface Science* **2005**, *245* (1-4), 202-207.
26. Beamson, G.; Briggs, D. *High-Resolution xPS of organic polymers, The Scienta ESCA300 database*; John Wiley & Sons Inc: Chichester (U.K.), New York, **1992**.
27. France, R. M.; Short, R. D.; Dawson, R. A.; Macneil, S. Attachment of human keratinocytes to plasma copolymers of acrylic acid/octa-1,7-diene and allylamine/octa-1,7-diene. *Journal of Materials Chemistry* **1998**, *8* (1), 37-42.
28. Kelly, J. M.; Short, R. D.; Alexander, M. R. Experimental evidence of a relationship between monomer plasma residence time and carboxyl group retention in acrylic acid plasma polymers. *Polymer* **2003**, *44* (11), 3173-3176.
29. Barz, J.; Haupt, M.; Hilgers, H.; Oehr, C. Ultrathin carbon-fluorine films. *International Conference on Phenomena in Ionized Gases, Proceedings, 27th, Eindhoven, Netherlands, July 18-22, 2005* **2005**, 03.
30. Vinogradov, I. P.; Lunk, A. Structure and chemical composition of polymer films deposited in a dielectric barrier discharge (DBD) in Ar/fluorocarbon mixtures. *Surface and Coatings Technology* **2005**, *200* (1-4), 660-663.
31. Denes, F. Synthesis and surface modification by macromolecular plasma chemistry. *Trends in Polymer Science (Cambridge, United Kingdom)* **1997**, *5* (1), 23-31.
32. Morgan, A. R.; Duc, T. M. The chemistry of deposits formed from acrylic acid plasmas. *Journal of Materials Chemistry* **1998**, *8* (4), 937-943.
33. Oran, U.; Swaraj, S.; Friedrich, J. F.; Unger, W. E. S. Surface analysis of plasma-deposited polymer films, 1 - ToF-SSIMS of plasma polystyrene before and after exposure to ambient air. *Plasma Processes and Polymers* **2004**, *1* (2), 123-133.
34. Lodish, H. *Biologia celular y molecular*; Mòdica Panamericana: Madrid, **2002**.
35. <http://www.bio.ph.ic.ac.uk/~erhard/Research.html> **2007**.
36. <http://www.upei.ca/pathclub/fig13.jpg> **2007**.
37. Sephel, G.; Tatoulian, M.; Sasaki, M.; Greatorex, D.; Martin, G. R.; Yamada, Y.; Kleinman, H. Laminin A is a chain synthetic peptide which supports neurite outgrowth. *Biochem Biophys Res Commun* **1989**, *162* (2), 821-829.
38. Ichikawa, N.; Kasai, S.; Suzuki, N.; Nishi, N.; Oishi, S.; Fujii, N.; Kadoya, Y.; Hatori, K.; Mizuno, Y.; Nomizu, M.; rikawa-Hirasawa, E. Identification of Neurite Outgrowth Active Sites on the Laminin alpha4 Chain G Domain. *Biochemistry* **2005**, *44* (15), 5755-5762.
39. Letourneau, P. C.; Condic, M. L.; Snow, D. M. Interactions of developing neurons with the extracellular matrix. *J. Neurosci.* **1994**, *14* (3), 915-928.
40. Shin, H.; Jo, S.; Mikos, A. G. Biomimetic materials for tissue engineering. *Biomaterials* **2003**, *24* (24), 4353-4364.
41. Chu, P. K.; Chen, J. Y.; Wang, L. P.; Huang, N. Plasma-surface modification of biomaterials. *Materials Science & Engineering, R: Reports* **2002**, *R36* (5-6), 143-206.
42. Lerouge, S.; Wertheimer, M. R.; Yahia, L. 'H. Plasma Sterilization: A Review of Parameters, Mechanisms, and Limitations. *Plasmas and Polymers* **2001**, *6* (3), 175-188.
43. Laroussi, M. Low temperature plasma-based sterilization: Overview and state-of-the-art. *Plasma Processes and Polymers* **2005**, *2* (5), 391-400.
44. Chan, C. M.; Ko, T. M.; Hiraoka, H. Polymer surface modification by plasmas and photons. *Surface Science Reports* **1996**, *24* (1/2), 1-54.
45. ATCC ATCC Cell Biology Collection. <http://www.lgcpromochem-atcc.com/common/catalog/numSearch/numResults.cfm?atccNum=CRL-1825> **2007**.

[CHAPTER 4]

MICROCANTILEVER SENSORS

CHAPTER 4

MICROCANTILEVER SENSORS

4.1 INTRODUCTION

Surface-active coatings have already found applications in many areas of technology and a number of wet chemical and dry techniques are available for their synthesis. It has been shown, that plasma assisted processes can be used to deposit thin films containing different densities of highly reactive groups which are available for reaction after deposition. The chemical reactivity of the deposits depends on the density and on the availability of the reactive groups. By careful control over the deposition conditions even monomers containing very labile groups can be deposited successfully.¹

Recently it was suggested that not only the functional groups on the surface, but also those embedded within the matrix are in principle available for reaction. This was inferred by DNA immobilization on plasma polymerised allylamine, for which a clear dependence of DNA immobilization on the film thickness was observed.² A major challenge in this kind of research is finding suitable analytical methods, which not only allow for in-situ measurements of chemical reactions of a thin film while immersed in solution, but also enables depth profiling of this reaction.

Microcantilevers sensor technology has proved to be a valuable technique to investigate material properties or the surface properties of thin films.^{3,4} The MC sensor set-up consists of an array of cantilevers which act as transducers, a reactive coating, and a read-out system. In the absence of external forces the deflection of the cantilevers is related to the differential mechanical stress generated between opposite sides of the cantilever. This offers unique possibilities to monitor small volume changes of thin films. Such volume changes could, for example, be a result of swelling processes owing to changes in environmental conditions such as temperature or humidity,⁵ or they could be a result of chemical reactions within the thin functional coating.⁶ In order to avoid misinterpretation of MC sensor data it is generally useful to combine it with other characterization techniques. In this section, the MC sensor technique has been used as a complementary method to FTIR to systematically study the reactivity of a low duty cycle pp-PFM film of known chemical structure and functional group density towards different amines. Pp-PFM is of particular interest as an active coating, since it offers a highly reactive ester group, which can potentially be utilized for binding biomolecules and promote cell adhesion and proliferation, as it has been presented in the precedent chapters and has already been published.^{7,8}

In order to understand the chemical reactivity of the pp-PFM surface towards biomolecules (i.e. proteins), we have investigated the basic reaction of the perfluoroester with simple amines. One particular aspect of interest was the influence of the molecular structure of the amines on their reactivity towards thin films. The amines studied ranged from different primary amines (1°) containing different substituents, secondary (2°), and tertiary (3°) amines.

Microcantilever sensors

The MC sensors technique was used in this work to investigate changes in stress in the thin film as a result of chemical reactions taking place. A systematic study on the reactivity of a low duty cycle pp-PFM film of known chemical structure and functional group density with different amines allows for some assumptions to be made on the extent of reaction at the liquid/solid interface or reaction within the film. This enables correlations to be made between functional group accessibility and type of reactant.

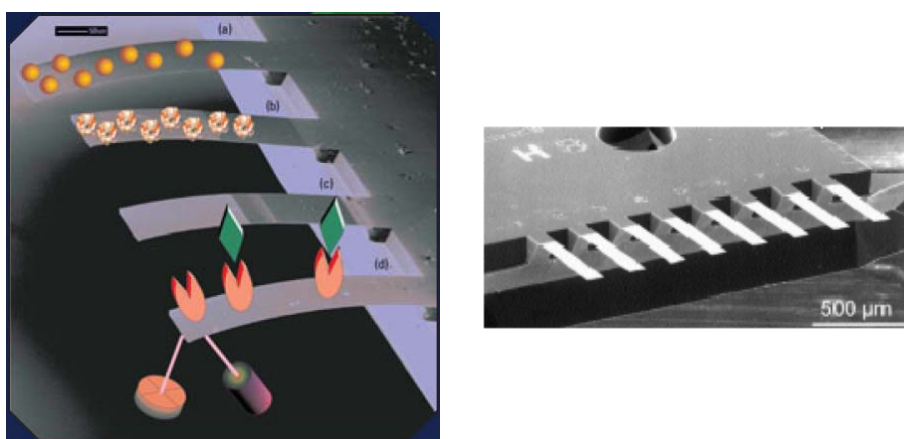


Figure 4.1 Illustration of a cantilever chemical sensor with optical lever readout. MC surfaces modified with (a) nanobeads, (b) cavitand receptors, and (c) thin polymeric film to improve cantilever response or selectivity. (d) Depiction of a bioaffinity interaction MC.⁹. SEM image of an array of eight silicon MCs, IBM⁴

In figure 4.1 a laser beam reflected near the end of a cantilever is displaced as the cantilever bends. This displacement is converted into an electronic signal by projecting the reflected laser beam onto a position-sensitive photodetector.⁹

In the absence of external forces the deflection of the cantilevers is related to the differential mechanical stress generated between opposite sides of the cantilever and thus offers unique possibilities to monitor small changes in stress at the interface between the MC and the thin film induced, for example, by a chemical

reaction of the selective coating. The stress at the interface is calculated from the deflection of the MC and can be used to evaluate volume changes resulting from the reaction of functional groups within the thin functional coating,⁶ or from swelling processes as a result of environmental changes (temperature, humidity).⁵

There are different approaches to understand how different coatings generate different responses on MC sensors. Among these models, one of big interest for this work is the one where an analyte is able to interact with a film thicker than a monolayer. The analyte is able to diffuse into the bulk of the film and interact with this, causing swelling of the coating, and by this, bending of the cantilever. This kind of mechanisms is presented in Figure 4.2.⁹

Further, it can reveal unique information about single binding events of molecules at interfaces. The MCS technique has, for example, been successfully used to detect the hybridization of DNA.¹⁰

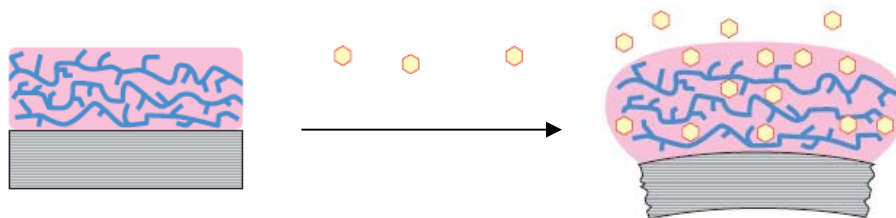


Figure 4.2 Mechanism of stress by the swelling of a thin film on a surface due to analyte absorption⁹

Working with thin films implies that the measurement of physical and chemical properties is often non trivial and only a limited number of current analytical tools are available. Several groups work to understand which parameters dominate the deflection of thin cantilevers. Godin and coworkers have combined the MCS technique with ellipsometry to compare in-situ the surface stress and thickness change of a alkanethiols which self assemble on gold.¹¹ Previous work in the MPIP group has shown that MCS data can easily be correlated to Surface Plasmon Resonance Spectroscopic data and FTIR data.^{5,6}

The deflection of each of the 8 MCs was monitored with a Scentris™ platform (Veeco, USA) based on the beam deflection detection principle (Figure 4.3). This technique allows for the sequential measurement of the deflection of 8 MC at a resolution <1 nm, over a range of several μm .

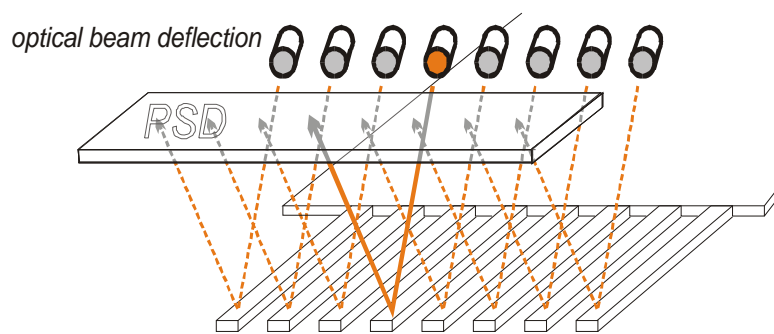


Figure 4.3 Schematic of the MCS array

4.1.1 EXPERIMENTAL SECTION

Materials

Isopropylamine (99%), diethylamine (99%), triethylamine (99%), 1,6-diaminohexane (99%) and hexylamine (99%) were purchased from Sigma-Aldrich and used as received.

OCTOSENSIS silicon micromechanical cantilever arrays (Micromotive, Germany) were used as transducers. Each chip consists of eight rectangular cantilevers, with a length of 500 μm , width of 90 μm and thickness of 2 μm arranged at a pitch of 250 μm . Typical variations of resonance frequencies within one array are less than 1%, indicating similar mechanical characteristics.

Sample preparation

Since most of the tests were to be performed under aqueous environment, the Si cantilever arrays need to be surface modified to ensure optimum adhesion between the functional coating and the Si surface. In addition, MCS data was compared to FTIR data on samples prepared by identical procedures. Thus the MCS were prepared in the same way as the glass slides used for IRRAS. The preparation involved the deposition of an adhesion layer of 1.5 nm of chromium to assist adhesion, subsequently a gold coating was evaporated (20 nm on the MCS, 80 nm on the glass substrate) followed by a modification of the gold with a self-assembled monolayer (SAM) of hexanethiol. The SAM was prepared by immersion of the one-side gold coated MC array into the 2mM hexanethiol ethanolic solution overnight. After thoroughly rinsing with absolute ethanol, the MC arrays were dried in atmosphere and subject to plasma polymerization. In order to avoid the deposition of pp-PFM on the bottom part of the cantilevers, a glass cover was located beneath cantilevers.

After the polymer deposition, reference MCs were prepared by exposing 4 MC within an array of 8 to concentrated isopropylamine for half an hour. The isopropylamine reacted with the active perfluorophenyl ester and deactivated the active ester groups. This deactivation procedure was performed within a cantilever

treatment station, a precise apparatus that allows the perfect alignment of the reference cantilever inside a capillar which contains the amine. In this way part of the MC sensor array could be used as a reference, while the other part served as the test sample. The functionalised MC arrays were stored under argon until MCS measurements.

Plasma Polymerization and Surface Analysis

Plasma polymerization was carried out in *system 1* as explained in the previous chapter in section 3.2. The typical plasma film thickness was $40 \text{ nm} \pm 4 \text{ nm}$.

Surface analysis was based on FTIR and profiler measurements as explained in section 3.2

Deflection measurements

The position of each cantilever was monitored for the simultaneous recording of deflection of all eight MC. Since the deflections of the cantilevers were determined independently, it was possible to calculate the differential deflection between a pp-PFM-coated MC and a reference MC, whereby drift temperature and unspecific absorption effects could be compensated.^{12,13} The low concentration of amine in the PBS did not induce noticeable changes in the refractive index of the PBS solution, such that we assume the absolute value of the deflection was not affected by exchanging the PBS solution with the amine solution.

Any influence due to the flow on the absolute deflection of the MC was avoided by working in quasi-stationary regime. The PEEK reaction cell was equipped with a glass window and had a volume was $30 \mu\text{L}$. An inlet and an outlet equipped with valves allowed for the exchange of the liquid. After injection of each solution, the inlet and the outlet valves of the reaction cell were closed such that there was no flow during measurements. The surface reactivity of the pp-PFM film could thus be monitored in real time and in-situ. This was done for different amines using a concentration of 1% amine in PBS buffer solution.

4.1.2 PP-PFM REACTIVITY ON MICROCANTILEVER SENSORS

Pp-PFM structure and deactivation

Film films achieved in chapter 3 with system 1 were used in this chapter for the Microcantilever Sensor studies.

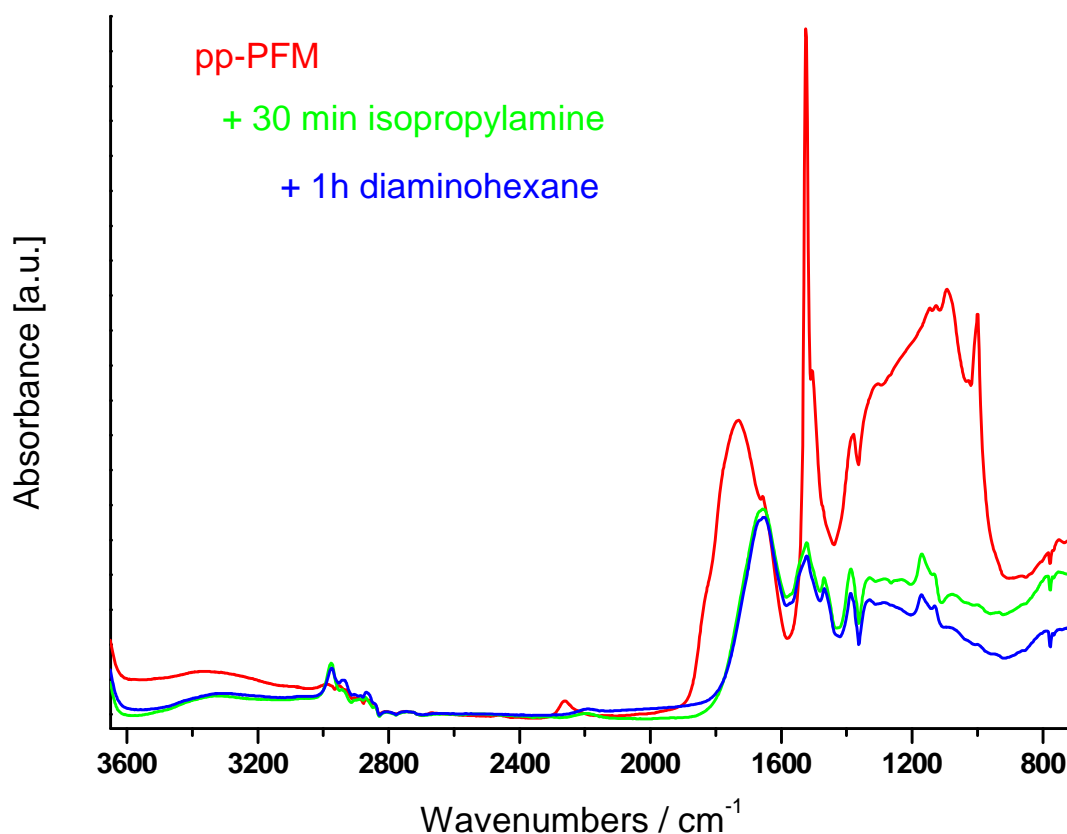


Figure 4.4 FTIR spectrum of pp-PFM deposited on the MCS and its deactivation reaction against of isopropylamine

The deactivation procedure of the MC sensor was optimised in a series of test in which an Au/SAM/pp-PFM substrate was exposed to concentrated isopropylamine for various periods of time.

IRRAS spectra presented in Figure 4.4 showed that after half an hour treatment with isopropylamine all the characteristic bands of the perfluorophenyl ester disappeared and a new band, characteristic of amide groups, appeared. The isopropylamine reacted with the active perfluorophenyl ester and deactivated the active ester group. Longer periods of time didn't show any improvement in the deactivation process, but showed a damage of the film. The later exposure of the deactivated film to 1,6-diaminohexane showed that the amine was not linking to the polymer. Therefore the success of the deactivation process was established. In this way part of the MC sensor array could be used as a reference, while the other part served as the test sample. The functionalised MC arrays were stored under argon until MCS measurements.

Reaction of the amines with pp-PFM on MCS¹⁴

After the deactivation of half of the Microcantilever Sensors, the array of microcantilevers was exposed to different amines. The reaction of the active ester with different amines will theoretically lead to different reaction products depending on the chemical structure of the amine used as is shown in Figure 4.5.

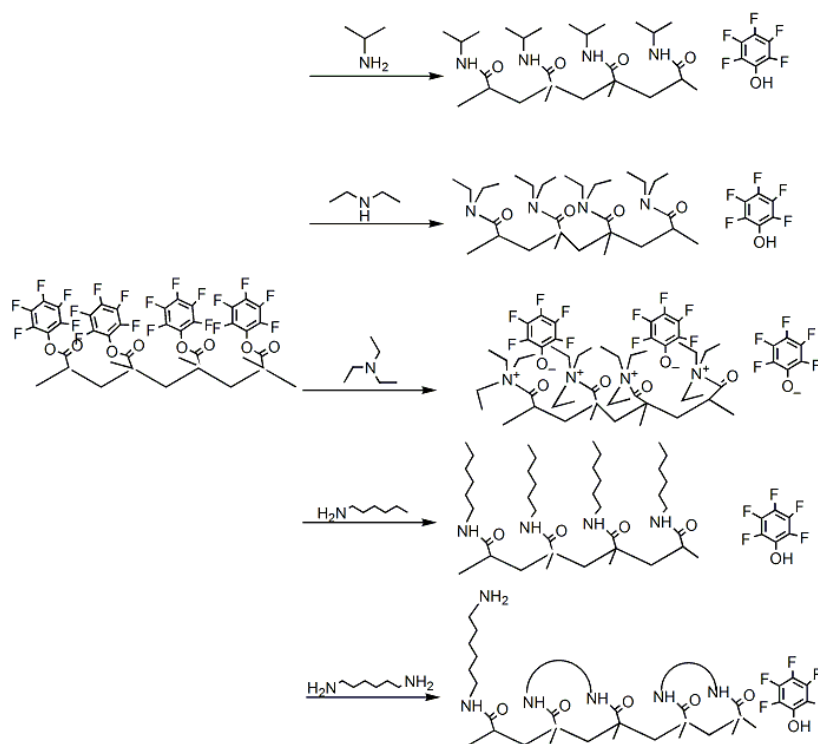


Figure 4.5 Schematic of the possible reactions occurring between pp-PFM and amines

Figure 4.6 presents the IRRAS and XPS spectra for pp-PFM films after 1h reaction with different amines. In this case, the amines used present different degree of substitution, having a primary, a secondary and a tertiary amine in each reaction.

Table 4.1 XPS data of the polymer after reaction with amines with various degree of substitution

Sample	Atomic percentage				Ratio		
	C1s	O1s	F1s	N1s	F/C	O/C	N/C
PFM	58.97	11.30	27.80	1.94	0.47	0.19	0.03
reacted hexylamine	71.20	8.15	12.59	8.07	0.18	0.11	0.11
reacted diethylamine	60.48	17.61	10.07	11.84	0.17	0.29	0.20
reacted triethylamine	56.51	19.50	9.18	14.81	0.16	0.35	0.26

The chemical structures of the different reaction products cannot be clearly differentiated by FTIR such that the spectra of all reacted surfaces show a trend towards the formation of amides as seen by the peak shift from 1735 cm^{-1} to 1654 cm^{-1} . Even so, subtle changes in the spectra can be observed.

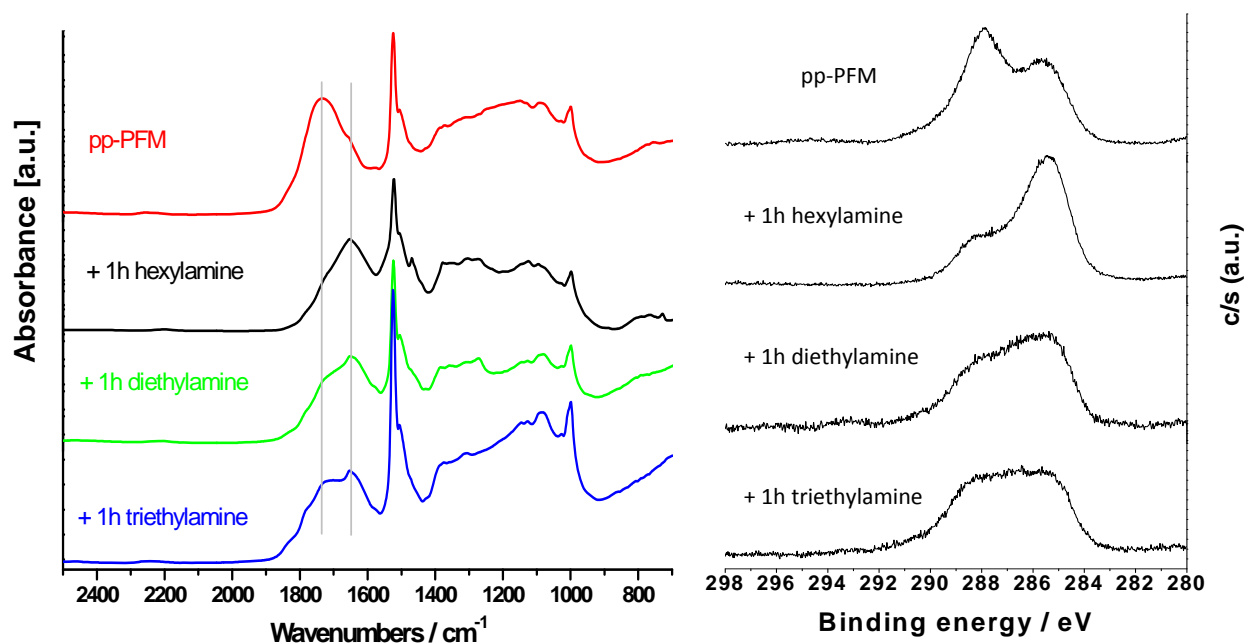


Figure 4.6 FTIR and XPS spectra of pp-PFM films after 1h exposure to amines with various degree of substitution

However, the shape of the IR spectra and the relative intensities of the bands after 1 hour exposure to different amine solutions allows for some predictions to be made about the reaction occurring. When comparing the relative intensities of the ester peak (1735 cm^{-1}) and the amide peak (1654 cm^{-1}) with respect to the chemical structure of the amine we observe a clear trend in going from the 1° to the 2° to the 3° amine reaction.

It can be seen that the relative intensity of the ester peak to the amide peak ($I_{\text{ester}}/I_{\text{amide}}$) decreases in the order $3^\circ > 2^\circ > 1^\circ$, suggesting a better conversion for the lower order amines. The FTIR spectra in Figure 4.6 hint almost complete transformation of the ester to the amide when using a 1° chain amine. Also the intensity decrease of the band at 1524 cm^{-1} (fluorinated ring) is the greatest for the reaction of the 1° amine, suggesting a significant loss of this group from the film surface. Higher order amines seem to be less reactive towards the PFM ester. This result is equivalent to the results presented by Eberhardt et al. on conventional pentafluorophenyl methacrylate polymers.¹⁵ We assume that this is a result of steric hindrance and thus a slower rate of diffusion of the 2° and 3° amine into the pp-PFM polymer network, which also prevents the amine to react with functional groups deeper within the polymer film.

The shape of the XPS curves shows how the degree of functionalization is higher when exposing the film to a primary amine, regarding the intensity of the C-F peak in front of the C-C peak. The atomic compositions

presented in Table 4.1 indicate that while working with the secondary and tertiary amine a damage of the films could be occurring, as the oxygen presence rises while also the nitrogen presence does. This indicates that not only the amine functionalities are being incorporated, but also oxygen groups are forming the superficial film, destroying the functionalities of the developed film. This fact can also be observed in the shape of the XPS curves, as the profiles for the secondary and tertiary amines present an involving curve, with less definition than the others, indicating the presence of a larger amount of groups in the XPS analysis. With these two results, it has been concluded that the primary amine is the amine that achieves better conversion of the ester groups in amide, linking the amine to the polymer.

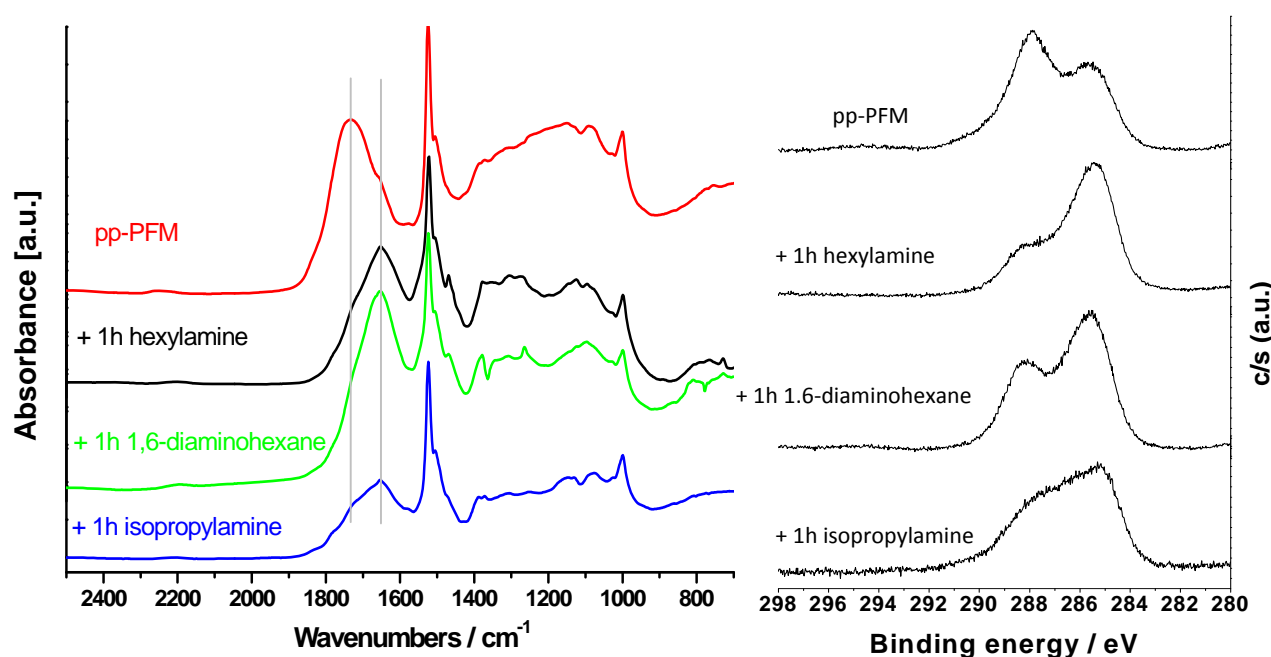


Figure 4.7 FTIR and XPS spectra of pp-PFM films after 1h exposure to various primary amines

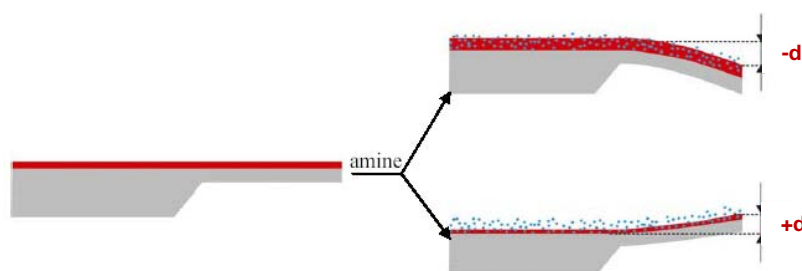
Figure 4.7 shows the FTIR spectra of the pp-PFM film after reaction (1 hour) with three primary amines of different chemical structure: one branched and two linear molecules with either one or two amino-groups. Hexylamine and 1,6-diaminohexane appear to undergo similar reactions such that the IRRAS spectra obtained are very similar. The XPS data, presented in Figure 4.7 and Table 4.2, suggest that the degree of functionalization for the hexylamine is higher than for the diaminohexane. After reaction with isopropylamine in PBS the presence of the peak at 1654 cm^{-1} suggests significant conversion from the ester to the amide, yet the high relative intensity of the band at 1525 cm^{-1} still suggests a significant amount of fluorinated phenyl groups. In this case, for the isopropylamine, the XPS data shows a rise of oxygen and nitrogen in front of the other elements.

Table 4.2 XPS data of the polymer after reaction with various primary amines

Sample	Atomic percentage				Ratio		
	C1s	O1s	F1s	N1s	F/C	O/C	N/C
PFM	58.97	11.30	27.80	1.94	0.47	0.19	0.03
reacted vs. hexylamine	71.20	8.15	12.59	8.07	0.18	0.11	0.11
reacted vs. diaminoethane	66.12	10.38	19.20	4.29	0.29	0.16	0.07
reacted vs. isopropylamine	61.77	15.89	9.80	12.54	0.16	0.26	0.20

Chemical analyses have shown the reaction of the primary amines with the polymer, as well as a reaction in some extent for the secondary amines. More precise information cannot be obtained and it still remains unclear if the amines are able to diffuse into the polymer.

During the conversion of the ester to the amide, a large pentafluorophenyl group is replaced by a smaller alkyl chain. Assuming that the bulky pentafluorophenyl group is able to diffuse out of the polymer network and into solution, this would lead to differences in the 3 dimensional arrangements of the polymer molecules and thus the film volume. This can lead to a change in the internal stress of the film and therefore to a bending of a microcantilever sensor, see Figure 4.8. Depending on the type of stress induced within the film, the film may either contract (compressive stress) leading to an upward bending, or it may expand (tensile stress) leading to a negative deflection or a downward bending of the cantilever, attributed to a volume increase within the film.^{4,6,16}

**Figure 4.8 Representation of MC deflection during the reaction**

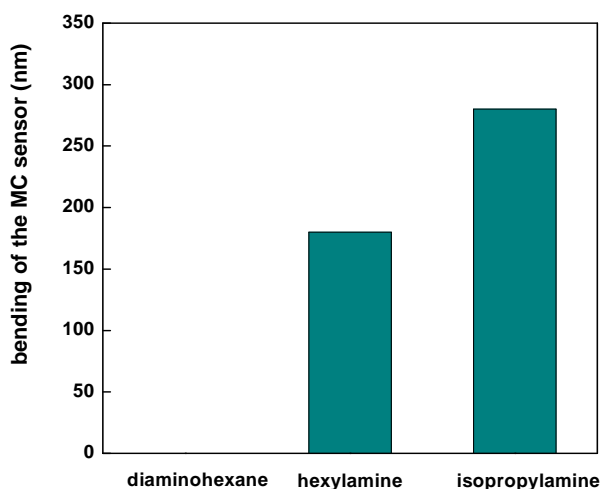
Experiment against different primary amines

Figure 4.9 Summary of the relative bending of the MC sensor coated with pp-PFM and reacted with 3 different primary amines for 1 hour

Figure 4.9 shows the relative bending of the modified MC arrays as a function of exposure time to different primary amines. The plot presents the average differential bending of the pp-PFM coated versus the reference MC sensors within one array after 1 hour exposure to the amine followed by the rinsing in PBS.

The data show clear differences for the reactions of the three 1° amines. Isopropylamine is the smallest of the three 1° amines with only three carbon atoms and clearly leads to the highest swelling and bending of the cantilever. Hexylamine is a linear molecule with six carbons which, after reaction also shows considerable swelling of the film leading to a bending of the MC. The absolute swelling is, however, lower than that observed for isopropylamine. This is believed to indicate that hexylamine does not diffuse into the polymer network as readily as isopropylamine. The reaction of diaminohexane, however, resulted in no significant overall bending. This may be because both functional groups of the molecule are able to react with the pp-PFM leading to a cross linking of the surface, which may lead to a “shielding” layer of reacted diaminohexane at the polymer-liquid interface preventing any further molecules to diffuse deeper into the polymer network.

These results are coherent with the chemical analyses results. The linkage on the polymer bulk is explored. With the small branched amine, isopropylamine. The isopropylamine appeared to show a higher penetration into the polymer structure and a bigger swelling of the film, and therefore a bigger degradation of the surface and higher loss of the C-F groups, as was already implied by the XPS and FTIR.

Experiment with different film thicknesses

The influence of the film thickness was studied against the most reactive amine, isopropylamine, on the deflection keeping all other conditions constant. The thicknesses were tuned by changing the plasma treatment time from 1 min to 5 min giving thicknesses of 40 nm and 120 nm respectively.

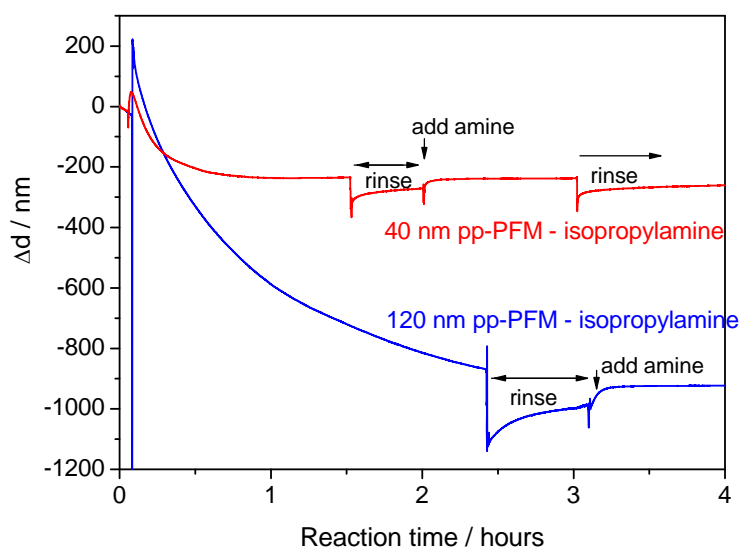


Figure 4.10 Evolution of the average differential deflection of a MC array functionalised with pp-PFM of different thickness during the treatment with 1 mM buffer solution of isopropylamine

When isopropylamine was reacted with the thicker film, a higher decrease in deflection ($\Delta d = -900$ nm) was found. Isopropylamine doesn't remain on the surface, but penetrates deeper inside the film and reacts within the bulk ester groups. If the reaction would occur only on the surface, no difference in the deflection would have been observed, as presented in Figure 4.10. Increasing the film thickness from 40 nm to approximately 120 nm led to an almost threefold change in the deflection over the duration of the experiment. The initial spike in the data is followed by a slow decrease in Δd , which did not reach a minimum after two and a half hours. Rinsing, followed by another immersion in the amine solution seemed to lead to a stabilization, such that after about three and a half hours no further change in the Δd was observed. Thus, while the reaction of the 40 nm thick film seemed to be complete within about one hour, the 120 nm thick film required approximately 3 hours.

In all the MCS experiments an initial sharp increase in Δd was observed, which can probably be associated with the initial approach and the reaction of the amines with perfluoroester groups at the pp-PFM solid/liquid interface. The subsequent slower decrease in Δd (for isopropylamine, hexylamine and diethylamine) is

thought to be related to a number of different processes taking place: (i) the diffusion of the amine into the polymer film, (ii) the reaction of the amine with the perfluoroester groups and (iii) the desorption of the latter. While a clear dependence on the size of the reagent was observed, the cantilever deflection also clearly showed a dependence on the film thickness.

4.1.3 SUMMARY

In this section the reaction of different amines on plasma polymerized PFM surfaces using IRRAS, XPS and MC sensors has been investigated. All the different techniques, XPS, IRRAS and the MCS indicated that the reaction of the pp-PFM was fastest for the 1° amine. The deflection of the pp-PFM functionalized MCS allows for some predictions on whether the reactions occur at the liquid/solid interface or within the matrix of the polymer. Each of the amines tested in this work has shown a unique response to the microcantilever sensor, which may give insights into the reaction mechanisms taking place. The largest difference was observed between the bi-functional amine and isopropylamine, the former showing tensile, the latter showing compressive stress on the pp-PFM film.

The combination of MC sensors and other surface sensitive techniques is believed to be a promising approach to study reactions and reaction mechanisms occurring in the bulk of thin films as well as on the polymer liquid interface.

Interesting experiments to be performed related to the present work, would be the reactivity of the pp-PFM films towards of peptides to corroborate the hypothesis of the pure surface reaction in this case.

4.2 REFERENCES

1. Forch, R.; Zhang, Z. H.; Knoll, W. Soft plasma treated surfaces: Tailoring of structure and properties for biomaterial applications. *Plasma Processes and Polymers* **2005**, *2* (5), 351-372.
2. Zhang, Z.; Chen, Q.; Knoll, W.; Foerch, R.; Holcomb, R.; Roitman, D. Plasma Polymer Film Structure and DNA Probe Immobilization. *Macromolecules* **2003**, *36* (20), 7689-7694.
3. Berger, R.; Delamarche, E.; Lang, H. P.; Gerber, C.; Gimzewski, J. K.; Meyer, E.; Guntherodt, H. J. Surface Stress in the Self-Assembly of Alkanethiols on Gold. *Science* **1997**, *276* (5321), 2021-2024.
4. Raiteri, R.; Grattarola, M.; Berger, R. Micromechanics senses biomolecules. *Materials Today (Oxford, United Kingdom)* **2002**, *5* (1), 22-29.
5. Igarashi, S.; Itakura, A. N.; Toda, M.; Kitajima, M.; Chu, L.; Chifen, A. N.; Forch, R.; Berger, R. Swelling signals of polymer films measured by a combination of micromechanical cantilever sensor and surface plasmon resonance spectroscopy. *Sensors and Actuators B: Chemical* **2006**, *117* (1), 43-49.
6. Igarashi, S.; Itakura, A. N.; Kitajima, M.; Chifen, A. N.; Foerch, R.; Berger, R. Surface stress control using ultraviolet light irradiation of plasma-polymerized thin films. *Applied Physical Letters* **2006**, *88* (14), 143119-1-143119-3.
7. Francesch, L.; Garreta, E.; Balcells, M.; Edelman, E. R.; Borros, S. Fabrication of bioactive surfaces by plasma polymerization techniques using a novel acrylate-derived monomer. *Plasma Processes and Polymers* **2005**, *2* (8), 605-611.
8. Francesch, L.; Borros, S.; Knoll, W.; Forch, R. Surface Reactivity of Pulsed-Plasma Polymerized Pentafluorophenyl Methacrylate (PFM) toward Amines and Proteins in Solution. *Langmuir* **2007**, *23* (7), 3927-3931.
9. Sepaniak, M.; Datskos, P.; Lavrik, N.; Tipple, C. Microcantilever transducers: A new approach to sensor technology. *Analytical Chemistry* **2002**, *74* (21), 568A-575A.
10. Fritz, J.; Baller, M. K.; Lang, H. P.; Rothuizen, H.; Vettiger, P.; Meyer, E.; Guntherodt, H.-J.; Gerber, C.; Gimzewski, J. K. Translating Biomolecular Recognition into Nanomechanics. *Science* **2000**, *288* (5464), 316-318.
11. Godin, M.; Laroche, O.; Tabard-Cossa, V.; Beaulieu, L. Y.; Grutter, P.; Williams, P. J. Combined in situ micromechanical cantilever-based sensing and ellipsometry. *Review of Scientific Instruments* **2003**, *74* (11), 4902-4907.
12. Lang, H. P.; Berger, R.; Andreoli, C.; Brugger, J.; Despont, M.; Vettiger, P.; Gerber, C.; Gimzewski, J. K.; Ramseyer, J. P.; Meyer, E.; Guntherodt, H. J. Sequential position readout from arrays of micromechanical cantilever sensors. *Applied Physics Letters* **1998**, *72* (3), 383-385.
13. Lang, H. P.; Hegner, M.; Meyer, E.; Gerber, C. Nanomechanics from atomic resolution to molecular recognition based on atomic force microscopy technology. *Nanotechnology* **2002**, *13* (5), R29-R36.
14. Queralto, N.; Bumbu, G. G.; Francesch, L.; Knoll, W.; Borros, S.; Berger, R.; Foerch, R. Investigation into the Chemical Reactivity of Plasma-Deposited Perfluorophenyl Methacrylate Using Infrared Reflection Absorption Spectroscopy and Microcantilever Studies. *Plasma Processes and Polymers* **2007**, *4* (S1), 790-793.
15. Eberhardt, M.; Mruk, R.; Zentel, R.; Theato, P. Synthesis of pentafluorophenyl (meth)acrylate polymers: New precursor polymers for the synthesis of multifunctional materials. *European Polymer Journal* **2005**, *41* (7), 1569-1575.
16. Tipple, C. A.; Lavrik, N. V.; Culha, M.; Headrick, J.; Datskos, P.; Sepaniak, M. J. Nanostructured microcantilevers with functionalized cyclodextrin receptor phases: Self-assembled monolayers and vapor-deposited films. *Analytical Chemistry* **2002**, *74* (13), 3118-3126.

[CHAPTER 5]

APPLICATIONS

CHAPTER 5

APPLICATIONS

The main goal of the work is to achieve a platform for covalent binding of biomolecules in an easy and fast way. This surface should then be able to support cell attachment and growing. The precedent chapters have been centered in the development of a plasma polymerized coating that would fulfill these parameters. The use of pentafluorophenyl methacrylate as monomer for the polymerization of the polymerization by pulsed plasma techniques, has been revealed as a possible way to achieve this platform and attach desired molecules, as amines or peptides. Cell culture on this surface was successfully achieved.

In this chapter an application is based on multi-sensor micro-devices for neuronal growth, where an enhancement of the cell attachment is needed.

5.1 CELL SIGNALLING PLATFORM THROUGH PEPTIDE ADHESION ON MODIFIED OXIDE SURFACES - APPLICATION FOR NEURONAL GROWTH

The work presented in this section is the result of a collaboration between the GEMAT group at the IQS and the Biomedical Application Group at the National Centre for Microelectronics (CNM-IMB, CSIC), in particular, Dr. Rosa Villa, Dr. Gemma Gabriel and Rodrigo Gómez.

The main idea was to improve cell attachment and growth of cells on some previously developed devices by the CNM, in the projects Microcell and Microtrans. These devices presented some problems in the control over the areas where neurons would grow, or in the case of the Microtrans needles, a problem of rejection for the *in vivo* assays. Therefore the use of the pp-PFM polymer was suggested, by the subsequent peptide attachment that showed promising results for cell growth presented in the third chapter, section 3.6.2. The polymer was already developed in the previous chapters, and the use of masks would help with the control over the growth areas.

5.1.1 INTRODUCTION

Long-term neural interfaces, as electrically active micro-devices that are able to record and stimulate neural signals in neurons and neural tissue, were first proposed in 1973.¹ The common basis for these devices is a silicon or glass substrate with deposited electrodes (typically Pt electrodes) and an associated circuit for signal conditioning.² Different shapes, substrates and electrode materials and layouts have been assayed. Conventional interfaces consist basically of an array of electrodes deposited in a grid layout, although there exist multiple variations including regenerative interfaces.^{3,4} Device shapes ranges from rectangular substrates containing arrays, such as in Micro-/Multi-Electrode Arrays (MEAs) for cell culture⁵⁻⁷ and cortical interfaces⁸, to flexible cuff interfaces for nerve wrapping⁹ and needle-shaped micro-devices for insertion into nerve or neural tissue¹⁰.

There have been many systems developed over the years, but long-term neural interfaces have still a series of problems first identified years ago.¹¹ Taking into account that the main goal behind most research proposals on neural interfaces is to result into clinical applications, and that almost all these applications involve the mid- or long-term placement of neural interfaces in (or in contact with) living tissue, the problem of long-term adhesion between neurons and electrodes must be specifically targeted.

Long-term adhesion has different but closely related troubles. The first problem concerns the initial inflammatory response towards the implanted interface. These initial inflammatory responses can easily develop into a chronic reaction¹², creating a highly resistive layer around the interface that renders it inoperative.¹³⁻¹⁵ Related to the inflammation is the problem that targeted neurons tend to migrate away from the immediate vicinity of the neural interface, probably because the implanted interface does not constitute the best of environments for cell growth and adhesion.

Even those materials generally considered to be biocompatible produce some degree of tissue response. Furthermore, once implanted the microelectrodes have to remain within the brain environment for a long time. Therefore, these devices must not be susceptible to attack by biological fluids, proteases, macrophages or any metabolic substances. However, although it has been reported that silicon-based shafts, silicon oxide based surfaces and other glass based products are highly biocompatible^{11,13,16}, there are chronic inflammatory reactions which affect both the neural tissue and the surface of the microelectrodes. These reactions often result in damage to neurons and microelectrodes and lead to the proliferation of a glial scar around the implanted probes, which prevents neurons to be recorded or stimulated.¹⁵

Electrode degradation does also often contribute to the failure of long-term implants. Electrodes are typically deposited on the substrate as a homogeneous layer by sputtering or chemical vapor deposition, and this layer is then patterned using microelectronic fabrication processes. With extended usage, and especially if higher potentials need to be applied due to the presence of fibrotic tissue, electrode materials tend to deteriorate

and detach from the substrate, leading to severely impoverished performances and raising concerns on their biocompatibility¹⁷⁻¹⁹.

Similar problems are also currant for MEA devices, especially when targeting long-term studies, with a long time scale of neuron culture on the surface.

With the above presented problem, developed devices that appear to have a good behavior *in vitro*, uses to be inoperative for *in vivo* assays. The challenge was to develop a cell friendly interface for tissue growth.

CNM-IMB has already been working on long-term interface in two projects: Microcell and Microtrans. The Microcell project involved a Micro-/Multi-Electrode Array for *in vitro* cell culture and the Microtrans project included the development of minimally invasive multi-sensor micro-probes for organ monitoring during transplantation.²⁰ Both devices presented the above exposed problems, and needed an interface improvement.

Figure 5.1 presents a picture of these devices, and a scheme of the layer distribution common to both. The substrates are based on Silicon, in this case, and have a silicon oxide layer. On top of this, a thin layer of titanium was deposited and on top of it, the platinum electrodes. A layer of silicon nitride is deposited avoiding the electrodes and on top of it, a second layer of silicon oxide is used to insure the SAM adhesion to the surface for posterior treatment.

The interface improvement was proposed by the pp-PFM polymerization on top of the surfaces and subsequent link of the peptide as used in chapter 2. In the case of the MEAs, a control over the polymerized areas was projected by the use of masks, to try to direct the neuronal growth on the substrates.

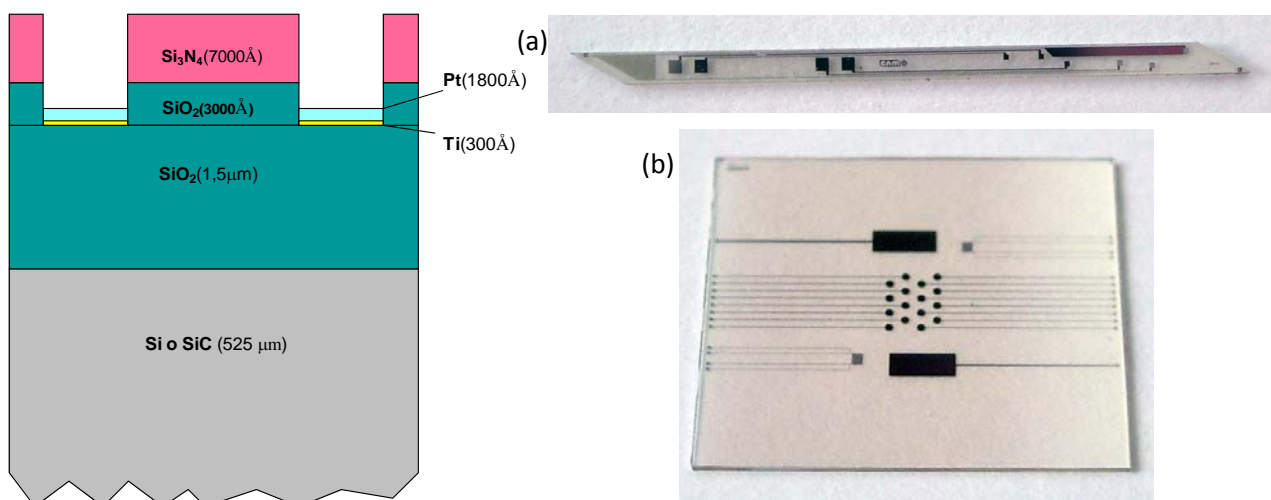


Figure 5.1 Scheme of layer distribution in the devices. (a) Pictures of the microneedles belonging to the Microtrans project and (b) cell culture microarrays of the Microcell project, developed in the CNM-IMB

In this last case, masks would leave part of the surface unmodified, and therefore protein non-covered. To get a passivating character of the remaining surface, a PEG-like SAM was deposited. The PEG-like surface has been reported to avoid protein adsorption by multiple groups²¹⁻²⁸ as well as resisting the adhesion of cells.^{29 30}

These characteristics are of high interest for our work, as it would avoid the peptide of interest to attach to the non-wanted areas, retaining the polymer pattern.

5.1.2 EXPERIMENTAL SECTION

Materials and substrates

The initial work was carried out on regular silicon wafers. The cellular culture microarrays and microneedles were also a silicon based system, developed by the System Integration Department and the Biomedical Applications Group in the National Centre for Microelectronics (CNM-IMB, CSIC) in Barcelona, Spain.

The masks for the selective polymerization were perforated silicon wafers 0,5mm thick.

Sample preparation

The substrates were coated with a silicon oxide layer to guarantee the good self assembly with a PEG-like system. These arrays were functionalized with an 2-[methoxy(polyethyleneoxy)propyl]trimethoxysilane self assembled layer, by the next procedure, to achieve a continuous system and avoid delaminating problems.

The silicon oxide substrates coming from clean room were sonicated in a methanol, a mixture of methanol/chloroform (1:1) and pure chloroform for 5 minutes each time. A 3mM PEG-silane solution in dry toluene with 0.8 ml of HCl_{conc}/L is prepared, and the samples introduced in it for 18h at room temperature. After this the samples were sonicated again in chloroform, chloroform-methanol mixture and methanol for 5 min each.³¹⁻³³

To ensure optimum adhesion of the plasma polymer on the platinum electrodes a second monolayer consisting of hexanethiol was self-assembled on the substrates before plasma polymerization. After the methanol samples were sonicated in ethanol for another 5 min. A 10 mM 1-hexanethiol in ethanol solution with several hours immersion was used for this second depositing the SAM. Samples were rinsed after in ethanol and finally dried with dry N₂.³⁴

This kind of selective functionalization with silanes and thiols SAMS has been already been used by some groups.²¹

Masks design

The masks were designed with several patterns of different shapes, corresponding to the different zones of electrodes of the microdispositives. This was done in order to functionalize them selectively and create guides to enhance cell growth.

The masks were manufacture in quartz, defining in chromium the patterns that would be transferred by lithographic methods later on.

The original design consists of three zones, presented in Figure 5.2:

In zone 1, the shape corresponds to the Microtrans microneedles. In zone 2, the pattern is defined as an equivalent of the CNM and IQS logos. In the last zone, the profiles are defined in relationship to the Microcell microarrays:

- a) pattern equivalent to the position of the electrode's array
- b) rectangle that includes all the array of electrodes
- c) diagonal channels that interconnect the microelectrodes
- d) chess pattern, that exposes just some of the electrodes to the plasma

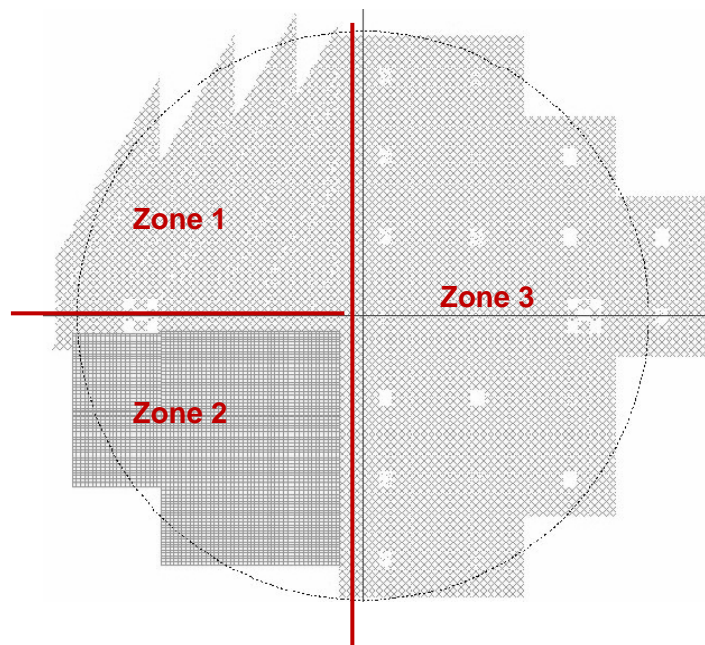


Figure 5.2 Design of the masks on a silicon wafer

The next figures give details of the different shapes with their dimensions in micrometers.

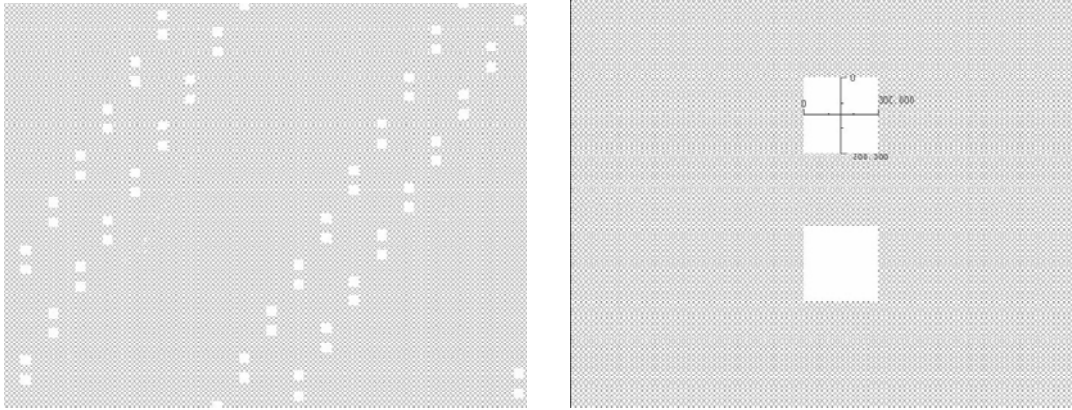


Figure 5.3 Detail of pattern in Zone 1

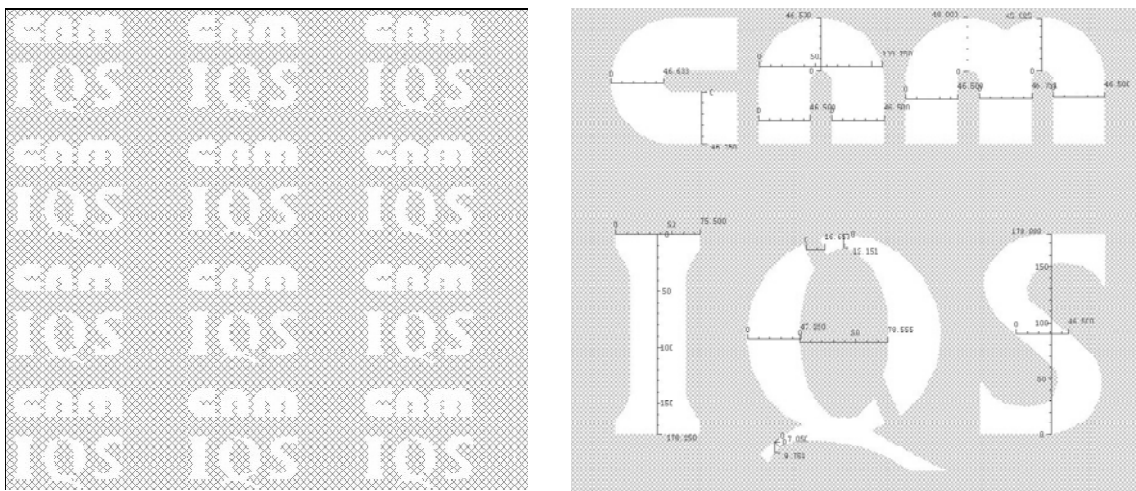


Figure 5.4 Detail of logos in zone 2

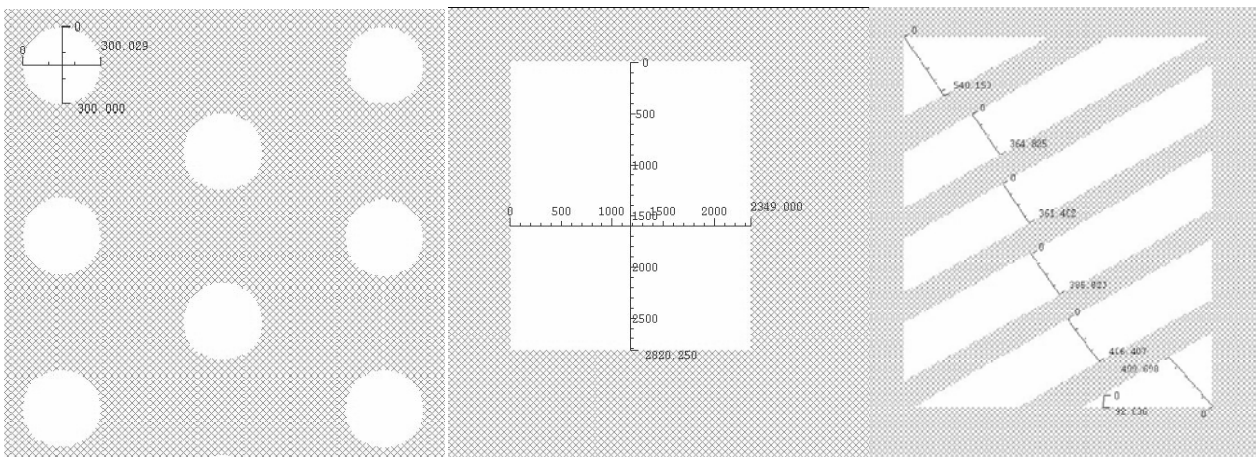


Figure 5.5 Detail of patterns in zone 3

Masks' manufacture

The process of manufacture of the masks was by perforation of a silicon wafer in a clean room from the already designed mask in the previous step. This design as well as the manufacture of the masks was developed by the CNM-IMB biomedical applications group.

The manufacture technique for the silicon engrave is the Silicon Deep Reactive Ion Etching (DRIE). This kind of engrave is done in a dry environment and is based in the combination of two gas mixtures that alternate in the reactor. This technique allows an engrave ratio of 30:1 (depth:width) and angles next to the walls of $90^{\circ} \pm 2^{\circ}$.

The major problems with this technique were found when working with zone 2. The logos presented different dimensions, what is one of the limitations of the DRIE technique. This technique is selective with the engrave dimensions, giving priority to the large measurements. When the small patterns are to be done, the original shape is deformed. For the logos in zone 2, one of the wafer sides, front side, presents better resolution than the other one, back side, as can be observed in Figure 5.6.

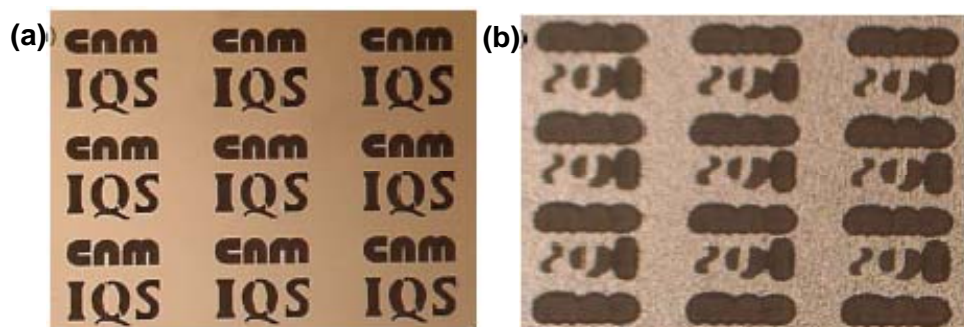


Figure 5.6 Details of the final appearance of the mask in zone 2, (a) front side and (b) back side

For the other two zones, the process is finished without remarks. The appearance of the masks is presented in Figure 5.7.

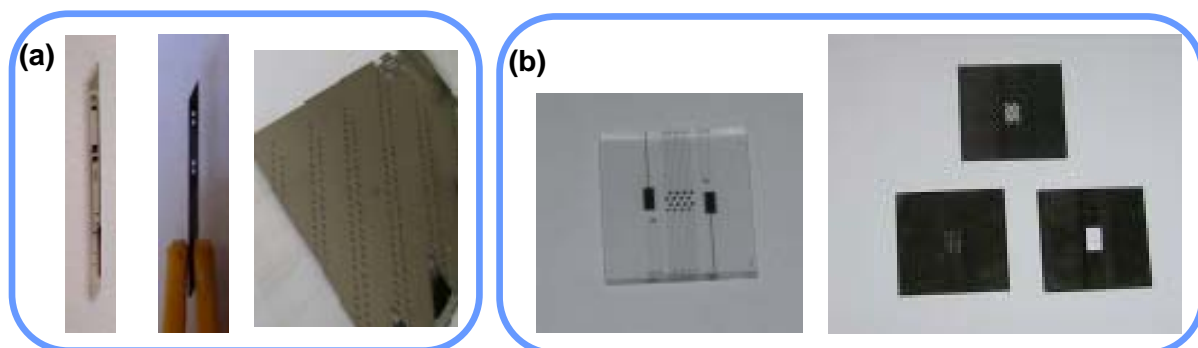


Figure 5.7 Details of the different masks, (a) masks belonging to the Microtrans needles, (b) masks of the Microcells arrays

Different masks thicknesses have been achieved. The original wafer thickness, 500 microns wasn't longer treated beside the pattern. 400 microns thick masks were achieved by polishing the already engraved masks and a last one of 150 microns was achieved by acid attack of the silicon wafer. Since all the masks were already engraved, these post-treatments also reflected changes in the patterns.

Plasma polymerization

The plasma polymerization was done in *system 2*, for the first tries with the masks on silicon wafer and for the microneedles, and in *system 1* for the real microarrays samples.

For both systems, the best conditions of polymerization to achieve the desired structure of pp-PFM were developed in chapter 2. First experiments were done with all the masks. When working with the mask of zone 2 (logos), a comparison between the front and the back side was done.

Surface analysis

The chemical characterization of the plasma polymerized coating has been discussed extensively in chapter 2, as well as its stability and reactivity. In this section, we have concentrated in the morphology of the achieved polymer when working with masks. The characterization has been done with a *Olympus SZ-40* stereozoom microscope, a *New View 100* interferometric microscope, from Zygo; and a *μSurf* confocal microscope, from Nanofocus.

The samples analyzed with the stereozoom microscope were the first tries on a silicon wafer. Therefore, these samples weren't treated with special consideration, and contamination by small particles can be seen on top of them. On the other side, part of this dust is also deposited on the microscope lenses.

These same samples analyzed by the interferometric microscope present degradation by manipulation like scratches. These belong to the manipulation and are not inherent of the polymerization.

5.1.3 POLYMERIZATION WITH MASKS: COATINGS DEVELOPED IN *SYSTEM 2*

The first experiments for this application were realized over simple silicon wafers in *system 2*. The purpose of these experiments was to visualize the final polymer pattern on the substrates when using the masks to induce a selective coverage of the substrate.

A polymerization was also performed on the Microtrans needles without mask. These needles had to be tested at different stages for the *in-vivo* assays. At this point of the research, their main problem was due to the rejection in the living tissue. Therefore a first try was done without taking care of the getting the pattern

only over the electrodes, and the polymerization was done over the whole needle. These experiments with the needles will be discussed later in section 5.1.6.

Pattern achieved with the “logos” mask, zone 2

The first mask tried was the mask in zone 2 with the two logos. As it has been explained earlier, this mask presents two different sides, due to the engraving method. Both sides were tested for the polymerization, exposing each of them to the plasma and comparing the results. An additional problem has to be taken in account for this mask, as the motives engraved are the smallest in all the designed masks.

As Figure 5.8 illustrates, the patterns achieved by exposing each side to the plasma are very different. Already comparing the stereozoom microscope images, it can be seen that the pattern gotten when exposing the back side to the plasma (b) has no definition in comparison to the front side (a) exposed to the plasma. This sample shows some of the letters belonging to the IQS logo, particularly the “IQ”. Even so, the CNM logo appears as a big mass, with no definition at all. The letters of this logo can’t be recognized.

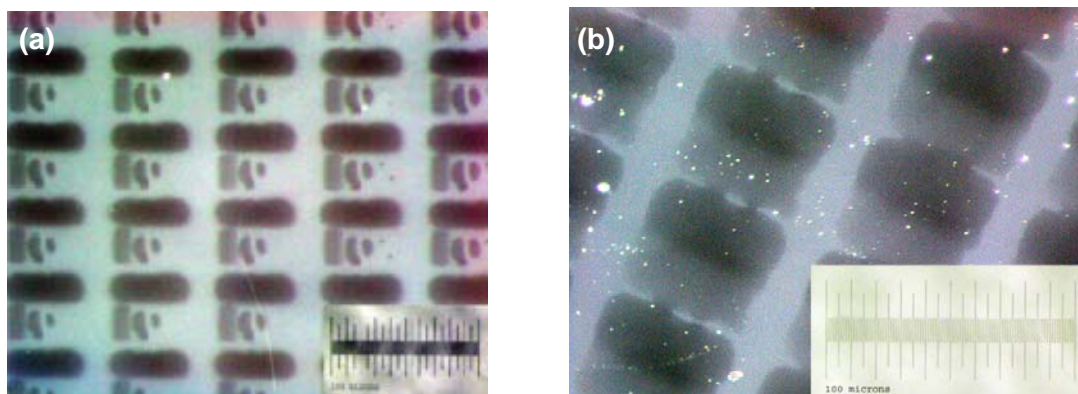


Figure 5.8 Surface obtained by polymerizing with the (a) front and the (b) back side exposed to the plasma

The “front side exposed” sample (a), has been studied with the interferometric microscope to have a better approach to the morphology of the achieved polymer. The resulting images are presented in Figure 5.9.

As it has already been discussed above, the “IQ” letters belonging to the IQS logo can be read, while the CNM logo (upper side of image b) remains unreadable. When observing the cross section in the IQ letters, it can be seen that in the zone where the letters are close, they don’t detach, losing the original definition of the mask. The thickness of the polymer achieved with this mask is around 17 nm.

When working with these masks, that present small motives, the definition of the pattern is lost in the polymerization. Therefore, another method is proposed to achieve these patterns on the surface.

A new study with Microcontact Printing of the molecules of interest on a previously polymer coated surface is suggested. Due to the lack of time, this path won't be explored in this work, but could be investigated later on.

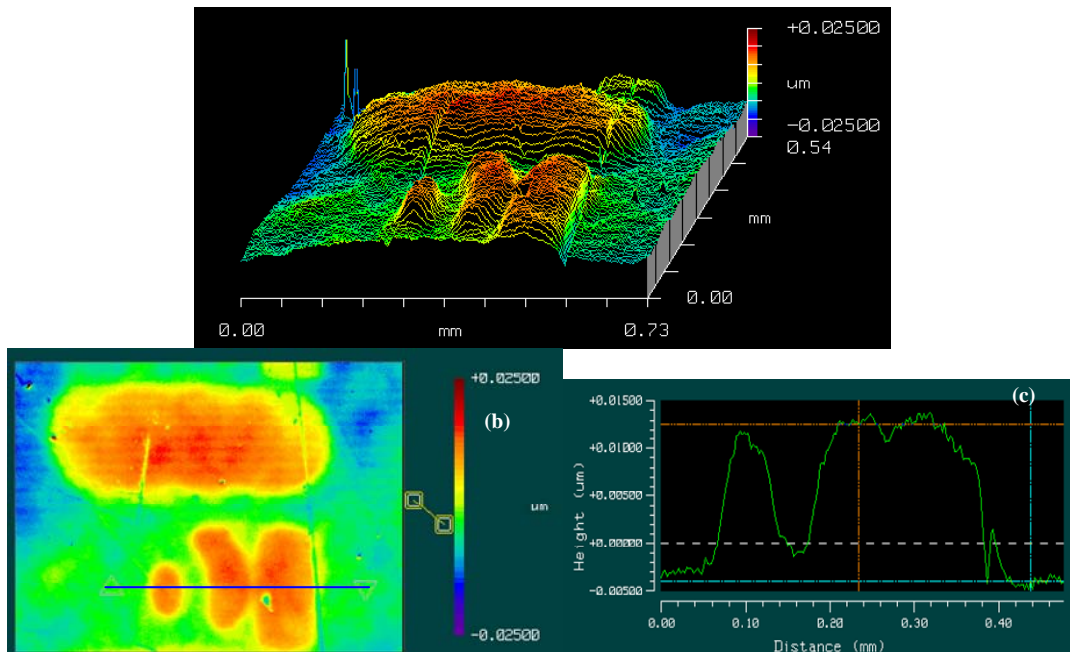


Figure 5.9 Images from the interferometric microscope belonging to the sample exposed in Figure 5.8 (a) Side image, (b) top image and (c) cross section of the IQS logo.

Pattern achieved with the mask in zone 1, “needles”, and zone 3, “chess pattern”

The results belonging to the polymerizations with the “needles” and the “chess pattern” in zone 1 and 3 are explained in this section.

Figure 5.10 shows the stereozoom microscope images of each polymerization. In both cases, the motives of the masks are well defined, being easily recognizable just with this technique.

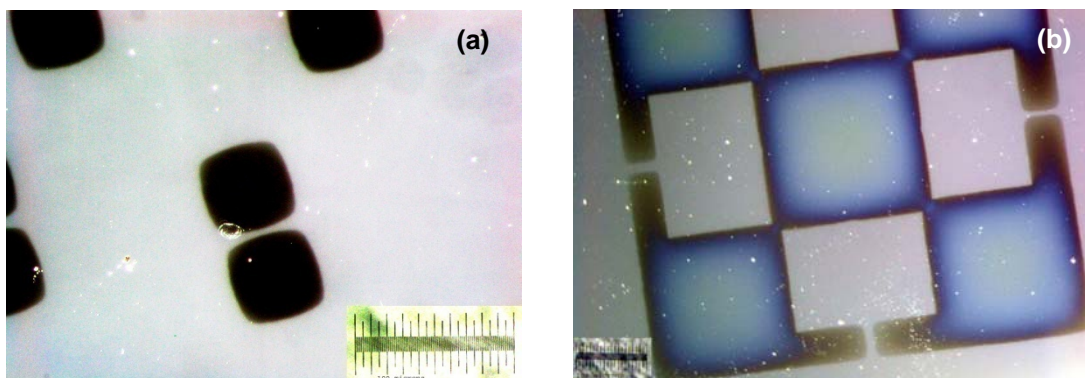


Figure 5.10 Images obtained with the stereomicroscope with the (a) needles mask and (b) “chess pattern”

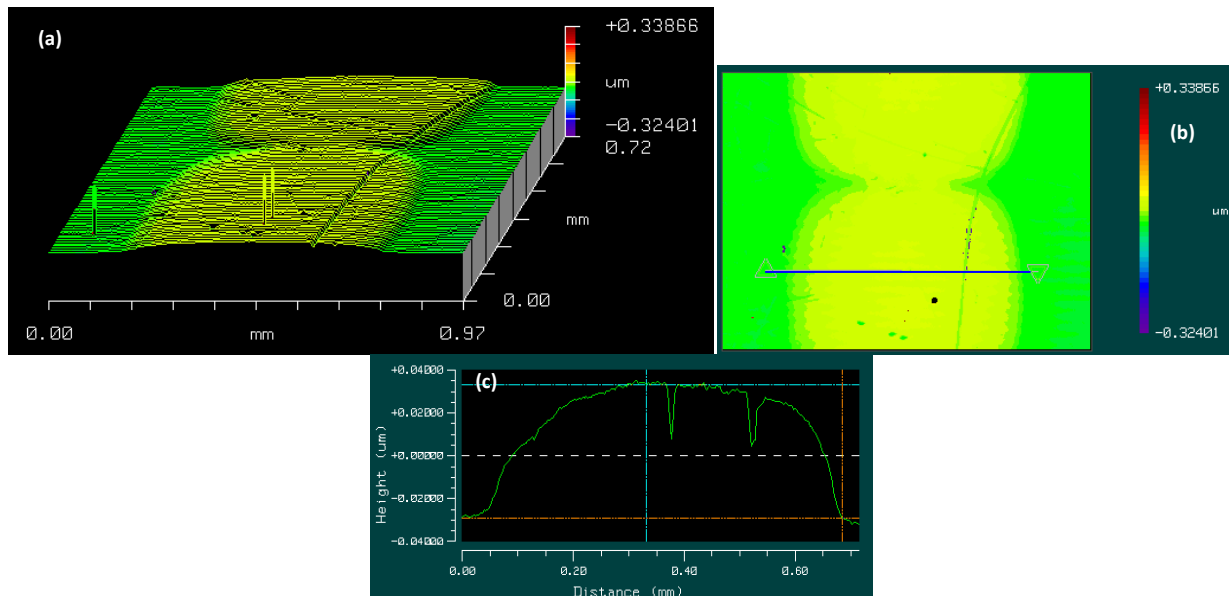


Figure 5.11 Images from the interferometric microscope belonging to the sample exposed in Figure 5.10 (a) Side image, (b) top image and (c) cross section of the polymer.

For a better quantification of the deposits, the analysis with the interferometric microscope was performed. Figure 5.11 shows the results for the “needles” mask, exposed in Figure 5.10 (a).

The pattern of the mask was to be recognized in the resulting polymer after the exposition to the plasma. The cross section gives a 62 nm thickness. By enlarging the measurements of the pattern, it is easier to polymerize thicker films than in the case of the “logos” mask. The width of the electrode’s pattern can be determined around 550-600 microns. This width is larger than the one of the mask, which is 300 microns, making clear that the polymer grows under the limits of the mask’s pattern. Even though, the polymer doesn’t grow all over the surface, but in the zones near the motive, following its form.

Figure 5.12 presents the interferometric microscope images obtained from the “chess pattern” mask, exposed in Figure 5.10 (b). The pattern is too big to be observed by the interferometric microscope as a whole. Therefore, just one box has been picked to characterize the film.

Taking a look at the cross section, it can be seen that polymer growth has been more marked in the center of the box. The thickness at this point is around 130 nm, while it is around 60 nm when getting near the edges of the mask. In this case, near the edge, the thickness of the film is in the same value that the thickness obtained with the previous mask (Figure 5.11). The width of the square is 1.4 mm. As in the previous sample, it can be seen that as the size of the motive gets larger, the polymerization makes a bigger progress. For the same polymerization times, the thickness of the films is higher.

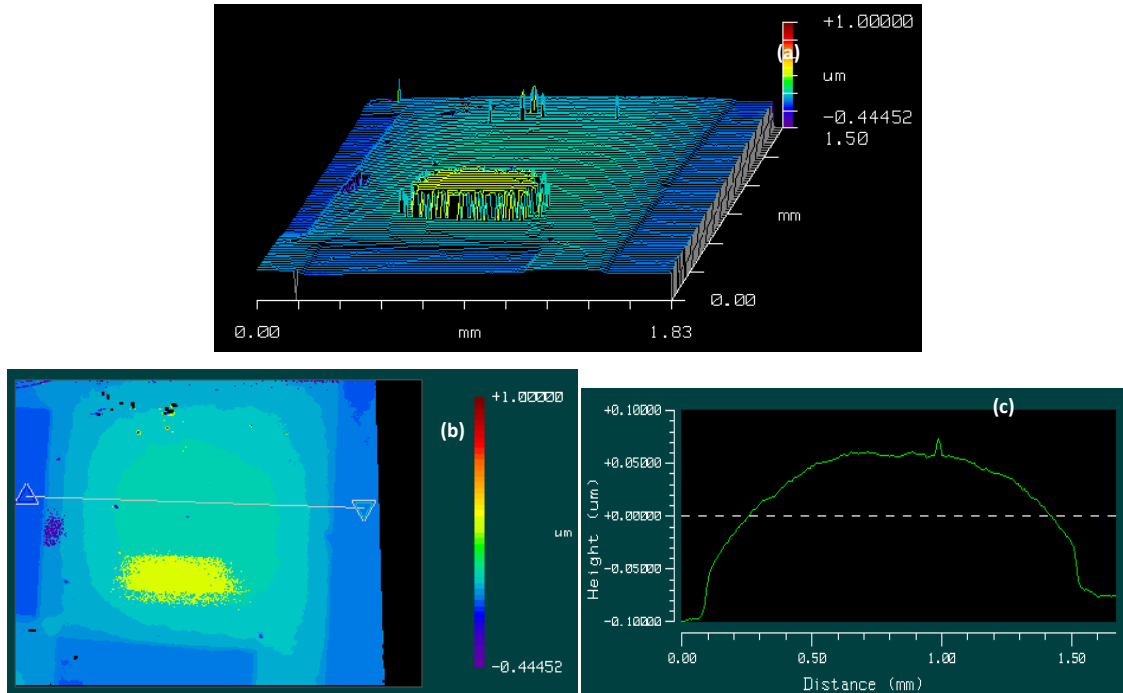


Figure 5.12 Images from the interferometric microscope belonging to the sample exposed in Figure 3.22 (a) Side image, (b) top image and (c) cross section of the coating.

This is an indication that with smaller patterns (like in the logos mask) an accessibility problem can be occurring for the polymerization. We think that a preferential polymerization can be occurring on the edges of the mask, avoiding the polymer to get to the surface of the substrate.

To try to clarify this point, masks with different thickness will be used for the subsequent polymerizations.

Pattern achieved with the mask zone 3, “electrodes array”

Masks with the same pattern but with different thicknesses will be used in the set of experiments, to see the influence of this thickness over the resulting polymeric pattern. In this case, the motive used is the “electrodes array” in zone 3.

The original wafer thickness was 500 microns. A 400 microns thick mask was done by polishing already engraved masks. As the polishing is a very aggressive method, it has to be noticed, that the original design of the pattern was changed, moving the electrodes’ holes apart from each other, to avoid mechanical breakage by the manipulation. A last mask with 150 microns thickness was achieved by acid attack of the silicon wafer original wafer. In this last case, by the acid attack, the pattern was also slightly changed, because the electrodes’ holes were enlarged by the procedure.

Figure 5.13 presents the resulting polymers explored with the stereozoom microscope:

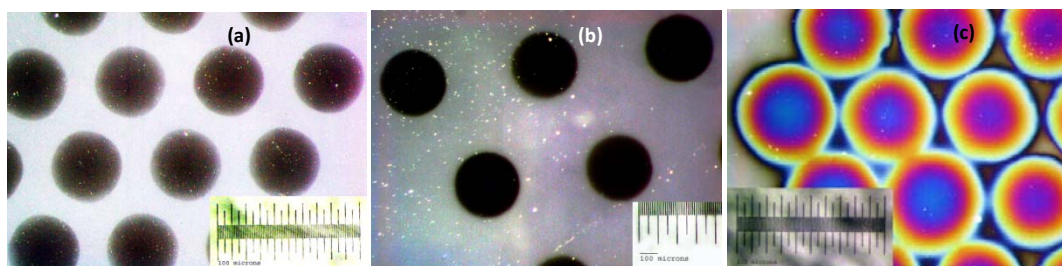


Figure 5.13 Images obtained with the stereozoom microscope with the (a) 500 microns (b) 400 microns and (c) 150 microns thick masks

Just by taking a look into the images, it is easy to recognize the difference between the polymerizations. Comparing the resulting polymer circles, the second set (b) presents a more distant distribution in contrast to the original mask's set (a). In the third case, the circles even come in contact with each other.

To have a better idea of the influence of the thicknesses, the interferometric microscope was used, obtaining the images exposed in Figure 5.14.

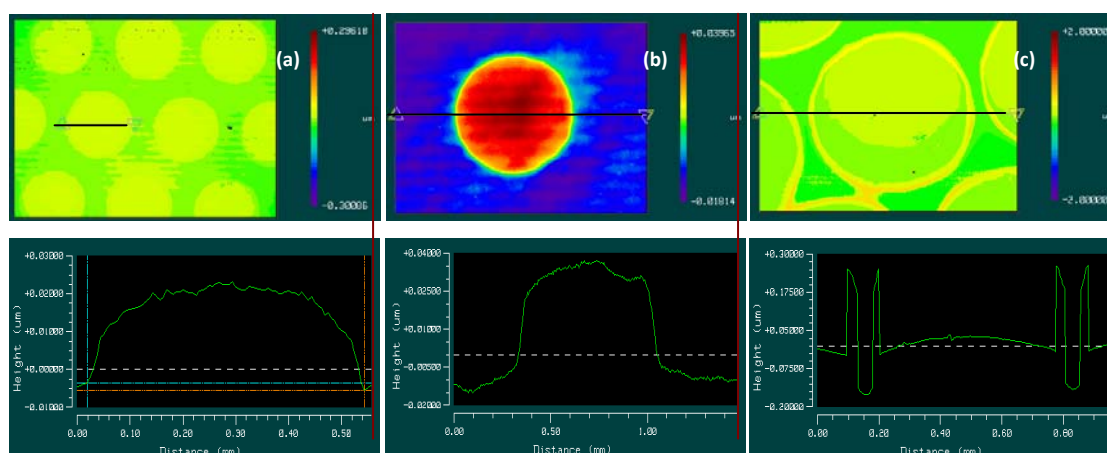


Figure 5.14 Images obtained with the interferometric microscope with the (a) 500 microns (b) 400 microns and (c) 150 microns thick masks

Interferometry shows the values of height and diameter of the circles achieved in each case, presented in Table 5.1.

Table 5.1 Height and diameter of the resulting circles obtained by polymerization of mask with different thickness

Mask thickness / μm	Height / nm	Diameter / μm
500	28	525
400	50	900
150	200	650

When using the 500 microns thick mask, the film thickness is around 28 nm. This shows that, even if the hole's diameter in the mask is equivalent to the one in the square side in the "needles" mask (300 microns), the geometry of the pattern has an influence on the thickness of the film. The film thickness in the case of the circle is smaller than in the case of the square.

When the thickness of the mask is reduced it can be observed that the height of the circle increases, getting to 200 nm for the sample corresponding to the 150 microns thick mask. In this case, it can be seen that there is a preferential polymerization around the edges of the pattern. In this zone, the thickness of the polymer rises up to more than 400 microns, resulting in polymer "hole".

When looking at the values of the circles' diameter, it is remarkable, that in all the cases they are higher than the mask's diameter. This phenomenon was already observed in the previous polymerizations, where the polymer was growing beyond the pattern's limits. This study brings up that by reducing the mask's thickness, this trend seems to rise, getting a higher polymer expansion. But when observing the last mask, that was 150 microns thick, the tendency appears to stop, showing a smaller diameter. By regarding the cross sections, this sample is the one showing a preferential polymerization around edges, which impedes the growing of the polymer in the covered areas of the substrates, far from the mask's holes.

This event has revealed a non-expected concept for the group over the preferential polymerization when using the masks. This will be explored further on in the next section 5.1.4, to see if the polymerization time has also an influence over it, in a way that it could be controllable.

Pattern achieved with the mask zone 3, "diagonals"

As in the previous case, masks with the same pattern but with different thicknesses will be used in the set of experiments. In this case, the motive used is the "diagonals" in zone 3.

The procedure for getting the different masks is equivalent to the one described above, including the design's changes. The resulting masks are 500, 400 and 150 microns thick.

Figure 5.15 (next page) presents the resulting polymers explored with the stereozoom microscope.

In these images, all samples seem to be different to each other. This mask is especially fragile, so that by its manipulation it is easy to "loose" diagonal bars. This is what happened for the first image, where the diagonal bars were lost, except in the two corners. In the case of the 400 microns thick mask, one of the diagonals has also been lost. This sample, due to the enlargement of the bars thickness in the design, presents a major definition of the pattern, than the other two.

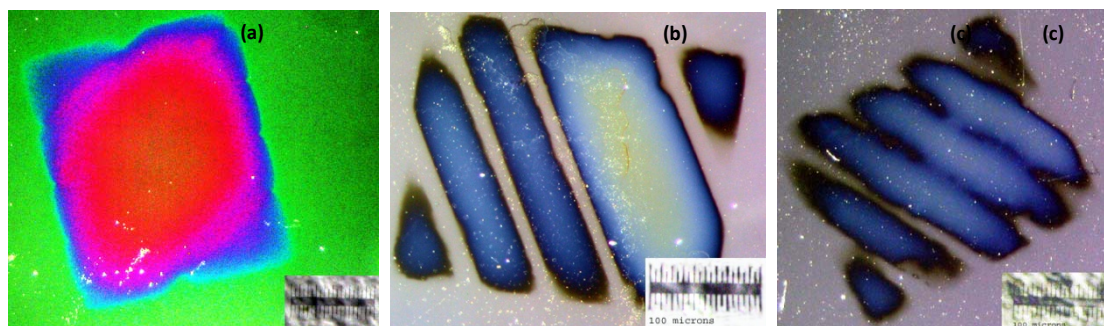


Figure 5.15 Images obtained with the stereozoom microscope with the (a) 500 microns (b) 400 microns and (c) 150 microns thick masks

For the interferometry measurements, the first sample has been avoided, as by the loss of the diagonal bars, its geometry is too changed from the original one, and its measurements would be confusing. Results for samples (b) and (c) are presented in Figure 5.16.

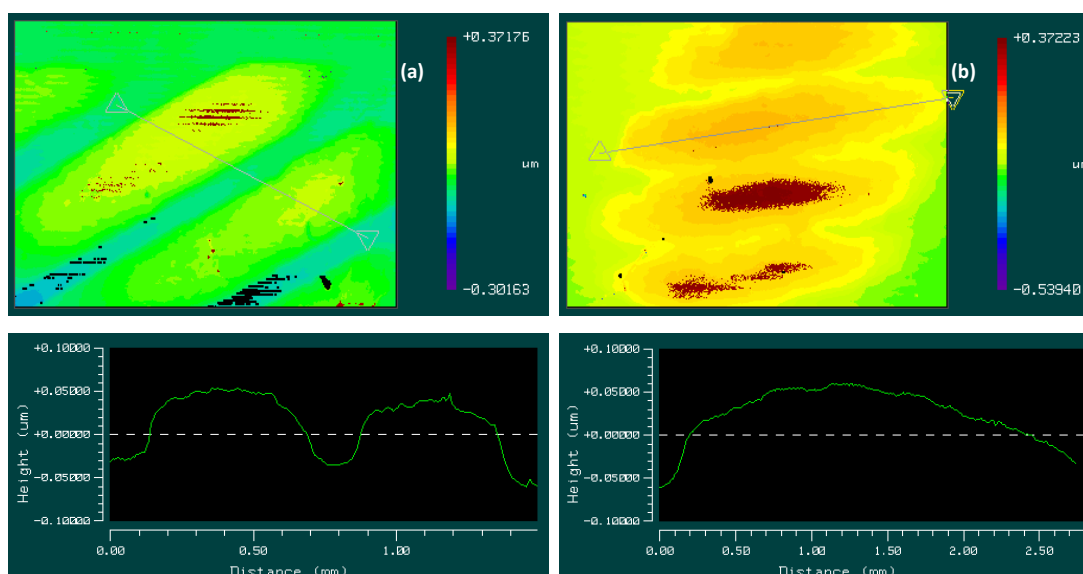


Figure 5.16 Images obtained with the interferometric microscope with the (a) 400 microns and (b) 150 microns thick masks

The thickness measurements for the two samples are 70 nm for sample polymerized with the 400 microns thick mask (a) and 110 nm for the one polymerized with the 150 microns thick mask (b).

The definition of the pattern was much higher in the case of the 400 microns mask, as was already pointed out above. In the case of the less thick mask, no preferential polymerization has been observed, and the polymer has expanded over the covered zones of the substrate. It has to be remarked that the covered zones of the substrate are smaller than in the case of the “electrodes” mask.

After all these experiences, a new study is proposed. This study should take into account the mask’s thickness as well as the polymerization time, to see if there are better results in the pattern resolutions.

5.1.4 POLYMERIZATION WITH MASKS: COATINGS DEVELOPED IN *SYSTEM 1*

As the final use of these polymer patterns is to be applied for biological studies with cells, the substrates should be sterile. The definitive Microcell electrodes microarrays and the masks must be therefore aligned in sterile conditions. This was hard to be done at this stage in the IQS laboratories. For these reason, it was performed in the MPIP installations. Hence, the rest of the studies would be done in *system 1* to achieve the best conditions for the polymerization with the masks.

Therefore, the use of the different masks was tested with the “electrodes” and “diagonals” mask in zone 3. From all the masks studied, this two presented the most suitable pattern for the studies with the Microcell electrodes arrays. The thinner masks, 150 and 400 microns, presented an enhancement in the polymers achieved above. The thicknesses of the polymers were improved in comparison to the thicker mask, for both masks, revealing a better access to the substrate for the growing polymer. In view of that, these thinner masks will be studied further, to determine the best polymerization conditions in *system 1*.

Pattern achieved with the mask zone 3, “electrodes array”

The polymerization conditions for *system 1* were fixed as they were developed in chapter 2. The times of exposure to the plasma were studied between 2 and 20 min, to see if there was any growing pattern by the use of masks.

The mask used for this first study was the 150 microns thick mask. Polymerization times were fixed in 2, 5 and 20 min. Figure 5.17 presents the confocal microscope images obtained from these samples.

The use of this mask in *system 1* reported similar shapes to the ones already observed. The first thing to be seen is that depending on the exposure time, the thickness of the layer changes, getting to the already observed ‘hole’ shape. The shape of the film goes from a “circle” to a “hole”, as polymerization time increases. Taking a deeper look into the thickness values (presented in Table 5.2, next page), it has to be remarked that in this system, the film growth is much faster than the growing in system 2. Already after 2 min of polymerization, the polymer thickness is around 200 nm, which was the thickness obtained after 20 min in the previous study. By increasing the exposure time to the plasma, the thickness also increased, to values around 600 nm after 5 min. When leaving the plasma on for 20 min, the “hole” shape appeared, revealing again the preferential polymerization around the pattern edges. The thickness of the polymer film inside the “hole” is around 600 nm also, as after the 5 min experience. The walls of the “hole”, on the other side, rise to more than 2 microns.

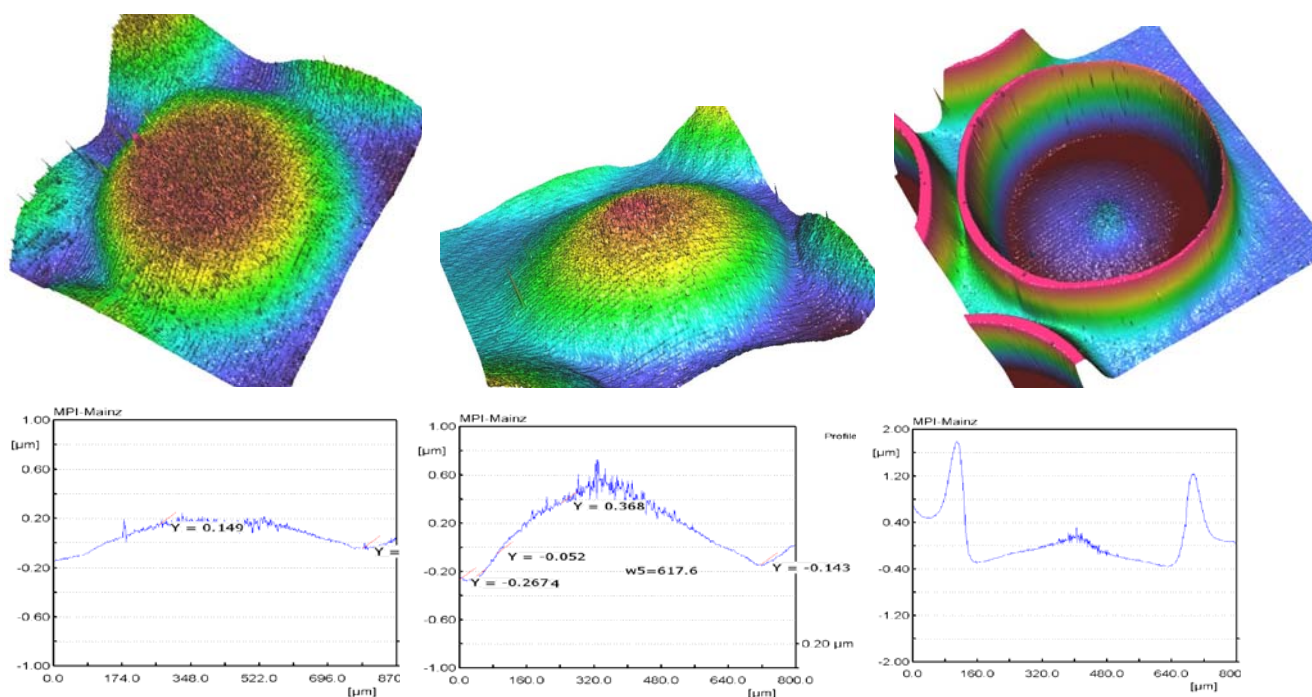


Figure 5.17 Images obtained with the confocal microscope for the polymerization with the 150 μm thick *electrodes* mask with (a) 2 min (b) 5 min and (c) 20 min polymerization time

The diameter of the circles or the “hole”, in the last case, are always around 600 microns, a value that was already present in the polymer obtained in *system 2* for this mask. This shows a maximal value for the pattern diameter with this mask.

The study was repeated for the 400 microns thick mask. In this group, polymerization times were fixed in 2, 5, 10 and 20 min. Figure 5.18 presents the confocal microscope images obtained from these samples.

Table 5.2 presents the thickness values for the films obtained with the two masks, depending on the polymerization time.

Table 5.2 Film thickness of the circles obtained by mask with different thickness and polymerization time

Mask thickness / μm	150	400
<i>Time / min</i>	<i>Film Thickness / nm</i>	
2 min	193	-
5 min	635	77
10 min	-	123
20 min	≈ 600	240

First thing to be observed in the values exposed above is that the 2 min polymerization for the 400 microns mask doesn't present any value. The polymerization did work for this exposure time, but the film was too thin to be detected with the confocal microscope. Besides this point, the rest of the polymerizations yield the expected circles pattern. Depending on the exposition time to the plasma, the circles were more defined, and distinguished better from the substrate. As in the previous case, the thickness of the polymer rises to higher values than in the precedent reactor, exceeding the values gotten for 20 min in *system 2*, 50 nm thickness, in 5 min of polymerization, around 80 nm. The growing of the polymer shows almost a linear trend with time, rising up to 240 nm thickness after 20 min of plasma exposure.

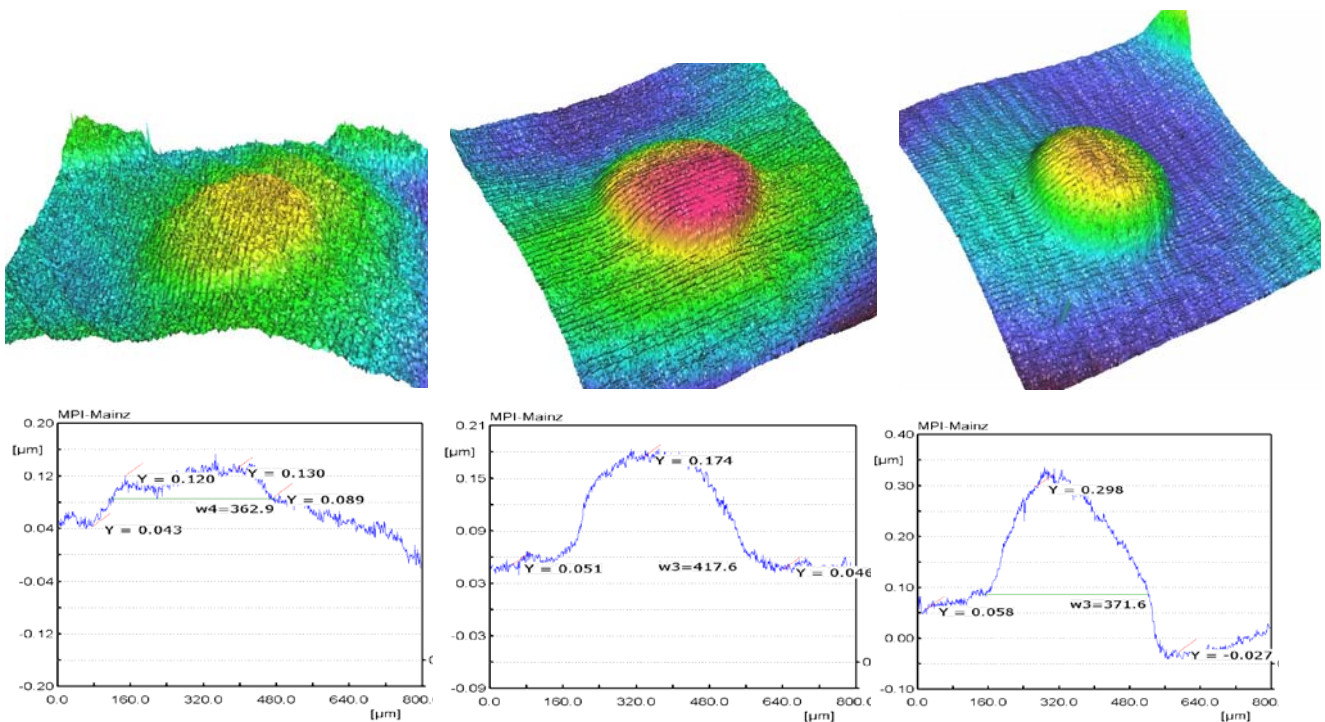


Figure 5.18 Images obtained with the confocal microscope for the polymerization with the 400 μm thick *electrodes* mask with (a) 5 min (b) 10 min and (c) 20 min polymerization time

By using this mask, no preferential polymerization around the pattern edges has been observed. The diameter of the circles registered by using this mask is around 350-400 microns, that is nearer to the value of the original design if the mask, that was 300 nm. In comparison with the experiment performed in *system 2*, these values represent a real enhancement in the polymerization. In that case, the diameter was increased to 900 microns diameter, showing a big expansion of the polymer. For this system, the polymer grows up nearer the pattern edges.

Comparing the two masks, and as expected, one can observe that the film thickness obtained for polymerization with the thinner mask are much higher than the ones for the 400 μm mask. Even though, the polymer geometry is more regular in the second case, obtaining coatings that present sharper edges at the

borders of the mask pattern. The diameters observed for the 400 microns mask represent a better retention of the original design. However it has to be remained that the “electrodes holes” of the 150 microns mask presented a higher diameter due to the acid attack the masks were exposed to, to achieve the 150 microns height. This can be a cause of the enlarging of the circles for the first set of samples.

Pattern achieved with the mask zone 3, “diagonals”

The set of experiments performed for the “electrodes” mask, will now be repeated for the “diagonals” mask. In this case, the polymerization times will be fixed to 5, 10 and 20 min.

Figure 5.19 presents the confocal microscope results obtained for the samples polymerized with the 150 microns thick mask, while Figure 5.20 does the same for the samples polymerized with the 400 microns thick mask. Table 5.3 shows the film thickness values obtained for both masks depending of the polymerization time.

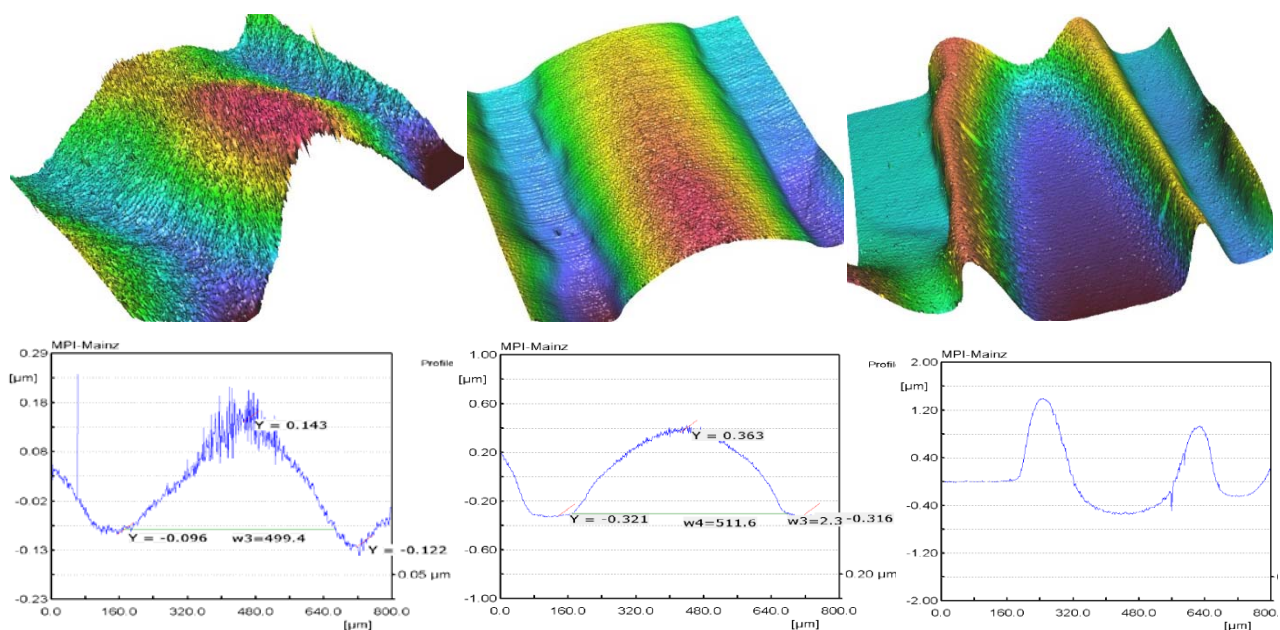


Figure 5.19 Images obtained with the confocal microscope for the polymerization with the 150 µm thick *diagonals* mask with (a) 5 min (b) 10 min and (c) 20 min polymerization time

The results obtained when working with the “diagonals” mask are comparable to the ones obtained with the ones obtained for the “electrodes” mask.

When taking a look into the samples polymerized with the 150 microns thick mask, the parallelism with the previous study is obvious. The polymer grows following the diagonal bands of the mask, increasing its thickness and definition, as the polymerization time increases. Again, the “band” shape is converted into a

“channel” as the exposure time to the plasma is 20 min, by a preferential polymerization at the pattern edges. The edge effects lead to these different shapes by getting changes in the e-field at the edges, with a final result of more deposition.

Table 5.3 Film thickness of the resulting lines obtained by polymerization of mask with different thickness and polymerization time

Mask thickness / μm	150	400
<i>Time / min</i>	<i>Thickness / nm</i>	
5 min	240	288
10 min	684	343
20 min	-	1390

The thickness of the film increases as the time rises, from 240 nm for 5 min polymers to around 680 nm for the polymer corresponding to 10 min. In the last case, the one with the “channel”, the cross section showing the profile was impossible to determine the thickness of the polymer inside the channel, as there wasn’t any uncovered substrate to compare with. Even though, it is possible to measure the channels walls height: This was found to be 2 μm , like in the case of the “hole” pattern.

In the three cases, the “band” or “channel” width is around 500 μm , staying constant as exposition time to the plasma increases.

Similar results are obtained when working with the 400 microns thick mask., in Figure 3.32. Again, the preferential polymerization on the edges of the pattern is avoided for the 20 min polymerization, as it was in the previous case.

Again the thickness increases with the polymerization time as it does the definition of the channels. The thickness shows similar values to the one for the 150 μm mask, around 250 nm, for this 400 μm mask. Even so, for the 10 min exposition, the growing of the film seems to stabilize, and presents values around 350 nm. When the time raises to 20 min, the film thickness goes up to 1400 nm, showing the highest value for all the coatings. This value is in the same order of the “channel” walls, but this time we are able to observe a whole band, with a sharp contour on the edges, following perfectly the motives of the mask.. Again, the width of the bands remains around 500 μm , following the original design of the masks.

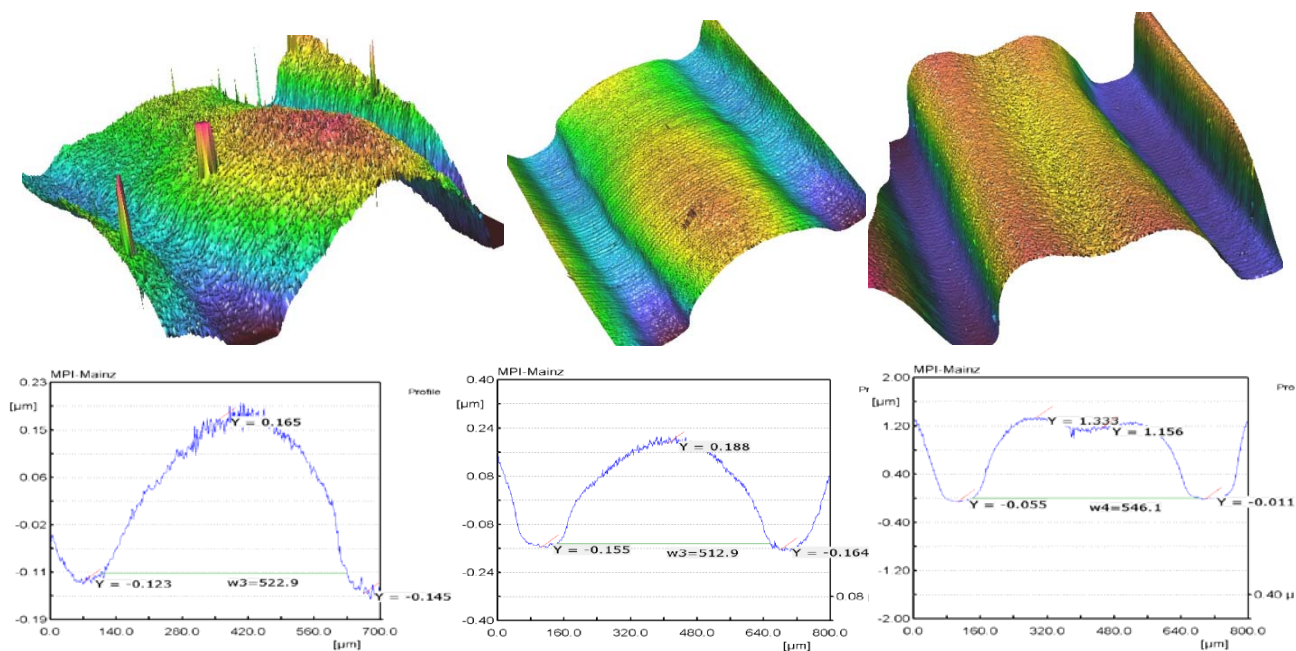


Figure 5.20 Images obtained with the confocal microscope for the polymerization with the 400 μm thick *diagonals* mask with (a) 5 min (b) 10 min and (c) 20 min polymerization time

In all the cases, the channels between bands are to be recognized, but they get more evident as the exposition time to the plasma grows.

The definition of the patterns is improved when the polymerization time rises, with these masks. The original motives have a different geometry than the “electrodes” mask, presenting a bigger exposition area, what enables an easier access of the growing polymer to the substrate surface. This is translated into fewer differences between using a 150 μm and 400 μm thick mask, than in the precedent case. Even so, when working with the thinner mask at high exposure times, the preferential polymerization at the motives edges turns out in a “channel” shape, as it was already observed for the electrodes mask.

After these two studies, it can be concluded that *system 1* presents an enhancement in the pattern of the polymers obtained, both for the polymer thickness and for the shape’s retention. The mask and the polymerization time will be chosen for further experiments in regard to these studies, depending on the shape and thickness of the films requested.

The formation of “holes” and “channels” when working at high polymerization times with opens a path to explore for the zone’s selective functionalization. Finding an easy way to selectively functionalize chosen areas is a hot topic in the patterning of surfaces. At this point, a deeper research needs to be done over this phenomenon to corroborate not only the obtained results, but also the possibility of having different

functionalities in and outside the patterns. This topic is out of the objectives of this thesis, and will be therefore not further studied. This way remains open for further researches.

5.1.5 EXPERIMENTS WITH THE MICROCELL ELECTRODES MICROARRAYS

Once the polymerization conditions studies have been done, the next step was to apply this knowledge to the “real” substrates, the Microcell electrodes array.

These arrays were covered with the PEG-like silane SAM and the thiol SAM on the electrodes, as explained before, to ensure the inorganic – organic phase continuity by the later polymerization by plasma. After this step, the substrates were sterilized in 70 % ethanol and dried in laminar flow fume hood. Also the masks were sterilized by this method.

The alignment of the electrodes on substrates and the pattern of the masks was done with the use of a Leica MS5 stereozoom microscope, with a vacuum system attach to it, placed in a laminar fume hood. The vacuum system holds the mask 1 mm above the sample that can be moved to achieve the alignment of the pattern and the electrodes. Once this is done, the vacuum is stop and the mask falls down on top of the substrate. To avoid movements of the mask and substrate as they are moved to the plasma reactor, the mask were stuck to the substrate by small piece of very thin carbon tape that is removed after polymerization.

The final conditions of polymerization were working at 50W with a duty cycle fixed at 2/52, as explained in chapter 3. At the end, there were two polymerizations. One with the “electrodes” motive mask, 400 μm thick during 5 min. The second one was done with the “diagonals” mask, 400 μm during 10 min. These two masks were chosen because of the higher resolution gotten in the shapes of the final polymer. The time of polymerization was fixed as the minimum needed to have the best definition by the smaller thickness of film.

Samples are stored in Argon for further experiments.

The polymerization procedure with the Microcells arrays have been done for practicing a cell culture on these samples. Therefore a sterilization procedure has been applied. Due to lack of time, this cell culture study was not done.

5.1.6 IMPLANTATION OF MICROTRANS NEEDLES IN RABBIT’S CORTEX

Microtrans needles are used for their implantation in rabbit’s cortex and following chronic analysis. This study will be performed in collaboration with the CNM and the Department of Hystology and the Institute of Bioengineering, Faculty of Medicine, under the coordination of Dr. Eduardo Fernández in the University Miguel Hernández, (Alacant, Spain).

Before doing the implantation, Microtrans needles were coated in *system 2*. Prior to polymerization, the needles were covered with the PEG-like silane in a self-assembled monolayer, as discussed above. As the surface was already assured to be silicon oxide, the steps of oxidation of the surface were avoided, preventing the possible damage of the platinum electrodes.

Once the needles were in the reactor, the sterilization procedure was equivalent to the one developed in chapter two. After this step, the needles were coated under 0.2 mbar monomer pressure, 50 W input power and pulsed plasma with a duty cycle 10/110. Polymerization time was fixed at 10 min and substrate's position within the reactor in position 4.

Subsequent reaction with Laminin A was done with the same conditions as the experiments in chapter 3, by exposing them to a 10g/ml (Cys0) - Laminin A (2091-2108) solution in PBS at 37°C for 1 hour and were rinsed after, always under sterility conditions.

The implantation was done in a male rabbit. Besides the Silicon-based Microtrans needles, other substrates developed in the CNM are used, but this time without the laminin coating. The electrodes are 3mm long, being distributed in function of its forming material. Figure 5.21 presents a picture of the SiC-based electrodes and its distribution in the rabbit's brain.

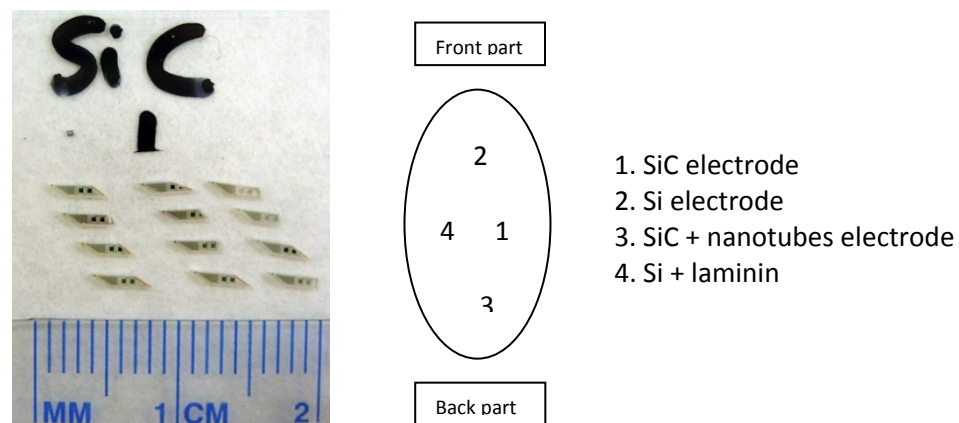


Figure 5.21 Picture of the SiC electrodes final aspect, and distribution of the electrodes in the cortex.



Figure 5.22 Experimental operating room at the Hystology department of the University Miguel Hernandez

Surgery was performed in a research operating room under asepsy conditions. Implantation of the needles was done in the south hemisphere, trying not to cross the brain cortex. The structure of the needles implies a hand implantation, with the above exposed distribution.

Macroscopic analysis

The rabbit was sacrificed after six months from the implantation, in healthy conditions.

Brain's dissection revealed the presence of connective material around all the electrodes, as shown in Figure 5.23.

There has been a movement on the original electrodes' placement. Furthermore, an expulsion from the initial placement has taken place, emerging almost totally from the cortex. A deeper analysis shows how the final placement is almost parallel to the cortex: There are no hints of implantation on the brain cortex. All electrodes present connective tissue around them of different aspect to the surrounding tissue, losing their connection to the cortex.

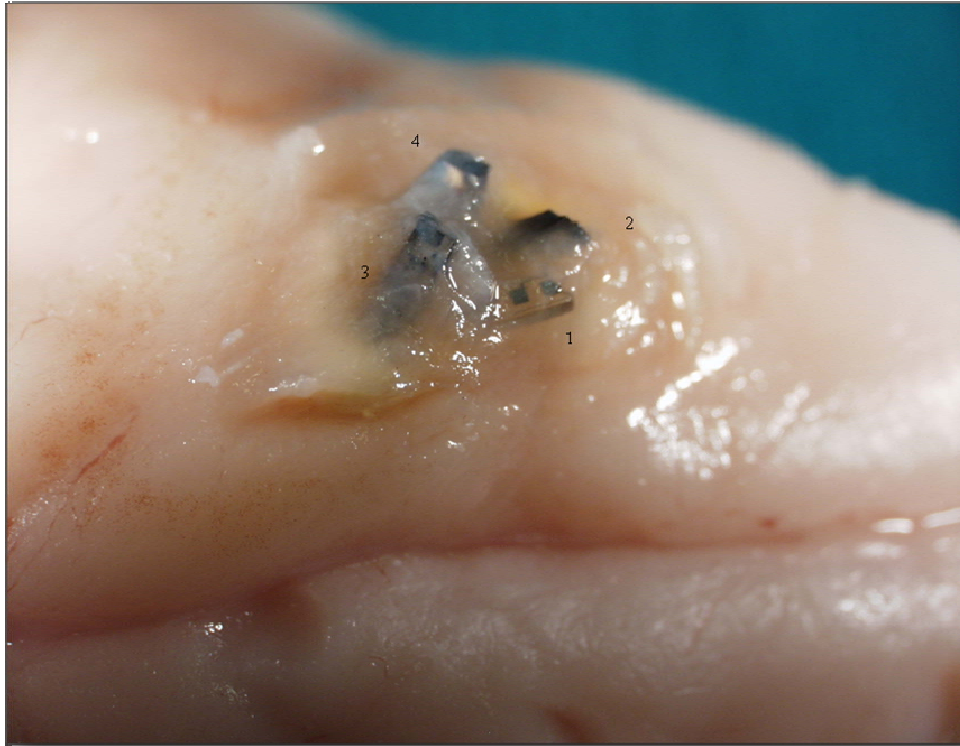


Figure 5.23 Distribution of the electrodes after six months of the implantation

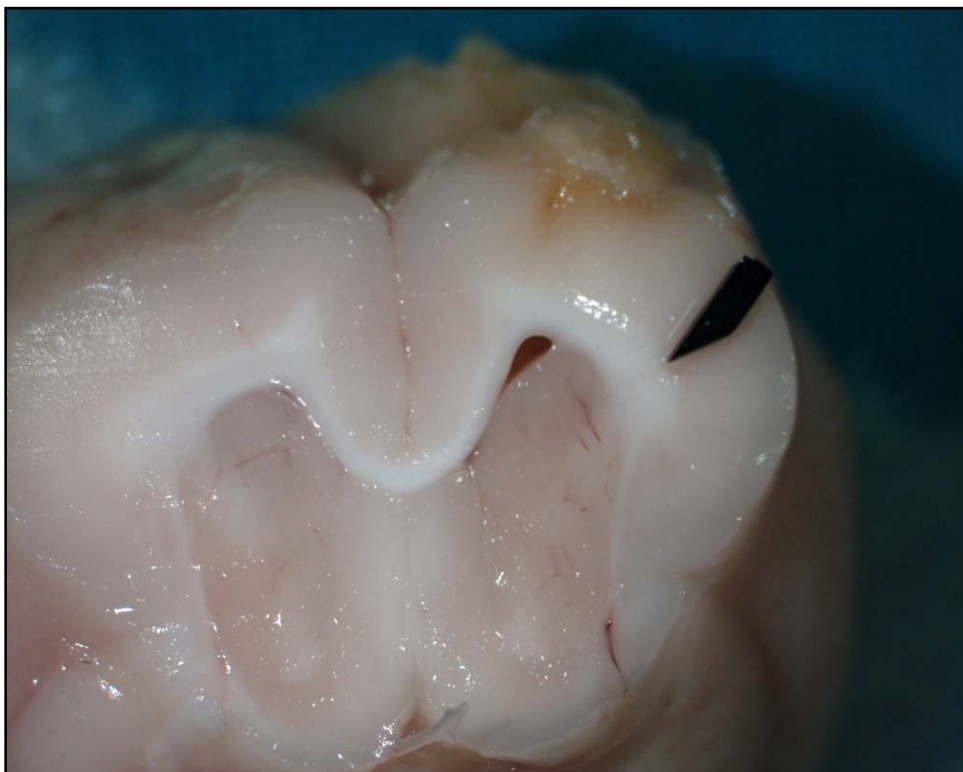


Figure 5.24 Cross section picture showing the depth of the implanted needle

Histological analysis

The tissue observed histologically with the use of hematoxylin-eosin dye didn't reveal a permanency of the needles in the brain's cortex. No samples were found where the implantation traces could be found. The outmost sections present a mainly connective tissue.

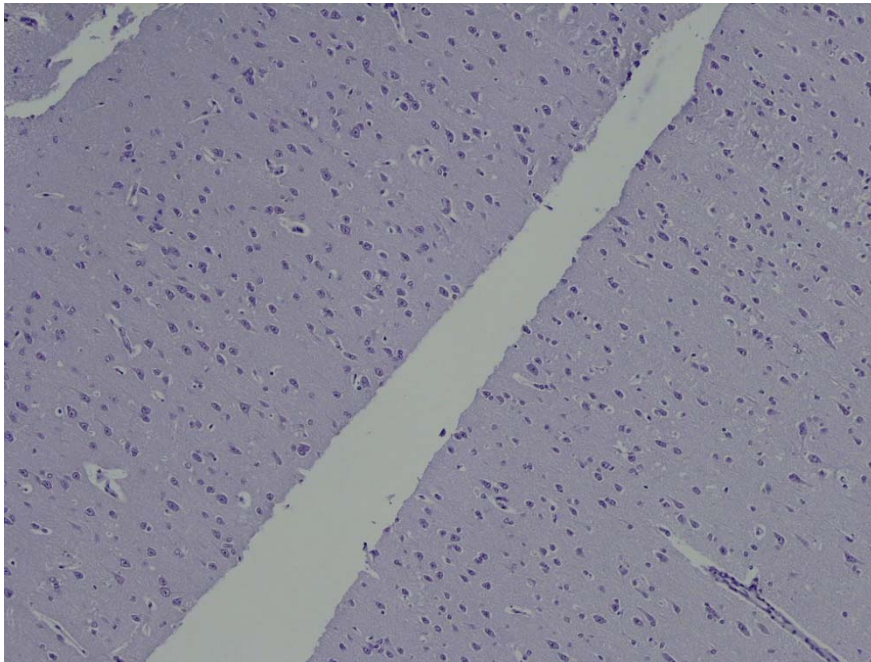


Figure 5.25 Hematoxylin-eosin tintion, 10x. There are no traces of electrodes presence

Inmunohistological analysis

Several cross sections of the studied tissue were treated with immunological techniques to try to localize regions which indicated the presence of the implanted electrodes.

The sections were incubated with glial fibrillary acidic protein (GFAP) protein antibodies: This protein is present in astrocytic glial cells, which are involved in the neurons' synapses. There is no presence of regions with glial healing that is caused by astrocytes.

The implantation of these first set of Microtrans needles has failed in term of connectivity with the brain's cortex. The connection between the materials and the living tissue hasn't been developed, by forming an external tissue to surround the artificial materials. Many factors could be contributing to this result, and a deeper study should be performed before the rejection of the developed needles.

5.1.7 SUMMARY

In this chapter; the plasma polymerization of pentafluorophenyl methacrylate in selected zones has been achieved by the use of the silicon masks developed in the CNM, in two different plasma systems.

The patterns have been reproduced on modified silicon wafer samples. For 500 μm thick masks the reproduction of big motives has been achieved successfully, even though small patterns (like the logo) are slightly defined.

By using thinner masks, the polymer deposition increases for the same exposition time. The definition of the patterns achieved with the thinnest masks (150 μm) is smaller, due in part to the motives enlarging by the mask's preparation. It can be observed that for high deposition times there is a formation of channels or holes depending on the pattern used, due to edge effects that lead to higher depositions near the masks edges. This phenomenon is independent of the polymerization system used.

The Microtrans needles were modified with pp-PFM and (cys0)-laminin attach to them. The in-vivo assays failed in term of connectivity with the brain's cortex. Even though, a positive result might be extracted out this experiment. Contrary to the precedent implantation experiments, the rabbit was able to survive during more than three months, until programmed death.

5.2 REFERENCES

1. Llinas, R.; Nicholson, C.; Johnson, K. In *Brain unit activity during behavior*, Phillips, M. I., Ed.; Springfield, IL: Thomas: **1973**; pp 105-111.
2. Edell, D. J. A Peripheral Nerve Information Transducer for Amputees: Long-Term Multichannel Recordings from Rabbit Peripheral Nerves. *Biomedical Engineering, IEEE Transactions on* **1986**, *BME-33* (2), 203-214.
3. Kovacs, G. T.; Storment, C. W.; Miller, M. H.; Belczynski, C. R.; Della Santina, C. C.; Lewis, E. R.; Maluf, N. I. Silicon-substrate microelectrode arrays for parallel recording of neural activity in peripheral and cranial nerves. *Biomedical Engineering, IEEE Transactions on* **1994**, *41* (6), 567-577.
4. Mensinger, A. F.; Anderson, D. J.; Buchko, C. J.; Johnson, M. A.; Martin, D. C.; Tresco, P. A.; Silver, R. B.; Highstein, S. M. Chronic Recording of Regenerating VIIIth Nerve Axons With a Sieve Electrode. *J Neurophysiol* **2000**, *83* (1), 611-615.
5. Regehr, W. G.; Pine, J.; Rutledge, D. B. A long-term in vitro silicon-based microelectrode-neuron connection. *Biomedical Engineering, IEEE Transactions on* **1988**, *35* (12), 1023-1032.
6. Potter, S. M.; DeMarse, T. B. A new approach to neural cell culture for long-term studies. *Journal of Neuroscience Methods* **2001**, *110* (1-2), 17-24.
7. Gross, G. W.; Kowalski, J. M. Experimental and Theoretical Analysis of Random Nerve Cells Dynamics. In *Neural Networks: Concepts, Applications and Implementations*, Antognetti, P., Milutinovic, V., Eds.; Prentice Hall: New Jersey, **1991**; pp 47-110.
8. Jones, K.; Campbell, P.; Normann, R. A glass/silicon composite intracortical electrode array. *Annals of biomedical engineering* **1992**, *20* (4), 423-437.
9. Veraart, C.; Grill, W. M.; Mortimer, J. T. Selective control of muscle activation with a multipolar nerve cuff electrode. *Biomedical Engineering, IEEE Transactions on* **1993**, *40* (7), 640-653.
10. Patterson, W. R.; Song, Y. Q.; Bull, C. W.; Ozden, I.; Deangellis, A. P.; Lay, A. P.; McKay, J. L.; Nurmikko, A. V.; Donoghue, J. D.; Connors, B. W. A microelectrode/microelectronic hybrid device for brain implantable neuroprosthesis applications. *Biomedical Engineering, IEEE Transactions on* **2004**, *51* (10), 1845-1853.
11. Najafi, K.; Ji, J.; Wise, K. D. Scaling limitations of silicon multichannel recording probes. *Biomedical Engineering, IEEE Transactions on* **1990**, *37* (1), 1-11.
12. McCreery, D. B.; Agnew, W. F.; Bullara, L. A. The Effects of Prolonged Intracortical Microstimulation on the Excitability of Pyramidal Tract Neurons in the Cat. *Annals of biomedical engineering* **2002**, *30* (1), 107-119.
13. Turner, J. N.; Shain, W.; Szarowski, D. H.; Andersen, M.; Martins, S.; Isaacson, M.; Craighead, H. Cerebral Astrocyte Response to Micromachined Silicon Implants. *Experimental Neurology* **1999**, *156* (1), 33-49.
14. Maynard, E. M.; Fernandez, E.; Normann, R. A. A technique to prevent dural adhesions to chronically implanted microelectrode arrays. *Journal of Neuroscience Methods* **2000**, *97* (2), 93-101.
15. Schwartz, A. B. Cortical neural prosthetics. *Annual Review of Neuroscience* **2004**, *27*, 487-507.
16. Sciaratta, V.; Vohrer, U.; Hegemann, D.; Muller, M.; Oehr, C. Plasma functionalization of polypropylene with acrylic acid. *Surface and Coatings Technology* **2003**, *174-175*, 805-810.
17. Robblee, L. S.; McHardy, J.; Agnew, W. F.; Bullara, L. A. Electrical stimulation with Pt electrodes. VII. Dissolution of Pt electrodes during electrical stimulation of the cat cerebral cortex. *Journal of Neuroscience Methods* **1983**, *9* (4), 301-308.
18. Cogan, S. F.; Guzelian, A. A.; Agnew, W. F.; Yuen, T. G. H.; McCreery, D. B. Over-pulsing degrades activated iridium oxide films used for intracortical neural stimulation. *Journal of Neuroscience Methods* **2004**, *137* (2), 141-150.
19. Moxon, K. A.; Kalkhoran, N. M.; Markert, M.; Sambito, M. A.; McKenzie, J. L.; Webster, J. T. Nanostructured surface modification of ceramic-based microelectrodes to enhance biocompatibility for a direct brain-machine interface. *Biomedical Engineering, IEEE Transactions on* **2004**, *51* (6), 881-889.
20. Gabriel, G.; Erill, I.; Caro, J.; Gomez, R.; Riera, D.; Villa, R.; Godignon, P. Manufacturing and full characterization of silicon carbide-based multi-sensor micro-probes for biomedical applications. *Microelectronics Journal* **2007**, *38* (3), 406-415.
21. Stapleton, M.-H.; Fraser, S. Biological sensors: probing nature's nanoscale world. *internet* **2007**.

22. Veisoh, M.; Zareie, M. H.; Zhang, M. Highly selective protein patterning on gold-silicon substrates for biosensor applications. *Langmuir* **2002**, *18* (17), 6671-6678.
23. Bremmell, K. E.; Kingshott, P.; Ademovic, Z.; Winther-Jensen, B.; Griesser, H. J. Colloid probe AFM investigation of interactions between fibrinogen and PEG-like plasma polymer surfaces. *Langmuir* **2006**, *22* (1), 313-318.
24. Bell, D. J.; Brody, J. P.; Yager, P. Using poly(ethylene glycol) silane to prevent protein adsorption in microfabricated silicon channels. *Proceedings of SPIE-The International Society for Optical Engineering* **1998**, 3258 (Micro- and Nanofabricated Structures and Devices for Biomedical Environmental Applications), 134-140.
25. Zhang, F.; Kang, E. T.; Neoh, K. G.; Wang, P.; Tan, K. L. Modification of Si(100) surface by the grafting of poly(ethylene glycol) for reduction in protein adsorption and platelet adhesion. *Journal of Biomedical Materials Research* **2001**, *56* (3), 324-332.
26. Zou, X. P.; Kang, E. T.; Neoh, K. G. Plasma-Induced Graft Polymerization of Poly(ethylene glycol) Methyl Ether Methacrylate on Si(100) Surfaces for Reduction in Protein Adsorption and Platelet Adhesion. *Plasmas and Polymers* **2002**, *7* (2), 151-170.
27. Zhang, F.; Kang, E. T.; Neoh, K. G.; Wang, P.; Tan, K. L. Surface modification of stainless steel by grafting of poly(ethylene glycol) for reduction in protein adsorption. *Biomaterials* **2001**, *22* (12), 1541-1548.
28. Malmsten, M. *Biopolymers at Interfaces: Second Edition, Revised and Expanded.*; 2 ed.; Marcel Dekker, Inc.: 2003; Vol. 110.
29. Ostuni, E.; Chapman, R. G.; Liang, M. N.; Meluleni, G.; Pier, G.; Ingber, D. E.; Whitesides, G. M. Self-assembled monolayers that resist the adsorption of proteins and the adhesion of bacterial and mammalian cells. *Langmuir* **2001**, *17* (20), 6336-6343.
30. Houseman, B. T.; Mrksich, M. The microenvironment of immobilized Arg-Gly-Asp peptides is an important determinant of cell adhesion. *Biomaterials* **2001**, *22* (9), 943-955.
31. Papra, A.; Gadegaard, N.; Larsen, N. B. Characterization of ultrathin poly(ethylene glycol) monolayers on silicon substrates. *Langmuir* **2001**, *17* (5), 1457-1460.
32. Backmann, N.; Zahnd, C.; Huber, F.; Bietsch, A.; Pluckthun, A.; Lang, H. P.; Guntherodt, H. J.; Hegner, M.; Gerber, C. A label-free immunosensor array using single-chain antibody fragments. *Proceedings of the National Academy of Sciences of the United States of America* **2005**, *102* (41), 14587-14592.
33. Padeste, C.; Sorribas, H.; Tlefemauer, L. Photolithographic Generation of Protein Micropatterns. *PSI Annual Scientific Report* **2000**.
34. Geissler, M.; Chen, J. Y.; Xia, Y. N. Comparative study of monolayers self-assembled from alkylisocyanides and alkanethiols on polycrystalline Pt substrates. *Langmuir* **2004**, *20* (17), 6993-6997.

[CHAPTER 6]

CONCLUSIONS

CHAPTER 6

CONCLUSIONS

The work described in this thesis concerns the surface tailoring of materials by plasma modification techniques, as plasma grafting and plasma polymerization. In particular, thin polymeric films bearing labile functionalities were synthesized by plasma polymerization of a monomer containing an active group, pentafluorophenyl. Different plasma systems were used in order to determine if the group retention was independent of the reactor used. In addition to the synthesis, attention was directed towards the characterization of these films, and the tailoring of their surface properties on a molecular level. The reactivity of the coatings towards amines and peptides was characterized. Finally, these reactive groups were used for the subsequent immobilization of peptides, cell culture and *in vivo* assays. From this work it can be concluded that:

1. A first approach to plasma polymerization and to plasma grafting has been developed. Control of the surface's characteristics has been achieved for the first time in our group. It has been possible to graft the PFM to the surfaces, and the linkage of proteins of interest, like biotin and streptavidin, has been done through its reactive side group. Through these proteins, the cell adhesion of endothelial cells is a reality.
2. Pentafluorophenyl methacrylate films have been achieved by polymerization techniques, leading to a reactive layer. It has been shown that even monomers containing reactive groups, such as pentafluorophenyl methacrylate, can be polymerized with high functional group retention using pulsed plasma deposition conditions. Polymerization parameters have been determined for each system in order to obtain good group retention. In the case of *system 1*, a maximum retention of the desired structure has been achieved by working at 50W with a duty cycle fixed at 2/52. The electrode's distance was fixed at 13 cm. In *system 2*, the parameters have been fixed at 50W with a duty cycle at 10/100, and the sample position has been revealed as a key factor to get a good structural retention.
3. It has been shown, that the reaction with aqueous buffer is much slower than that with primary amines. Thus, the reaction between an amine terminated reagent and the ester groups will always dominate reaction pathways in an aqueous solvent environment. It has been further shown, that the reactivity of the plasma deposits is reduced considerably if the surfaces are immersed in aqueous solution prior to reaction with the amine. These insights are of particular importance when applying these surfaces as support for the covalent attachment of peptides and other biomolecules containing amines or alcohols. Furthermore, the binding to

the surface of a peptide, (Cys0) Laminin A (2091-2108) by the presence of amino terminated groups has been achieved.

4. A new protocol has been developed to prepare the samples for cells seeding and culture experiments on modified substrates. After binding of a peptide to the surface, cells seeding has been accomplished, by a successful growing of neurons living up to 13 days on the platform. The fact that cells are able to grow on top of the polymerized surface after covalent peptide attaching shows a promising platform for cell-substrate interaction.

5. The reaction of different amines on plasma polymerized PFM surfaces using IRRAS, XPS and MC sensors has been investigated. These techniques indicated that the reaction of the pp-PFM was the fastest for the 1° amine. The deflection of the pp-PFM functionalized MCS allows for some predictions on whether the reactions occur at the liquid/solid interface or within the matrix of the polymer. Each of the amines tested in this work has shown a unique response to the microcantilever sensor, which may give insights into the reaction mechanisms taking place. The largest difference was observed between the bi-functional amine and isopropylamine, the former showing tensile, the latter showing compressive stress on the pp-PFM film.

6. Plasma polymerization of pentafluorophenyl methacrylate in selected zones has been achieved by the use of the silicon masks in two different plasma systems. The patterns have been reproduced on modified silicon wafer samples. For 500 µm thick masks the reproduction of big motives has been achieved successfully, even though small patterns are slightly defined.

By using thinner masks, the polymer deposition increases for the same exposition time. The definition of the patterns achieved with the thinnest masks (150 µm) is smaller, due in part to the motives enlarging by the mask's preparation. It can be observed that for high deposition times there is a formation of channels or holes depending on the pattern used, due to edge effects that lead to higher depositions near the masks edges. This phenomenon is independent of the polymerization system used.

7. The Microtrans needles were modified with pp-PFM and (cys0)-laminin attach to them. The in-vivo assays failed in term of connectivity with the brain's cortex. Further experiments would be needed in order to determine the different factors influencing these results. However, a positive result might be extracted out this experiment. Contrary to the precedent implantation experiments, the rabbit was able to survive during more than three months, until programmed death.

All these results are encouraging for the use of pp-PFM modified materials in the future, as reactive films for platforms for cell culture in biomaterials and biosensors.

[APPENDIX]

SURFACE CHARACTERIZATION METHODS

APPENDIX

SURFACE CHARACTERIZATION METHODS

The surface characterization techniques have developed remarkably in the last decades. This fact has favored the developing of the thin coating's field, providing accurate information about the chemical composition or morphology, among other characteristics of the films. The characterization methods used in this thesis are briefly discussed in this appendix.

a. FOURIER TRANSFORMED INFRARED SPECTROSCOPY

Infrared (IR) spectroscopy is a chemical analytical technique that highly indicated for polymer characterization.¹ It measures the infrared intensity versus the wavelength (wavenumber) of light. The technique can detect the vibration characteristics of chemical functional groups in a sample.

When an infrared light interacts with the matter, chemical bonds will stretch, contract and bend. By these movements, chemical functional groups of organic compounds tend to show characteristic vibrations, absorbing defined regions in the infrared spectra. These vibrations correspond mainly to the functional group regardless of the structure of the rest of the molecule, making possible the identification of the functional group by the absorption band.²

The wavenumber positions where functional groups absorb are consistent, even with the effect of temperature, pressure, sampling, or change in the molecule structure in other parts of the molecules.³

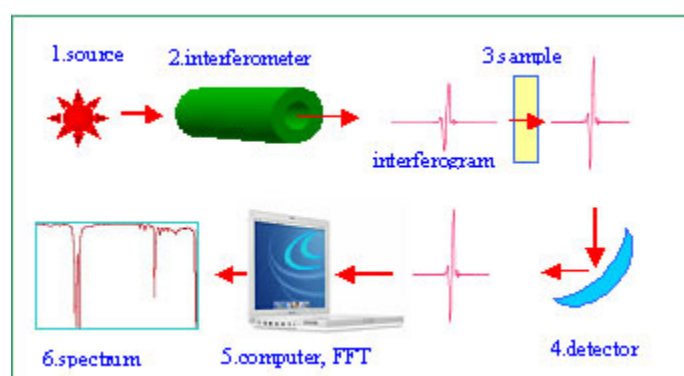


Figure a.1 Schematic illustration of FTIR system³

Fourier Transformed Infrared Spectroscopy was developed to profit the IR technique with the advances in computer technology. Figure a.1 shows the scheme of an FTIR system. The basic principle is based on the

simultaneous registration of all IR frequencies by the detector, using a polychromatic light source. Applying a mathematical transformation, the Fourier transformed, a single beam spectrum is generated.⁴

The final transmittance/absorbance spectrum is usually independent of all instrumental and environmental contributions, and only presents the features of the sample, as a reference background spectrum is obtained.⁵

Grazing Angle FTIR or Infrared Reflection-Adsorption Spectroscopy (IRRAS)⁶

Infrared reflection-adsorption spectroscopy (IRRAS) or grazing angle FTIR is used for characterization of thin films or monolayer on metal substrate, because it has advantage of high surface sensitivity.⁷

The IRRAS is dependent upon the optical constants of the thin film and substrate, the angle of incidence, as well as the polarization of the incident IR radiation.

Figure a.2 shows the incident and reflected electric vectors of the so-called p and s components of radiation where p refers to parallel polarized radiation and s to perpendicular polarized radiation with respect to the plan of incidence.

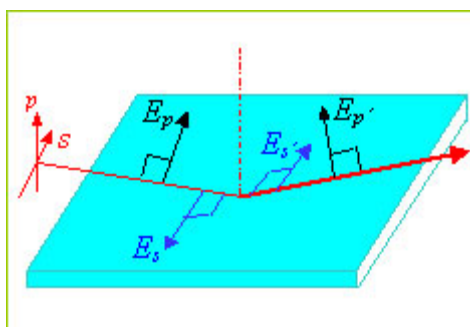


Figure a.2 Schematic illustration of the p and s polarization radiation⁶

The interaction with the surface of the sample is done only by the p -component radiation. Hence, the active vibrations that can be detected in IRRAS must have a component of the dynamic dipole polarized in the direction normal to the surface of sample, turning molecules that lie on the surface invisible to the beam.⁸ These results give the so-called “surface selection rule” for IRRAS.

The main features of IRRAS can be summarized as:

Maximum spectral intensity is detected when the angle of incidence is near grazing incidence ($ca. \sim 80^\circ$).

The dipole transition moment of the surface molecules must have a component orientated along the surface normal in order to absorb the IR incident radiation.

The absorption of the parallel component of the incident radiation is directly proportional to the film thickness when the film is thin enough ($< 10\text{nm}$).

The grazing angle FTIR analyses done in this work were carried out using a Nicolet 850 spectrometer in the reflection mode on approximately 80nm thick gold films. A polarizer was used in this system to have a better resolution of the side groups perpendicular to the polymer surface.

b. X-RAY PHOTOELECTRON SPECTROSCOPY

X-Ray Photoelectron Spectroscopy (XPS), also known as ESCA, is the most widely used surface analysis technique because of its relative simplicity in use and data interpretation.⁹

It is a surface analytical technique, which is based upon the photoelectric effect. Each atom in the surface has core electron with the characteristic binding energy that is conceptually, not strictly, equal to the ionization energy of that electron. When an X-ray beam directs to the sample surface, the energy of the X-ray photon is adsorbed completely by the core electron of an atom. If the photon energy, $h\nu$, is large enough, the core electron will then escape from the atom and emit out of the surface. The emitted electron with the kinetic energy is referred to as the photoelectron.

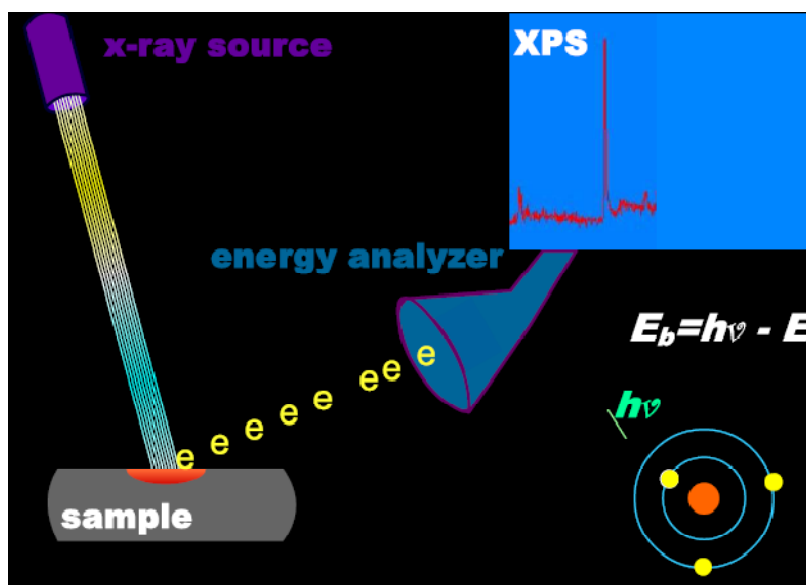


Figure b.1 Scheme of the XPS function¹⁰

An electron energy analyzer determines the binding energy of the emitted photoelectrons. From the binding energy and intensity of a photoelectron peak, the elemental identity, chemical state, and quantity of an element are determined.

For insulating samples, once the photoelectrons are emitted out of the sample surface, a positive charge zone will establish quickly in the sample surface. As a result, the sample surface acquires a positive potential that

has to be offset. In order to neutralize the surface charge during data acquisition, a low-energy electron flood gun is used to deliver the electrons to the sample surface.

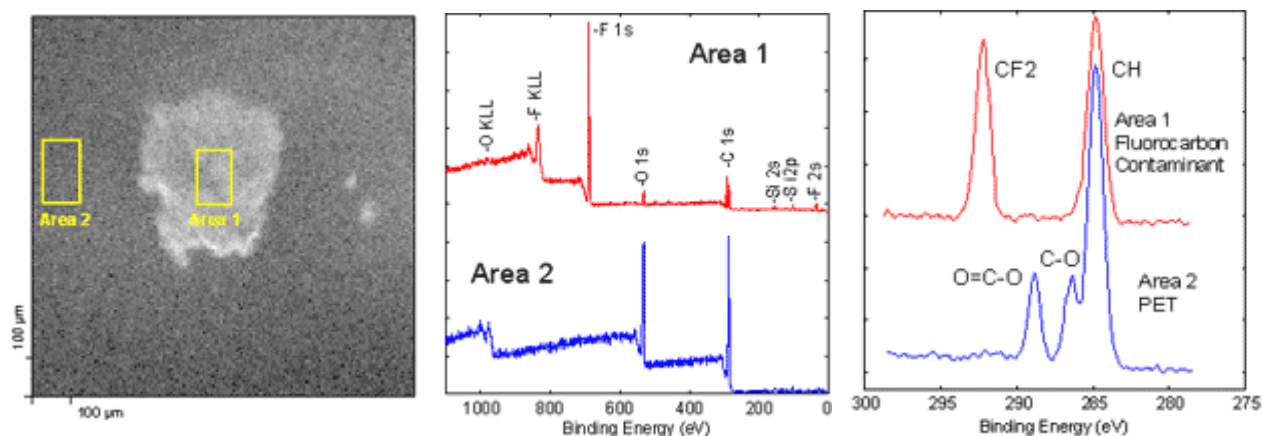


Figure b.2 X-ray beam induced secondary electron image, survey spectra and High resolution carbon 1s spectra from selected areas on a contaminated polymer surface that show the presence of fluorine in the contaminated area.¹⁰

The core electron of an element has a unique binding energy, which seems like a "fingerprint". Thus almost all elements except for hydrogen and helium can be identified *via* measuring the binding energy of its core electron. Furthermore, the binding energy of core electron is very sensitive to the chemical environment of element. The same atom is bonded to the different chemical species, leading to the change in the binding energy of its core electron. The variation of binding energy results in the shift of the corresponding XPS peak, ranging from 0.1eV to 10eV. This effect is termed as "chemical shift", which can be applied to studying the chemical status of element in the surface.¹¹

In this work, X-ray photoelectron spectroscopy analyses for the samples in *system 1* were performed within 2 days using a Perkin Elmer PHI 5500 spectrometer, equipped with a 300 W monochromatized Mg K α X-rays source. Pass energy for the acquisition of C1s photoelectrons narrow scans was 11.75 eV.

The XPS analyses for samples from *system 2* were performed also using a Perkin Elmer PHI 5500 spectrometer, equipped with a 350 W monochromatized Al K α X-rays source. Pass energy for the acquisition of C1s photoelectrons narrow scans was 11.75 eV.

All XPS spectra were recorded at a take-off angle of 45° relative to the sample surface. Surface charging of the nonconductive films was neutralized using an electron flood gun. Data analysis was carried out using Multipax (PHI) and ORIGIN software. Deconvolution of the C 1s peak was performed using ORIGIN software assuming a 70:30 Lorentzian/ Gaussian peak shape.

c. ATOMIC FORCE MICROSCOPY

Atomic Force Microscopy (AFM) is the result of the Nobel Prize Winning investigations on Scanning Tunneling Microscope by Binnig, Rohrer, Gerber and Weibel in 1982, at IBM in Zurich.¹² The microscope was developed around the mid eighties, and produces high resolution, three-dimensional images by scanning a sharp tip over the sample surface. The tip is part of a flexible cantilever on one end of a cylindrical piezoelectric tube mounted near the top of the microscope.

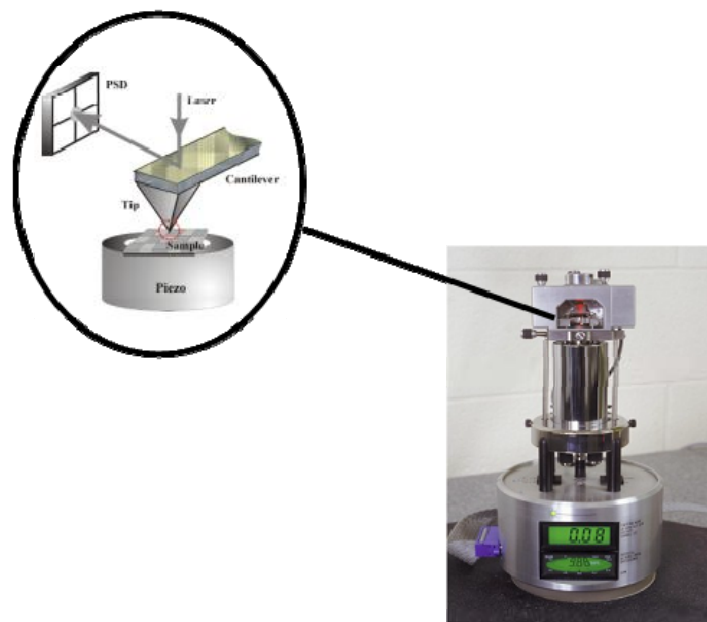


Figure c.1 Image of an Atomic Force Microscope

The Atomic Force Microscopy is one of the surface analytical tools of highest resolution. This technique is based in the measurements of small forces of attractive and repulsive atomic interaction, around 10^{-7} a 10^{-9} N, between the microscope's tip and the sample's surface. The interaction force value depends on the distance between this tip and the surface, what enables mapping the topography with practically atomic resolution.¹²

There are different kinds of forces that rule the tip and the surface interaction:

Short range repulsive forces (distances around 0.1 nm), that are a consequence of the interaction between the electrons clouds between the tip and the sample.

Long range forces (around 1 nm), caused by the attractive Van der Waals forces or by electric and magnetic forces, which can be either attractive or repulsive.

Both types of forces contribute to the total acting force on the cantilever, but only the repulsive interatomic force is able to give high resolution images, due to its extreme short range nature. Imaging of the surface is done by measuring these interaction forces via deflection of the soft cantilever while scanning the tip across

the surface.¹² A deeper explanation on the forces applying to the atomic force microscopy is presented in the review by Butt et al.¹³

Atomic force microscopes work usually in two modes, either contact or non-contact mode. The *contact* mode works with the tip around 0.1-0.3 nm from the sample's surface, and is based on the repulsive forces that govern the interaction. The *non-contact* mode locates the tip at distances fixed around 1 and 2 nm, where the attractive forces dominate the interaction. The variation of these forces, as a consequence of the different topology of the sample allows obtaining the image.

There a third mode present usually in the commercial available microscopes, the *tapping* mode. This mode is a intermittent contact mode, where the cantilever oscillates with an amplitude typically from 20 to 100 nm, causing this intermittent contact within the sample and the tip. This variation on the methods tries to reach the best resolution obtained by the contact mode, avoiding the friction forces that appear between the tip and the sample, getting less damage on soft samples.

By the oscillation, as the cantilever moves vertically, the reflected laser beam deflects in a regular pattern over a photodiode array, generating a sinusoidal, electronic signal.

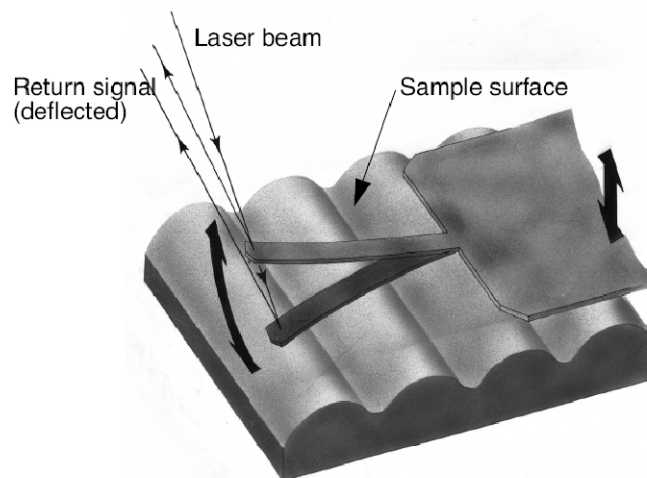


Figure c.2 Tapping Cantilever on Sample Surface¹⁴

Figure c.2 represents the cantilever at the sample surface. Although the cantilever substrate is excited with the same energy, the tip deflects in its encounter with the surface. The reflected laser beam reveals information about the vertical height of the sample surface and characteristics of the sample material itself.¹⁴

In order to describe the roughness of the surfaces, by the images obtained with the AFM, general parameters are calculated. The roughness parameters are R_a , R_q y R_{max} . R_a presents the arithmetic average of the absolute values of the surface height deviations measured from the mean plane. R_q gives the root mean

square average of height deviations taken from the mean data plane and R_{\max} the maximum vertical distance between the highest and lowest data points in the image.

In this work, AFM analysis was performed in tapping mode using a Nanoscope III Instrument (Digital Instruments, Santa Barbara, CA, USA). The roughness of the coatings was measured in terms of arithmetic average roughness (R_a), root mean square roughness (R_q) and maximum roughness height (R_{\max}).

d. ToF-SIMS

ToF-SIMS has been revealed to be very useful in the characterization of organic materials' surfaces, as it has a real surface sensitivity (outermost 15 Å), a high analytical sensitivity, and the direct relationship between the surface structure and the SIMS fragmentation patterns. Therefore SIMS has turned into a very interesting tool to investigate plasma deposited films. It provides spectroscopy for characterization of chemical composition, giving information about the unsaturation, branching or crosslinking and the aromatic or aliphatic character of a sample¹⁵, imaging for determination of distribution of chemical species and depth profiling for thin film characterization.¹⁶⁻²³ Figure d.1 presents a figure of the imaging process.

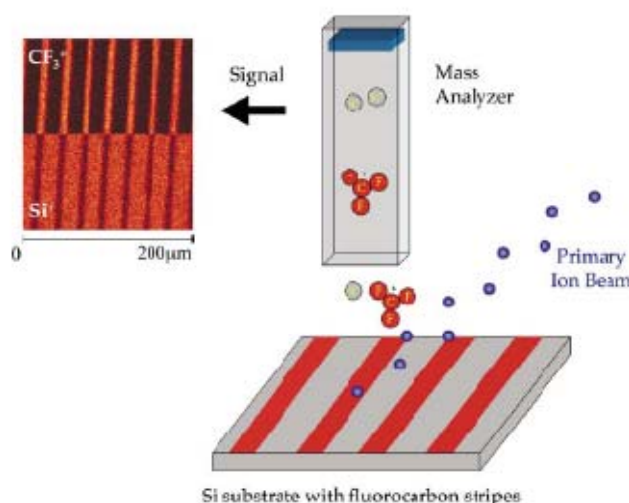


Figure d.1 A cartoon of the static ToF SIMS imaging process. A primary ion beam is scanned across the surface, which results in the ejection of secondary ions. They are then mass analyzed to generate an image of the patterned surface.²⁴

SIMS is the mass spectrometry of ionized particles which are emitted when the surface is bombarded by energetic primary particles, usually ions.

ToF-SIMS uses a pulsed primary ion beam (for example Ar^+ , Ga^+ , Cs^+) to desorb and ionize species from a sample surface. The emitted secondary particles are electrons, neutral species atoms or molecules, and atomic and cluster ions. The majority of species emitted are neutral, but it is the secondary ions which are

accelerated into a mass spectrometer, where they are mass analyzed by measuring their time-of-flight from the sample surface to the detector.²⁵

The working principle is the following: When a high energy beam of ions or neutral (primary ion source) bombards a surface, the particle energy is transferred to the atoms of the solid by collisions. A “collision cascade” occurs inside the solid, and some collisions return to the surface resulting in the emission of atoms and atoms clusters, some of which are ionized when leaving the surface. The emitted secondary ions are extracted into the ToF analyzer by applying a potential between the sample surface and the mass analyzer.

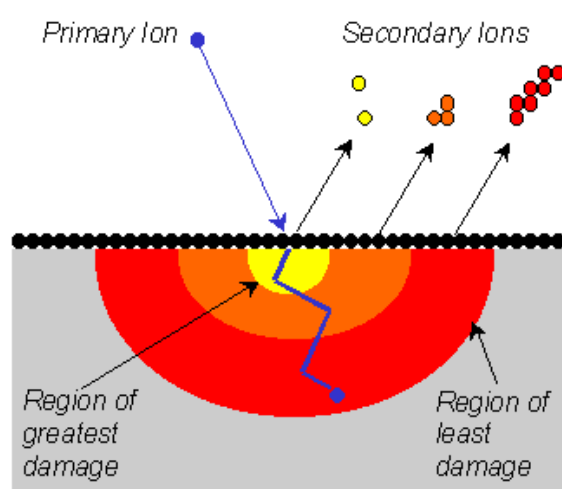


Figure d.2 Schematic diagram of the SIMS process²⁶

ToF-SIMS spectra are generated using a pulsed ion source (very short pulses of <1 ns). Secondary ions travel through the ToF analyzer with different velocities, depending on their mass to charge ratio. For each primary ion pulse, a full mass spectrum is obtained by measuring the arrival times of the secondary ions at the detector and performing a simple time to mass conversion.²⁵

To avoid the technique to be destructive, the static mode is used with an extremely low dose of primary ions, less than 10^{12} ions/cm², permitting that less than 1% of the top surface layer of atoms or molecules receives an ion impact during the experiment. With this application, in the spectroscopy and imaging modes, only the outermost (1-2) atomic layers of the sample are analyzed.

ToF-SIMS analysis in this thesis was performed with by a time-of-flight secondary ion mass spectrometer ToF-SIMS IV by Ion-ToF GmbH, Münster, Germany. Targets were bombarded by a 10 keV Cs⁺ primary ion beam with a pulsed primary ion current of 0.75 pA. For each analysis the ion beam scanned a $1\mu\text{m}^2$ area. The total acquisition time was fixed to 8 s. Positive and negative spectra were obtained with the same dose of primary ions.

Analyses of the obtained data were done by using ORIGIN Software. There is not a standard procedure to approach the analysis of the mass spectral data. The amount of information given by a simple spectrum is huge, as many masses are present on each sample. There are many ways to come close to the data, depending on the different authors, without any kind of consensus. Many groups present their ToF-SIMS analyses without any kind of normalization of the data, based on the fact of presenting only the mass spectrum, without importance to the masses' relative intensities, or by regarding these intensities just for specific masses by the ratio between each other.^{16,17,20,27-29} For other groups, the normalization of the data remains important, but no general trends are being applied. Some authors present a normalization based on the total intensities by specific ranges of masses^{18,19}, other based on reference peaks intensities³⁰, but mainly a data normalization is done by dividing by the total ion intensity in each spectrum of all the selected peaks.^{21,31-}
³⁴ This procedure is the one applied in this work over all the ToF-SIMS data gotten in the different spectra, also the ones not presented directly, in order to follow the peaks relative intensity throughout the different experiments performed.

e. SURFACE PLASMON RESONANCE

The fundamentals of surface plasmons and the experimental set up are well established and have been summarized in a number of reviews and articles.³⁵⁻³⁷ SPR is a particularly valuable tool for quantitatively studying binding reactions on surfaces if the surface itself does not change its optical properties during the binding event. SPR spectroscopy is a highly sensitive optical method for probing changes in the optical thickness ($\Delta n d$) of ultrathin adlayers on a metallic (generally gold or silver) substrate.

Surface plasmons are oscillations of the quasi-free electron gas in a metal that are coupled to an electromagnetic wave at the surface. They propagate along the interface between a metal and a dielectric medium.³⁸ Their evanescent field peaks at the interface, and decays exponentially into the metal and the dielectric medium.

Experiments were carried out on a home-built SPR setup based on the configuration introduced by Kretschmann and Raether. A thin metal layer (typically Ag or Au) is evaporated on a glass slide, and placed on the base of a prism. The light from a HeNe laser is linearly polarized, reflected at the base of the prism, and monitored with a detector. If the angle of incidence is scanned, a sharp minimum in the reflected light intensity occurs, when the light is resonantly coupled to the surface plasmon modes. At this angle, the energy and the momentum between the incoming photons and the surface plasmon waves are matched, and the reflectivity goes virtually to zero.

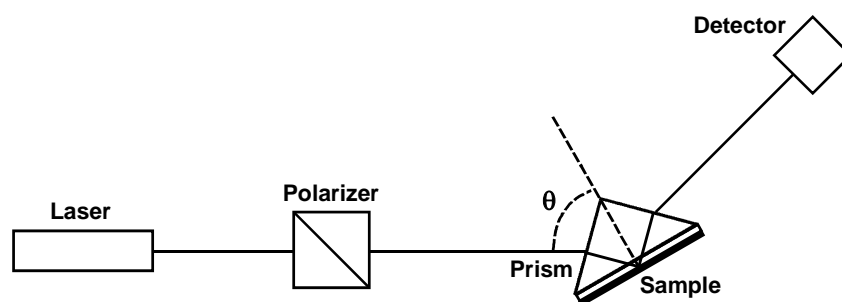


Figure e.1 Scheme of the SPR setup

Kinetic information can also be obtained from SPR spectroscopy. In these measurements, the angle of incidence is kept constant, on the left side of the initial reflectivity minimum, in the range where the resonance decreases linearly. Then the change in the reflectivity is measured as a function of time, until equilibrium is reached.³⁹

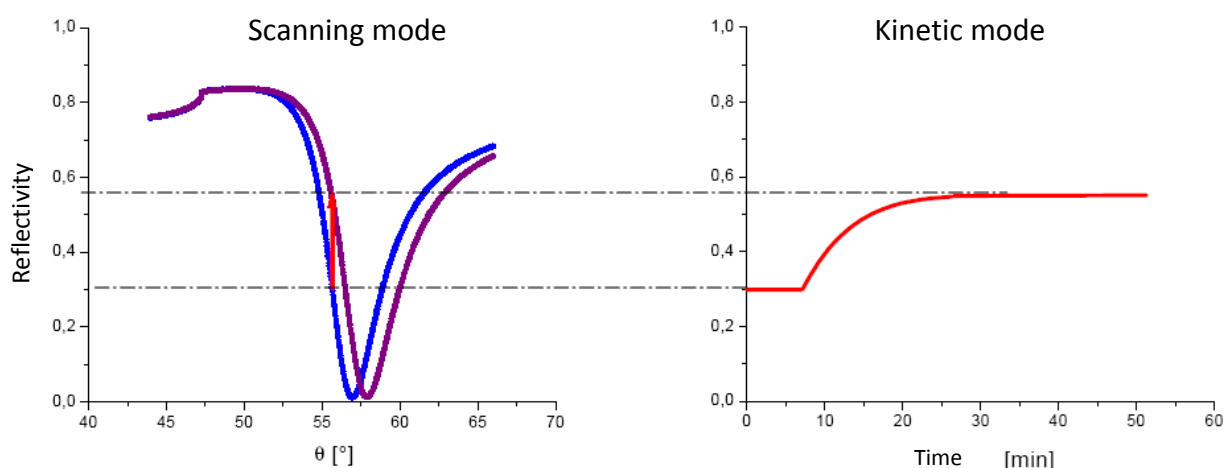


Figure e.2 SPR Operation modes

Surface Plasmon Resonance spectroscopy in this work was carried out on a home built spectrometer equipped with a Teflon reaction cell (see Figure e.3). While in previous work it has been generally studied the reaction kinetics of "stable" surfaces (i.e. those surfaces which were fully swollen)^{40,41}, in the present work the SPR technique was used to monitor a fast adsorption process which is accompanied by a slow swelling and desorption processes. Experimentally, this leads to an unstable baseline in the kinetic measurements and it was observed a broadening of the plasmon peak as well as a shift in the resonance angle. The combination of these effects makes it extremely difficult to discriminate between the different processes seen in the reflectivity mode at constant angle. In order to at least partially overcome this, the base line was monitored over a long time and kinetic measurements were performed by a dynamic tracking of the minimum giving direct access to the actual resonance angle.

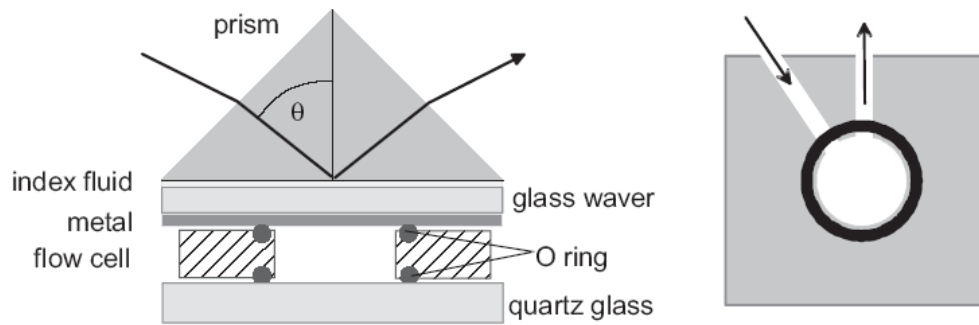


Figure e.3 Mounting of the prism and the sample flow cell

f. CONTACT ANGLE GONIOMETRY

Contact angle measurements give information about the top several Å of a plasma film.⁴² The contact angle is defined as the angle between a solid surface and the tangent of the liquid-vapour interface of a liquid drop.⁴³ Contact angle measurements with water can be used to determine if a plasma film is hydrophilic (low contact angle) or hydrophobic (high contact angle). In static measurements, the angle θ is measured at a stationary liquid front.⁴⁴ Figure f.1 shows a picture of a sessile drop on a solid surface.

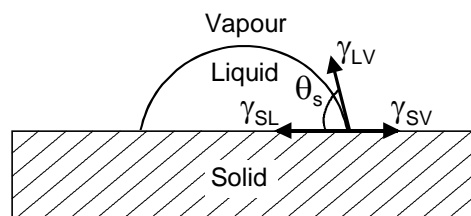


Figure f.1 Schematic diagram of the measurement of the sessile contact angle.

Contact angle measurements were performed with a DSA 10 Krüss Drop shape analysis system.

g. REFERENCES

1. Koenig, J. L. Fourier transform infrared spectroscopy of polymers. *Advances in Polymer Science* **1984**, *54* (Spectrosc.: NMR, Fluoresc., FT-IR), 87-154.
2. Hesse, M.; Meier, H.; Zeeh, B. *Metodos espectroscopicos en Quimica Organica*; 5 ed.; Editorial Sintesis: Stuttgart, New York, **1999**.
3. <http://www.nuance.northwestern.edu/KeckII/ftir1.asp> **2007**.
4. Hesse, M.; Meier, H.; Zeeh, B. *Metodos espectroscopicos en Quimica Organica*; 5 ed.; Editorial Sintesis: Stuttgart, New York, **1999**.
5. Smith, B. C. *Fundamentals of Fourier Transform Infrared Spectroscopy*; CRC press: **1996**.
6. <http://www.nuance.northwestern.edu/KeckII/ftir3.asp> **2007**.
7. Raacke, J.; Giza, M.; Grundmeier, G. Combination of FTIR reflection absorption spectroscopy and work function measurement for in-situ studies of plasma modification of polymer and metal surfaces. *Surface and Coatings Technology* **2005**, *200* (1-4), 280-283.
8. Malmsten, M. *Biopolymers at Interfaces: Second Edition, Revised and Expanded.*; 2 ed.; Marcel Dekker, Inc.: **2003**; Vol. 110.
9. <http://www.phl.com/techniques/xps.html> **2007**.
10. <http://www.nuance.northwestern.edu/KeckII/xps1.asp> **2007**.
11. *Surface analysis method in materials science*; Springer-Verlag: Heidelberg, **1992**.
12. Friedbacher, G. Scanning Probe Microscopy. In *Surface and Thin Film Analysis*, Bubert, H., Jenett, H., Eds.; Wiley-VCH Verlag GmbH: **2002**; pp 276-290.
13. Butt, H. J.; Cappella, B.; Kappl, M. Force measurements with the atomic force microscope: Technique, interpretation and applications. *Surface Science Reports* **2005**, *59* (1-6), 1-152.
14. Dimension TM 3100 Manual. Digital Instruments Veeco Metrology Group: **2000**.
15. Oran, U.; Swaraj, S.; Friedrich, J. F.; Unger, W. E. S. Surface analysis of plasma-deposited polymer films by Time of Flight Static Secondary Ion Mass Spectrometry (ToF-SSIMS) before and after exposure to ambient air. *Surface and Coatings Technology* **2005**, *200* (1-4), 463-467.
16. Turri, S.; Radice, S.; Canteri, R.; Speranza, G.; Anderle, M. Surface study of perfluoropolyether-urethane cross-linked polymers. *Surface and Interface Analysis* **2000**, *29* (12), 873-886.
17. Kinmond, E. J.; Coulson, S. R.; Badyal, J. P. S.; Brewer, S. A.; Willis, C. High structural retention during pulsed plasma polymerization of 1H,1H,2H-perfluorododecene: an NMR and TOF-SIMS study. *Polymer* **2005**, *46* (18), 6829-6835.
18. O'toole, L.; Beck, A. J.; Short, R. D. Characterization of Plasma Polymers of Acrylic Acid and Propanoic Acid. *Macromolecules* **1996**, *29* (15), 5172-5177.
19. Ward, A. J.; Short, R. D. A t.o.f.s.i.m.s. and x.p.s. investigation of the structure of plasma polymers prepared from the methacrylate series of monomers: 2. The influence of the W/F parameter on structural and functional group retention. *Polymer* **1995**, *36* (18), 3439-3450.
20. Morgan, A. R.; Duc, T. M. The chemistry of deposits formed from acrylic acid plasmas. *Journal of Materials Chemistry* **1998**, *8* (4), 937-943.
21. von Gradowski, M.; Jacoby, B.; Hilgers, H.; Barz, J.; Wahl, M.; Kopnarski, M. ToF-SIMS characterisation of ultra-thin fluorinated carbon plasma polymer films. *Surface and Coatings Technology* **2005**, *200* (1-4), 334-340.
22. Zhu, F.; Kong, E. S.-W.; Zhang, J.; Zhang, Y. Surface modification of TiO₂ nanoparticles through plasma polymerization of acrylic acid. *Chemical Physics Letters* **2006**, *423* (4-6), 270-275.
23. Rossini, P.; Colpo, P.; Ceccone, G.; Jandt, K. D.; Rossi, F. Surfaces engineering of polymeric films for biomedical applications. *Materials Science and Engineering: C* **2003**, *23* (3), 353-358.
24. Castner, D. G.; Ratner, B. D. Biomedical surface science: Foundations to frontiers. *Surface Science* **2002**, *500* (1-3), 28-60.
25. Vickerman, J. C.; Briggs, D. TOF-SIMS: Surface Analysis by Mass Spectrometry. **2001**; p 789.

26. <http://www.phl.com/techniques/tof-sims.html> **2007**.
27. Fraser, S.; Short, R. D.; Barton, D.; Bradley, J. W. A Multi-Technique Investigation of the Pulsed Plasma and Plasma Polymers of Acrylic Acid: Millisecond Pulse Regime. *J. Phys. Chem. B* **2002**, *106* (22), 5596-5603.
28. Mackie, N. M.; Castner, D. G.; Fisher, E. R. Characterization of pulsed-plasma-polymerized aromatic films. *Langmuir* **1998**, *14* (5), 1227-1235.
29. Briggs, D.; Fletcher, I. W.; Gonçalves, N. M. Positive secondary ion mass spectrum of poly(methyl methacrylate): a high mass resolution ToF-SIMS study. *Surface and Interface Analysis* **2007**, *29* (5), 303-309.
30. Feng, J.; Chan, C. M.; Weng, L. T. Influence of chain sequence structure of polymers on ToF-SIMS spectra. *Polymer* **2000**, *41* (7), 2695-2699.
31. Huang, H. L.; Goh, S. H.; Lai, D. M. Y.; Huan, C. H. A. ToF-SIMS studies of poly(methyl methacrylate-co-methacrylic acid), poly(2,2,3,3,3-pentafluoropropyl methacrylate-co-4-vinylpyridine) and their blends. *Applied Surface Science* **2004**, *227* (1-4), 373-382.
32. Oran, U.; Swaraj, S.; Friedrich, J. F.; Unger, W. E. S. Surface analysis of plasma-deposited polymer films, 3 - In situ characterization of plasma-deposited ethylene films by ToF-SSIMS. *Plasma Processes and Polymers* **2004**, *1* (2), 141-152.
33. Oran, U.; Swaraj, S.; Friedrich, J. F.; Unger, W. E. S. Surface analysis of plasma deposited polymer films, 5 - ToF-SSIMS characterization of plasma deposited allyl alcohol films. *Plasma Processes and Polymers* **2005**, *2* (7), 563-571.
34. Oran, U.; Swaraj, S.; Friedrich, J. F.; Unger, W. E. S. Surface analysis of plasma-deposited polymer films, 1 - ToF-SSIMS of plasma polystyrene before and after exposure to ambient air. *Plasma Processes and Polymers* **2004**, *1* (2), 123-133.
35. Kambhampati, D. K.; Knoll, W. Surface-plasmon optical techniques. *Current Opinion in Colloid & Interface Science* **1999**, *4* (4), 273-280.
36. Knoll, W. In *Handbook of Optical Properties*, Hummel, R. E., Wissmann P., Eds.; **1997**; pp 373-400.
37. Nakamura, R.; Murguruma, H.; Ikebukuro, K.; Sasaki, S.; Nagata, R.; Karube, I.; Pedersen, H. A plasma polymerized film for surface plasmon resonance immunosensing. *Analytical Chemistry* **1997**, *69* (22), 4649-4652.
38. Aust, E. F.; Ito, S.; Sawodny, M.; Knoll, W. Investigation of polymer thin films using surface plasmon modes and optical waveguide modes. 2 ed.; **1994**; pp 313-323.
39. Green, R. J.; Frazier, R. A.; Shakesheff, K. M.; Davies, M. C.; Roberts, C. J.; Tendler, S. J. B. Surface plasmon resonance analysis of dynamic biological interactions with biomaterials. *Biomaterials* **2000**, *21* (18), 1823-1835.
40. Zhang, Z.; Chen, Q.; Knoll, W.; Forch, R. Effect of aqueous solution on functional plasma polymerized films. *Surface and Coatings Technology* **2003**, *174-175* (Complete), 588-590.
41. Zhang, Z.; Menges, B.; Timmons, R. B.; Knoll, W.; Foerch, R. Surface plasmon resonance studies of protein binding on plasma polymerized di(ethylene glycol) monovinyl ether films. *Langmuir* **2003**, *19* (11), 4765-4770.
42. Anand, M.; Cohen, R. E.; Baddour, R. F. Surface modification of low density polyethylene in a fluorine gas plasma. *Polymer* **1981**, *22*, 361-371.
43. d'Agostino, R. *Plasma Deposition, Treatment and Etching of Polymer Films*; Academic Press: Boston, MA, **1990**.
44. Chan, C. M. *Polymer Surface Modification and Characterization*; Hanser/Gardner Publications, Inc.: Cincinnati, OH, **1994**.